

Diss. ETH No. 15276

**A Spatio-Temporal Matching Algorithm
for 3D Particle Tracking Velocimetry**

A dissertation submitted to the
Swiss Federal Institute of Technology Zurich

for the degree of
Doctor of Technical Sciences

presented by

JOCHEN WILLNEFF

Dipl. Ing. Vermessungswesen, Universität Fridericiana zu Karlsruhe

born 14th of March, 1971
citizen of Germany

accepted on the recommendation of

Prof. Dr. Armin Grün, ETH, examiner

Prof. Dr. Hans-Gerd Maas, Dresden University of Technology, Germany, co-examiner

September 2003

Contents

Abstract	1
Zusammenfassung	3
1. Introduction	5
2. Flow measurement	7
2.1. Mathematical description of flow fields	7
2.1.1. Eulerian representation	7
2.1.2. Lagrangian representation	7
2.2. Techniques for flow measurement	8
2.2.1. Thermo-electric velocity measurement techniques	9
2.2.1.1. Hot Wire Anemometry / Constant Temperature Anemometry (CTA)	9
2.2.1.2. Pulsed Wire Anemometry (PWA)	10
2.2.2. Optical velocity measurement techniques	10
2.2.2.1. Laser Doppler Anemometry (LDA)	10
2.2.2.2. Laser-2-Focus Anemometry (L2F)	11
2.2.2.3. Laser Induced Fluorescence (LIF)	12
2.2.2.4. Particle Image Velocimetry (PIV)	12
2.2.2.5. Particle Tracking Velocimetry (PTV)	14
2.2.3. Comparison of flow measurement techniques	16
3. Photogrammetric aspects for 3D PTV	17
3.1. Mathematical model	17
3.2. Handling of the mathematical model	18
3.3. Multimedia geometry	19
3.4. Epipolar line intersection technique	19
4. Hardware components of a 3D PTV system	23
4.1. Visualization of the flow	23
4.2. Illumination	24
4.3. Sensors	24
4.3.1. Video norm	24
4.3.2. Image acquisition with High Definition TV cameras	25
4.3.3. IEEE-1394 technology (Firewire)	26
4.3.4. Integration modes	26
4.3.5. Fill factor and light sensitivity	26
4.3.6. Cameras with CMOS technology	27
4.3.7. Synchronization	27
4.4. System calibration	28
4.5. Hardware of the 3D PTV system at ETH	28
4.6. Potential of 3D PTV	29

5. Overview on particle tracking methods	31
5.1. Coordinate based spatio-temporal assignment	32
5.2. Algorithmic aspects for spatio-temporal matching for 3D PTV	32
5.3. Image space based tracking techniques	33
5.4. Object space based tracking techniques	35
6. 3D PTV based on image and object space information	39
6.1. Spatio-temporal consistency in multiocular image sequences	39
6.2. Spatio-temporal matching algorithm for 3D PTV	41
6.3. Alternative criteria for temporal assignment in image sequences	43
6.4. Tracking procedure using kinematic motion modelling	45
6.5. Exploitation of redundant information for ambiguity reduction	48
6.6. Non-algorithmic limitations of trajectory lengths	50
6.7. Parameter settings for PTV processing	51
7. Tests of the spatio-temporal matching algorithm	53
7.1. Definition of performance characteristics	53
7.2. Tests using simulated data	54
7.2.1. Generation of simulated image sequences	54
7.2.2. Simulation of a vortex flow field	55
7.3. Tests using real data	59
7.3.1. Data set 'Trinocular'	60
7.3.2. Data set 'Forward facing step'	63
7.3.3. Data sets for investigation of velocity derivatives	66
7.3.3.1. Turbulent flow generation by electromagnetic forcing	67
7.3.3.2. Length scale and Kolmogorov time	68
7.3.3.3. Setup for the experiment 'copper sulphate'	69
7.3.3.4. Setup for the experiments '1.0' and '2.5'	70
7.3.3.5. Optimization of the experimental setup	71
7.3.3.6. Experiment 'copper sulphate'	72
7.3.3.7. Experiment '1.0'	74
7.3.3.8. Experiment '2.5'	77
7.3.3.9. Statistical basis for Lagrangian analysis	79
7.4. Application of 3D PTV in space 'MASER 8 Project'	80
7.4.1. Description of the four headed camera system	81
7.4.2. Calibration of the image acquisition system	82
7.4.2.1. Image quadruplet used for the calibration	82
7.4.2.2. Results of the calibration	83
7.4.3. Image preprocessing	84
7.4.4. Parabolic flight campaign	86
7.4.4.1. Processing of parabolic flight data	86
7.4.5. MASER 8 campaign	88
7.4.5.1. Processing of MASER 8 data	88
7.4.5.2. Tracking results from data set 'MASER 8'	90
7.5. Results	91
7.5.1. Examples from the data set 'simulated vortex'	91
7.5.2. Examples from real experiment data	93
7.5.3. Accuracy considerations and trajectory smoothness	94

7.5.4. Performance characteristics applied to the PTV data sets	96
8. Conclusions and perspectives	99
8.1. Conclusions	99
8.2. Future work	100
8.2.1. Simplification of the calibration procedure by DLT	100
8.2.2. Investigation of the traceability of particles	101
8.2.3. Further developments of 3D PTV systems	101
9. Acknowledgements	103
Appendix	105
A.1 Handling of the 3D PTV software	105
A.2 Running the 3D PTV software under different operation systems	105
A.3 Parameter files for 3D PTV	105
A.4 Data Input	107
A.5 Examples for the parameter files name.ori and name.addpar	111
A.6 Calibration of the image acquisition system	112
A.7 Processing of a single time step	113
A.8 Display of image sequences	113
A.9 Processing of image sequences	114
A.10 Tracking of particles	114
A.11 Options	115
A.12 Visualization of tracking results	115
References	117
Curriculum Vitae	123

Abstract

3D Particle Tracking Velocimetry (PTV) offers a flexible technique for the determination of velocity fields in flows. In the past decade the successful research work performed by the Institute of Geodesy and Photogrammetry at ETH Zurich led to an operational and reliable measurement tool used in various hydrodynamic applications. In cooperation with the Institute of Hydromechanics and Water Resources Management (IHW) at ETH Zurich further progress has been achieved in the improvement of the existing hard- and software solutions.

Regarding the hardware setup the image acquisition system used at the ETH Zurich was upgraded from analogue intermediate storage to online image digitization. The latest hardware setup was used for the data acquisition in experiments for the investigation of velocity derivatives in turbulent flow measured with 3D PTV. The recently employed system is capable to record image sequences of four progressive scan cameras at a frame rate of 60 Hz over 100 s, which corresponds to 6000 frames. The reasons for the development of a 60 Hz system was the promise of an improved particle traceability and an increased number of frames per Kolmogorov time leading to a higher overall performance not only in quality but also in the amount of statistical data available.

Major progress was made regarding the software implementation. Within the framework of the research project “Entwicklung eines spatio-temporalen Zuordnungsalgorithmus für 3D PTV” (Grant No 2100-049039.96/1) of the Swiss National Science Foundation a new spatio-temporal matching algorithm was developed, implemented and tested. In former approaches the reconstruction of the particle trajectories was done in two steps by establishing the spatial and temporal correspondences between particle images separately. The previous 3D PTV solution at the Institute of Geodesy and Photogrammetry applying an object space based tracking algorithm was improved in a way that the redundant information in image and object space is exploited more efficiently. The enhanced method uses a combination of image and object space based information to establish the spatio-temporal correspondences between particle positions of consecutive time steps. The redundant image coordinate observations combined with the prediction for the next particle position should allow the establishment of spatio-temporal connections even when the velocity field has a high density or the movement of the tracer particles is fast. The use of image and object space based information in combination with a prediction of the particle motion was intended to lead to enhanced results in the velocity field determination. In the case of ambiguities in the epipolar line intersection method particle trajectories are often interrupted for one or several time steps. With the new algorithm these gaps can be bridged reliably and even the continuation of a trajectory is possible when the redundant information is exploited in a correct way. The tracking procedure is performed bidirectional, which leads to further improvements of the results. The most important result of this work is a substantial increase of the tracking rate in 3D PTV.

A reduction of the trajectory interruptions due to unsolved ambiguities can multiply the yield of long trajectories and thus the usefulness of the results of 3D PTV, which further enlarges the application potential of the technique. Long trajectories are an absolute pre-requisite for a Lagrangian flow analysis, as integral time and length scales can only be determined if long correlation lengths have been recorded. In addition, the number of simultaneous trajectories should be large enough to form a sufficient basis for a statistical analysis. Compared to the former implementation the tracking efficiency has been increased and the reconstruction of longer trajectories was obtained.

To offer easy handling for the user the data processing with the PTV implementation should also provide a high degree of automatization. Controlled by a graphical user interface and after

the adjustment of experiment dependent parameters the processing of the image sequences is done fully automatically, directly generating the requested result data for hydrodynamic analysis as well as for visualization purposes.

Tests of data sets from simulated and real experiments were performed to ensure the method's operability and robustness. The great variety of the data sets that were processed during the development of the new spatio-temporal matching algorithm show its general applicability for a wide range of different 3D PTV measurement tasks.

Zusammenfassung

Mit 3D Particle Tracking Velocimetry steht eine flexible Methode zur Bestimmung von Geschwindigkeitsfeldern in Strömungen zur Verfügung. Die im vergangenen Jahrzehnt am Institut für Geodäsie und Photogrammetrie der ETH Zürich geleistete Forschungsarbeit führte zu einem einsatzfähigen und zuverlässigen Messinstrument für verschiedenste Anwendungen in der Hydrodynamik. In Zusammenarbeit mit dem Institut für Hydromechanik und Wasserwirtschaft (IHW) der ETH Zürich wurden weitere Fortschritte in der Verbesserung der vorhandenen Hard- und Softwarelösungen erzielt.

Bezüglich der Hardware wurde das System zur Bilddatenerfassung der ETH Zürich von analoger Zwischenspeicherung und anschliessender A/D-Wandlung auf eine online-Digitalisierung umgestellt. Das neueste System wurde zur Datenerfassung in Experimenten für die Untersuchung von Geschwindigkeitsableitungen in turbulenten Strömungen aus PTV Messungen eingesetzt. Das zuletzt eingesetzte System kann die Bildsequenzen von vier Progressive Scan Kameras mit einer Bildrate von 60 Hz über einen Zeitraum von 100 s beziehungsweise 6000 Bildern aufzeichnen. Von der Entwicklung eines 60 Hz Systems versprach man sich eine verbesserte Partikelverfolgung und eine gesteigerte Anzahl von Zeitschritten pro Kolmogorov Länge, was nicht nur die Gesamtleistungsfähigkeit, sondern auch die zur Verfügung stehende Datenmenge erhöht.

Grosse Fortschritte wurden im Bereich der Auswertesoftware erzielt. Im Rahmen des Forschungsprojektes “Entwicklung eines spatio-temporalen Zuordnungsalgorithmus für 3D PTV” (Grant No 2100-049039.96/1) des Schweizer Nationalfonds wurde ein neuer spatio-temporaler Zuordnungsalgorithmus entwickelt, implementiert und getestet. Bisherige Methoden zur Rekonstruktion von Partikeltrajektorien lösten das Problem der räumlichen und zeitlichen Zuordnung von den Partikelabbildungen in zwei getrennten Schritten. Die frühere 3D PTV Methode des Instituts für Geodäsie und Photogrammetrie, welche einen objektraumbasierten Trackingalgorithmus verwendete, wurde dahingehend verbessert, dass die redundante Information aus Objekt- und Bildraum effizienter genutzt wird. Die verbesserte Methode nutzt die Kombination aus objekt- und bildraumbasierter Information um die spatio-temporalen Verknüpfungen zwischen den Partikelpositionen in aufeinanderfolgenden Zeitschritten zu lösen. Die redundanten Bildkoordinatenbeobachtungen, kombiniert mit einer Vorhersage der nachfolgenden Partikelposition, sollte die Lösung der spatio-temporalen Zuordnungen selbst dann ermöglichen, wenn die Partikeldichte hoch ist oder die Partikel sich schnell bewegen. Die Verwendung der bild- und objektraumbasierten Informationen in Kombination der Vorhersage der Partikelbewegung sollte zu deutlich verbesserten Ergebnissen der Messung von Geschwindigkeitsfeldern führen. Mehrdeutigkeiten, wie sie bei der Kernlinienschnittmethode auftreten, führen oft zu Unterbrechungen der Partikeltrajektorie von einem oder mehreren Zeitschritten. Mit der neuen Methode ist es möglich, diese Lücken zuverlässig zu schliessen und sogar die Fortsetzung einer Trajektorie kann mittels geeigneter Ausnutzung der redundanten Information erfolgen. Das Tracking wird zeitlich in beide Richtungen durchgeführt, was zu einer weiteren Verbesserung der Ergebnisse führt. Das wichtigste Ziel der Arbeit war die Steigerung der Erfolgsrate des Trackings mit 3D PTV.

Eine Reduktion der mehrdeutigkeitsbedingten Unterbrechungen der Partikeltrajektorien vervielfacht die Anzahl langer Trajektorien und erhöht dadurch die Nutzbarkeit der 3D PTV Ergebnisse, was wiederum zur erweiterten Einsatzfähigkeit dieser Technik beiträgt. Lange Trajektorien sind eine absolute Grundvoraussetzung für Langrange'sche Strömungsanalysen, da integrales Zeit- und Längenmass nur bestimmbar sind, wenn ausreichend lange Korrelationslängen gemessen werden konnten. Zusätzlich sollte die Anzahl gleichzeitig beobachteter

Trajektorien eine ausreichende Basis für statistische Analysen darstellen. Verglichen mit der bisherigen Implementation wurde sowohl eine gesteigerte Trackingrate, als auch die vermehrte Rekonstruktion längerer Trajektorien erzielt.

Um dem Anwender die Prozessierung der Daten zu erleichtern, sollte die PTV Auswertesoftware einen hohen Automatisierungsgrad aufweisen. Gesteuert über eine graphische Benutzeroberfläche kann nach der Einstellung von experimentabhängigen Parametern eine vollautomatische Auswertung erfolgen, die sofort die Ausgabe der Ergebnisse in geeigneter Form sowohl für hydrodynamische Analysen als auch für Visualisierungszwecke ermöglicht.

Durch umfangreiche Tests sowohl mit simulierten Datensätzen, als auch von realen Experimenten ist die Einsatzfähigkeit der Methode gewährleistet. Betrachtet man die grossen Unterschiede in den einzelnen Datensätzen, die während der Entwicklung des neuen spatio-temporalen Zuordnungsalgorithmus erfolgreich bearbeitet wurden, kann diese Methode als geeignet zur Lösung verschiedenster 3D PTV Messaufgaben angesehen werden.

1. Introduction

3D Particle Tracking Velocimetry (PTV) is a technique for the determination of 3D velocity fields in flows. The method is based on the visualization of a flow with small, neutrally buoyant particles and recording of stereoscopic image sequences of the particles. The results of PTV are not only three-dimensional velocity vectors in a three-dimensional object space provided with a certain temporal resolution, but also three-dimensional trajectories, the particles distribution and their temporal behaviour. Due to this ability of the method it can deliver both Eulerian as well as Lagrangian flow properties. Research activities in this field have been performed at the Institute of Geodesy and Photogrammetry for more than a decade and have reached a status of an operable and reliable measurement method used in hydrodynamics and also space applications.

In cooperation with the Institute of Hydromechanics and Water Resources Management at ETH Zurich further progress is achieved in the improvement of the existing hard- and software solutions.

The PTV method was already successfully used in many applications as the investigation of different flow phenomena like turbulence and turbulent dispersion, flow separation, convection and velocity derivatives. Within the framework of the research project “Entwicklung eines spatio-temporalen Zuordnungsalgorithmus für 3D PTV” of the Swiss National Science Foundation (Grant No 2100-049039.96/1) a new spatio-temporal matching algorithm was developed and implemented.

The most important result that was expected from this work was a substantial increase of the tracking rate in 3D PTV. This is of importance mainly in the context of a Lagrangian analysis of particle trajectories, which can be considered the actual domain of the technique. Long trajectories are an absolute pre-requisite for a Lagrangian flow analysis, as integral time and length scales can only be determined if long correlation lengths have been recorded. In addition, the number of simultaneous trajectories should be large enough to form a sufficient basis for a statistical analysis. Due to interruptions of particle trajectories caused by unsolved ambiguities the number of long trajectories decreases exponentially with the trajectory length. Very long trajectories over hundred and more time instances can so far only be determined if the probability of ambiguities is reduced by a low seeding density, thus concurrently reducing the spatial resolution of the system and the basis for a statistical analysis. A reduction of the interruptions of the trajectories due to unsolved ambiguities increases the yield of long trajectories and thus the usefulness of the results of 3D PTV and further enlarge the application potential of the technique.

2. Flow measurement

In the field of hydromechanics, many theories to describe different aspects of turbulence and turbulent diffusion have been developed in the past. These theories are often based on assumptions and approximations since exact experimental data is difficult to obtain. Much research work in fluid dynamics is exclusively based on Computational Fluid Dynamics (CFD), which often requires long computation times. The comparison between numerical calculations and results of flow measurements provide the basis for the verification of the theoretical models used in fluid dynamics. This indicates the necessity of a reliable velocity field determination for flow experiments to validate the numerical simulations and to verify results from CFD codes.

After a short introduction concerning the mathematical description of flow fields this chapter gives an overview about the different operational techniques used for flow measurement.

2.1. Mathematical description of flow fields

The determination of the local flow velocity as well as the velocity distribution in complex flows is a fundamental task in the field of fluid dynamics. The motion in a flow field can be described in two ways. The way of description implies directly the measurement techniques used for the determination of the observed flow field.

2.1.1. Eulerian representation

One possible description is the determination of the direction and norm of the velocity vector at prescribed positions. This Eulerian description regards the velocity \vec{u} as a function of position \vec{x} and time t :

$$\vec{u} = \vec{u}(\vec{x}, t) \quad (1)$$

For a three-dimensional flow this vector consists of three components. Depending on the flow to be measured the velocity vector determination might be reduced to one or two components in some cases. Most of the theoretical investigations and experimental measurements in the field of fluid mechanics refer to the Eulerian approach. Many of the operable instruments measure fluid properties at fixed positions and provide Euler-flow field information directly. Fig. 1 shows an Eulerian representation (left) of a flow at one instant of time.

2.1.2. Lagrangian representation

Alternatively, the motion can be described in the Lagrangian way. In the Lagrangian representation a trajectory of an individual fluid element is defined to be a curve traced out as time progresses. Thus, a trajectory is a solution of the differential equation:

$$\frac{d\vec{x}}{dt} = \vec{u}(\vec{x}(t), t) \quad (2)$$

2.2. Techniques for flow measurement

The fluid elements are identified at some initial time t_0 with position \bar{x}_0 . Thus $\bar{x} = \bar{x}(\bar{x}_0, t - t_0)$ where $\bar{x}_0 = \bar{x}(t_0)$. The velocity of a fluid is therefore the time derivative of its position:

$$\vec{u}(\bar{x}_0, t - t_0) = \frac{\delta}{\delta t} \bar{x}(\bar{x}_0, t - t_0) \quad (3)$$

Although Lagrangian quantities are difficult to obtain several phenomena are formulated in this flow representation. Fig. 1 shows the Lagrangian representation (right) of a flow, due to the fact that the Lagrangian representation is based on trajectories of fluid elements it requires more than one time instant compared to the Eulerian representation.

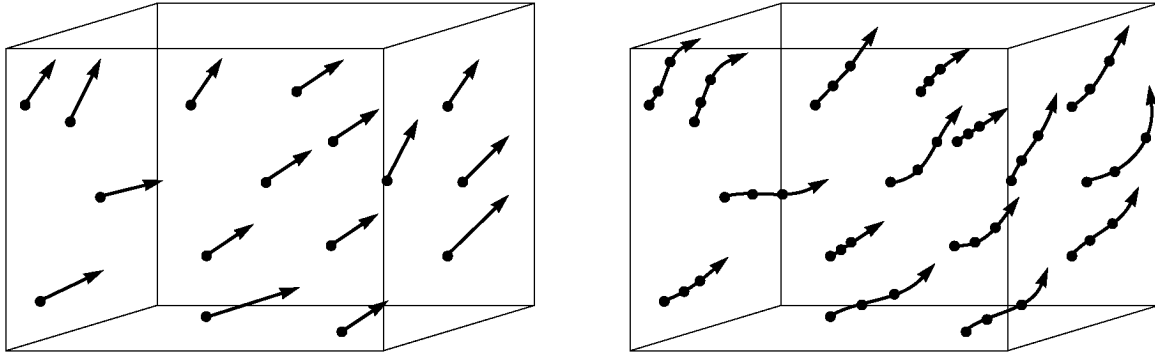


Fig. 1: Flow modeled as Eulerian (left) and Lagrangian (right) representation

2.2. Techniques for flow measurement

Several different operable techniques have been developed for flow measurement distinguishing by their applicability, performance and the kind of results they deliver. Most of today's fluid dynamics measurements are performed with point-based techniques. Others allow global measurements in a plane or even throughout an object volume. The three-dimensional flow velocity information can be obtained by scanning of layers as well as simultaneous full field measurements.

Flow measurements can be performed intrusive with probes put into the flow or non-intrusive. Among the today's flow measurement techniques the most common are classified to these two types in Table 1. The results are velocities in one, two or three dimensions or trajectories over time. Relevant performance characteristics of the different techniques are summarized in Table 2 in section 2.2.3.

A brief overview about these common techniques, a comparison of the result and their performance is given in (Maas, 1992b), more details about some of the mentioned methods can be found in (Nitsche, 1994).

Table 1: Overview on the different flow measurement techniques

Classification	Method	Type of measurement
intrusive	Hot Wire Anemometry / Constant Temperature Anemometry (CTA)	measurement at single probe locations, thermo-electric
	Pulsed Wire Anemometry (PWA)	measurement at single probe location, thermo-electric
non-intrusive	Laser Doppler Anemometry (LDA)	measurement at single probe locations, optical, particles
	Laser-2-Focus Anemometry (L2F)	measurement at single probe locations, optical, particles
	Laser Induced Fluorescence (LIF)	scanning lightsheet, optical, flourescin
	Particle Imaging Velocimetry (PIV)	(scanning) lightsheet, optical, particles
	Particle Tracking Velocimetry (PTV)	object volume, optical, particles

2.2.1. Thermo-electric velocity measurement techniques

Thermo-electric velocity measurement techniques are widely common and appropriate for the measurement of time series in one, two or three-dimensional gas and liquid flows. The temporal resolution of these techniques can be considered as high where spatial resolution is rather limited to a few number of probe locations. The thermo-electric velocity measurement techniques cannot be classified as non-intrusive.

2.2.1.1. Hot Wire Anemometry / Constant Temperature Anemometry (CTA)

Hot Wire Anemometry - or Constant Temperature Anemometry (CTA) - is a widely accepted tool for fluid dynamic investigations in gases and liquids and has been used as such for more than 50 years (Dantec, 2003). It is a well-established technique that provides single point information about the flow velocity. Its continuous voltage output is well suited to digital sampling and data reduction. Properly sampled, it provides time series that can form the basis for statistical evaluation of the flow microstructure.

The velocity is measured by its cooling effect on a heated sensor. A feedback loop in the electronics keeps the sensor temperature constant under all flow conditions. The voltage drop across the sensor thus becomes a direct measure of the power dissipated by the sensor. The anemometer output therefore represents the instantaneous velocity in the flow. Sensors are normally thin wires with diameters down to a few micrometers. The small thermal inertia of the sensor in combination with a very high servoloop amplification makes it possible for the Hot Wire Anemometry to follow flow fluctuations up to several hundred kHz and covers velocities from a few cm/s to well above the speed of sound. A scheme of a Constant Temperature Anemometer is shown in Fig. 2.

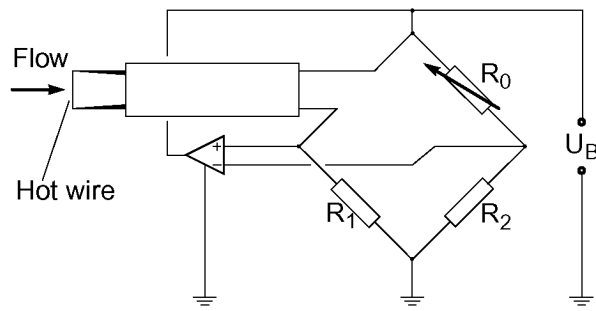


Fig. 2: Circuit diagram of a CTA system

The method's particular advantages are high temporal resolution, making it particularly suitable for the measurement of very fast fluctuations in single points. It requires no special preparation of the fluid (e.g. seeding with tracers) and the small dimensions of the probe permit measurement in locations that are not easily accessible. The heat-transfer relation governing the heated sensor includes fluid properties, temperature loading, sensor geometry and flow direction in relation to the sensor. Due to the complexity of the transfer function a calibration of the anemometer is mandatory before its use.

2.2.1.2. Pulsed Wire Anemometry (PWA)

Pulsed Wire Anemometry (PWA) is based on the principle of measuring velocity by timing the flight of a passive tracer over a known distance (Venas et al., 1999). A pulsed wire probe has three wires, one pulsed and two sensor wires. The pulsed wire emits a heated spot, a small slightly heated region of fluid, which is convected with the instantaneous flow and after a short time sensed by one of the sensor wires - giving a "time of flight" and thus a velocity sample if the distance between the wires is known. A sensor wire is placed on either side of the pulsed wire to be able to detect flow in both - forward and backward - directions.

Like Hot Wire Anemometry the spatial resolution of this technique is limited to a few number of probe locations providing pointwise information about the flow velocity. The individual measurements are usually performed with a temporal resolution of 5 - 10 Hz. To yield reliable results - depending on the turbulence of the flow - over 500 up to 5000 single measurements are averaged. Compared to Hot Wire Anemometry the range of flow velocities, which can be measured reliably with this technique is rather small and should not exceed 15 m/s.

2.2.2. Optical velocity measurement techniques

All the optical velocity measurement techniques described in the following sections are non-intrusive and therefore do not influence the flow directly. Nevertheless indirect influences can occur e.g. due to the used illumination facility, which may produce a significant amount of heat leading to unwanted thermal forcing of the flow.

2.2.2.1. Laser Doppler Anemometry (LDA)

Laser Doppler Anemometer, or LDA, is also a very common technique for fluid dynamic investigations in gases and liquids and has been used as such for more than three decades (Dantec, 2003). LDA allows measuring velocity and turbulence at specific points in gas or liquid flows. LDA requires tracer particles in the flow. Liquids often contain sufficient natural seeding, whereas gases must be seeded in most cases. Typically the size range of the particles is between 1 up to 10 μm , the particle material can be solid (powder) or liquid (droplets).

The basic configuration of a LDA system consists of:

- Continuous wave laser
- Transmitting optics, including a beam splitter and a focusing lens

- Receiving optics, comprising a focusing lens and a photodetector
- Signal conditioner and a signal processor

The laser beam is divided into two and the focusing lens forces the two beams to intersect. The photodetector receives light scattered from tracer particles moving through the intersection volume and converts the light intensity into an electrical current. The scattered light contains a Doppler shift, the Doppler frequency, which is proportional to the velocity component perpendicular to the bisector of the two laser beams. With a known wavelength of the laser light and a known angle between the intersecting beams, a conversion factor between the Doppler frequency and the velocity can be calculated. The addition of one or two more beam pairs of different wavelengths to the transmitting optics and one or two photodetectors and interference filters permits two or all three velocity components to be measured. Each velocity component also requires an extra signal processor channel.

The basic configuration gives the same output for opposite velocities of the same magnitude. In order to distinguish between positive and negative flow direction, frequency shift is employed. An acousto-optical modulator - the "Braggcell" - in the transmitting optics introduces a fixed frequency difference between the two beams. The resulting output frequency is the Doppler frequency plus the frequency shift. Modern LDA optics employs optical fibres to guide the laser light from the often bulky laser to compact probes and to guide the scattered light to the photodetectors.

Beside being a non-intrusive method, its particular advantages are the very high temporal resolution (the sampling rate can exceed 100 kHz), no need for calibration and the ability to measure in reversing flows. LDA offers the possibility of pointwise measurements, which results in rather low spatial resolution. With big technical effort it is possible to obtain simultaneous measurements at a few number of probe locations (5 - 10 points). Under the assumption of a stationary flow field, velocity profiles can be measured by scanning the object volume along a traverse.

2.2.2.2. Laser-2-Focus Anemometry (L2F)

The Laser-2-Focus Anemometry (L2F) is a technique suitable for measurement of flow velocities in gases and liquids (Förstner, 2000), (Krake/Fiedler, 2002). The velocity of extremely small particles is recorded, which are usually present in all technical flows or may be added if required. The light scattered by the particles when irradiated by a light source is used in this technique. The required particles are in the size range of the light wavelength (less than one μm) and follow the flow even at high accelerations so that correlation between particles and flow velocity is assured. In the observation volume of the L2F device, two highly focussed parallel beams are projected, which function as a time of flight gate. Particles, which traverse the beams in this area each emit two scattering light pulses that are scattered back and are detected by two photodetectors each of which is assigned to a beam in the measuring volume (Förstner, 2000).

Should a particle traverse both beams, then it transmits two scattering signals whose time interval provides a value for the velocity component in the plane perpendicular to the beam axis. The measurement principle is shown in Fig. 3. Two associated double signals are only obtained when the plane through which the two beams are spread out is nearly parallel to the flow direction. The beam plane is rotatable and its angular position α is determined. The beam plane for a L2F measurement is adjusted in various angular positions in the range of the mean flow direction and some thousands of time-of-flight measurements are carried out for each position. The evaluation of the data results in the two components - magnitude and direction - of the mean flow vector in the plane perpendicular to the optical axis of the measuring system.

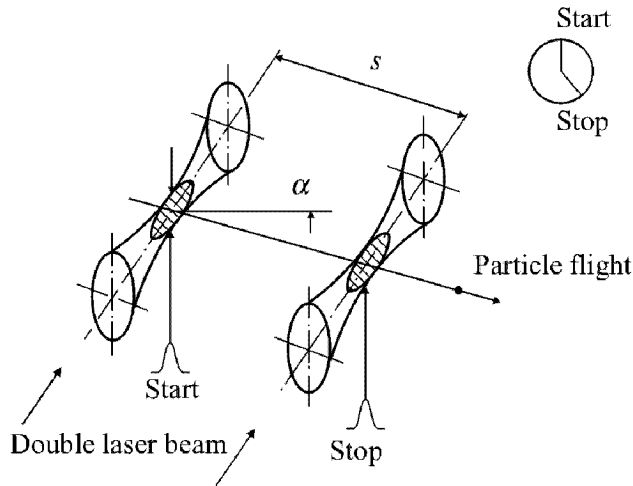


Fig. 3: Measurement principle of L2F, taken from (Krake/Fiedler, 2002)

Recently a new three component system was developed, which operates with the same confocal optical set-up as a two component L2F system, thus enabling three component measurements even under difficult conditions of limited optical accessibility. The two velocity components in the plane perpendicular to the optical axis are measured by the conventional L2F time of flight technique. Since the velocity component in the direction of the optical axis causes a frequency shift of the scattered light due to the Doppler effect, the third component can be measured by analyzing the scattered light frequency. The individual measurements are performed with a high temporal resolution.

tion, but to yield reliable results around 5000 single measurements are averaged. In comparison to LDA a longer measuring time is required. Again the spatial resolution is limited to a few probe locations.

2.2.2.3. Laser Induced Fluorescence (LIF)

Laser Induced Fluorescence (LIF) is suitable for the examination of mixing processes in turbulent flows. Fluorescein absorbs light of a certain wavelength and emits light of a different usually higher wavelength. It can be visualized by a laser beam, which is widened to a light-sheet by a cylindrical lens. Primarily LIF provides 2D information from single illuminated lightsheets. Three-dimensional information can be obtained by scanning of an observation volume, where the illuminated lightsheet is moved stepwise in depth direction (Dahm/Dimotakis, 1990), (Dahm/Southerland, 1990), (Dahm et al., 1991) and (Merkel et al., 1993). Synchronized with the scanning, images are recorded layer by layer by a high-speed solid state camera, generating volume image datasets.

From these data, velocity fields can be determined by different techniques, e.g. three-dimensional least squares matching. If the relation between the grey values in the digital images and the concentration of fluorescein in the flow is known from a radiometric calibration of the system, these datasets represent tomography sequences of the mixing process of the flows.

Research activities in this field were performed by the Institute of Geodesy and Photogrammetry at ETH, a description of the method is given in (Maas, 1993), detailed information about the used template matching can be found in (Grün, 1985) and (Grün/Baltsavias, 1988).

2.2.2.4. Particle Image Velocimetry (PIV)

Particle Image Velocimetry (PIV) is a method providing practical quantitative whole-field turbulence information (Adrian, 1986). The technique is based on the processing of doublepulsed particle images captured by a camera observing a flow field. The PIV measurement process involves:

- The flow is visualized with seed particles, which are suspended to trace the motion and to provide a signal. In airflows the seeding particles are typically oil drops in the range of 1 to 5

μm . For water applications polystyrene, polyamide or hollow glass spheres in the range of 5 to 100 μm are used as flow markers.

- A thin slice of the flow field is illuminated by a light-sheet, the illuminated seeding scatters the light. A camera placed at right angles to the light-sheet detects this. The light-sheet is pulsed (switched on and off very quickly) twice at a known interval.
- The first pulse of the laser freezes images of the initial positions of seeding particles onto the first frame of the camera. The camera frame is advanced and the second frame of the camera is exposed to the light scattered by the particles from the second pulse of laser light. There are thus two camera images, the first showing the initial positions of the seeding particles and the second their final positions due to the movement of the flow field. Alternative approaches apply single-frame recording with double- or multi-pulses.
- The two camera frames are then processed to find the velocity vector map of the flow field. The PIV techniques do not evaluate the motion of individual particles, but correlates small regions between the two images taken shortly in sequence. This involves dividing the camera frames into small areas called interrogation regions. In each interrogation region, the displacement of groups of particles between the two frames is measured using correlation techniques. The velocity vector of this area in the flow field can be calculated when the distance between the camera's CCD chip and the measurement area is known.
- This is repeated for each interrogation region to build up the complete 2D velocity vector map.

An experiment arrangement for PIV is shown in Fig. 4. Most of the PIV studies are confined to two-dimensional flow fields, however the need for three-dimensional measurements has been emerging for many applications. In conventional PIV systems, the third velocity component is not determinable due to the geometry of the imaging. A PIV system can be extended to measure all three velocity components. Generally the additional hardware required for the extension is a second camera. The concept is to use the two cameras forming a stereoscopic configuration to resolve the out-of-plane motion. For the concepts to extend the PIV method to three-dimensional measurements see (Lai, 1996) and (Hinsch/Hinrichs, 1996).

Dantec Dynamics introduced a further development of the PIV technology. To get information throughout a complete object volume a new system solution (*FlowMap Volume Mapping PIV*) was designed (Dantec, 2003). A proposed hardware configuration consists of two cameras and a light sheet illumination facility mounted on a traverse. The system delivers multiple 3D stereoscopic PIV mappings in cross-sections of a flow within short time intervals, while the integrated software (*FlowManager*) controls all PIV system elements and the traverse mechanism. In an example the total execution time for recording six cross sections, each including 2300 vectors, is specified with less than 10 minutes. The total volume mapped had the dimensions of 60 x 160 x 250 mm³.

An alternative approach is realized with holographic PIV systems, which allow true three-dimensional measurements for a volumetric domain. Compared to stereoscopic PIV the complexity of the method is increased substantially (Lai, 1996). The approach is based on a holographic recording of a particle field with a certain depth range. The flow field of the tracer particles can be reconstructed by the so-called off-axis holography (Hinsch/Hinrichs, 1996). More details about the holographic PIV method and its application for flow studies are given in (Rood, 1993).

The PIV techniques yield dense vector maps with velocities in the range from zero to supersonic. The spatial resolution per single light sheet is high, but as only a thin slice of the object volume is observed per instant the temporal resolution of PIV is low. Results of PIV measure-

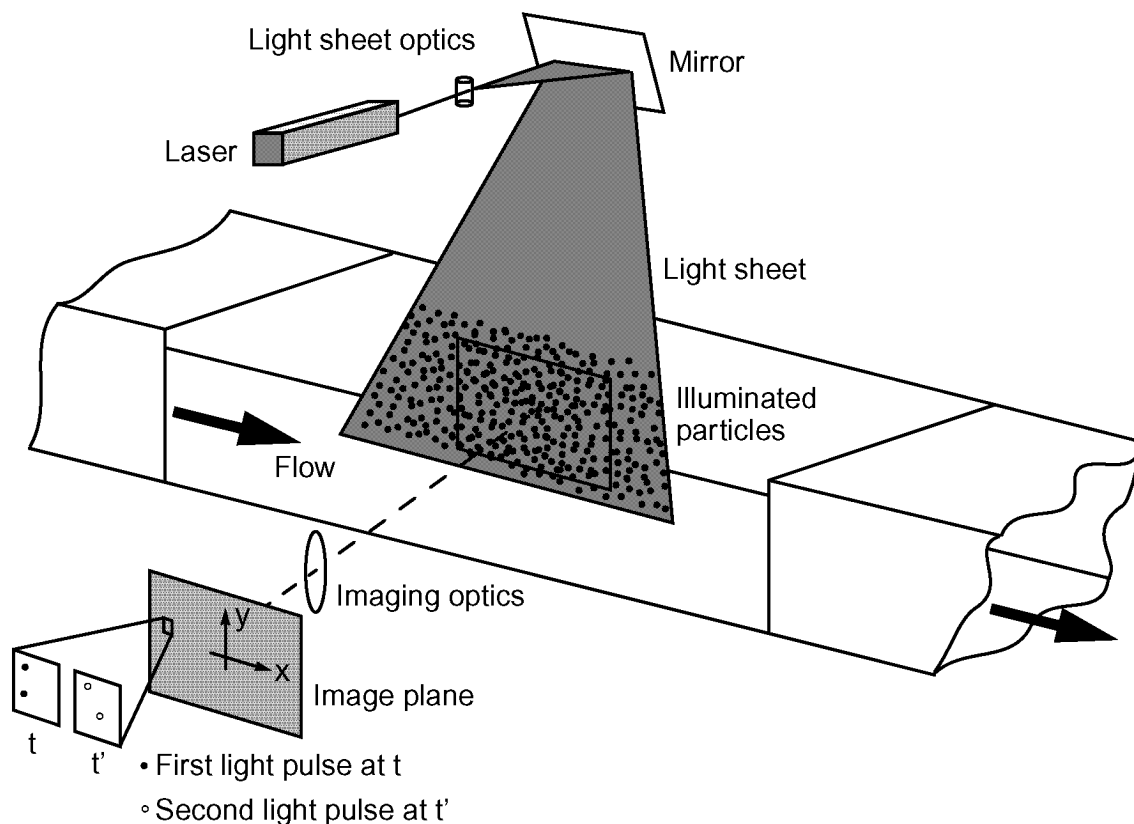


Fig. 4: Experimental arrangement for particle image velocimetry in a wind tunnel, taken from (Raffel et al., 1998)

ments are Eulerian flow fields, which represent the flow as a function of space and time. Only velocity vectors are measured by PIV, therefore it is not possible to obtain the Lagrangian representation of the flow field with this extensively used method.

2.2.2.5. Particle Tracking Velocimetry (PTV)

Optical 3D measurement techniques are used in an increasing number of applications. Also for flow measurement tasks they can offer a suitable solution. In 1988 Adamczyk and Rimai presented a 2-dimensional PTV method, which was used for the determination of a fluid velocity field in a test section (Adamczyk/Rimai, 1988a). In a further development they extended their system enabling the reconstruction of 3-dimensional flow field from orthogonal views (Adamczyk/Rimai, 1988b). The first application of a 3D PTV system at ETH is described in (Papantoniou/Dracos, 1989) and (Papantoniou/Maas, 1990). Other systems were developed at the University of Tokyo (Nishino/Kasagi, 1989) and at the University of Heidelberg (Netzsich/Jähne, 1993).

The measurement principle is based on the acquisition of image sequences from different views recording the motion of particles. In contrast to PIV, in which the mean displacement of a small group of particles is sought for, PTV tries to reconstruct the trajectories of individual particles in three-dimensional object space. To visualize the flow the observation volume is seeded with particles and illuminated by a suitable light source. One major advantage of optical approaches is the non-intrusive acquisition of three-dimensional information about objects or dynamic processes. In the case of PTV this offers the possibility to measure velocity

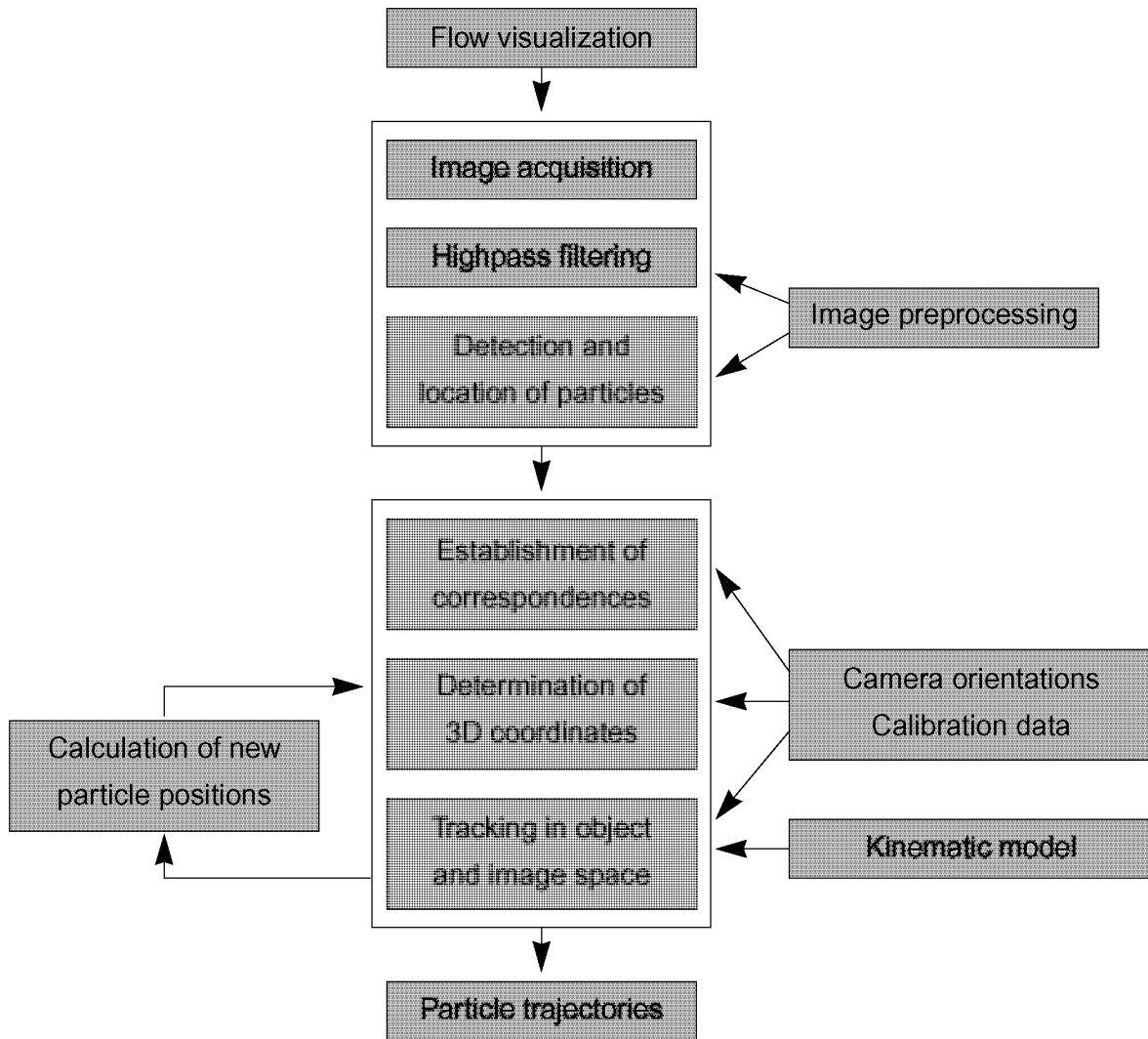


Fig. 5: PTV processing scheme

fields without disturbing the flow. Except the tracers, which are used to visualize the flow can be considered as an intrusive component of the method, but with the right choice of particles leads to minimal and negligible disturbances (see in 4.1.). The particle motion is recorded by at least two synchronized cameras. In most PTV applications the cameras observe the flow from outside the object volume thus being located in a different optical medium than the particles. If the motion in a fluid is observed through a glass plate the optical ray passes through air, glass and fluid and is broken twice according to the refractive indices. If different media are involved in the optical setup then the optical geometry has to be modelled (see 3.3.).

After an on- or offline digitization the image sequence data is processed to segment the particle images and to extract their image coordinates. After the assignment of corresponding particle images from different views it is possible to determine the 3D particle position in object space by forward intersection. A tracking procedure reconstructs the particle trajectories. The existing PTV solutions either work with an image or object space based tracking algorithm. The new spatio-temporal matching algorithm, which was developed during the presented research work, uses the information of image and object space for the tracking procedure simultaneously. The different PTV solutions are described in detail in chapter 5.

The implementation at ETH uses a fully automated image processing procedure to extract the particle positions in image space (Maas, 1992b). As a first step a highpass filtering of the images to remove non-uniformities of the background intensity level is performed. After that, the particles are segmented by a thresholding algorithm. The image coordinates of the particles are determined by a greyvalue-weighted centre of gravity. With the knowledge of camera orientation data determined in a system calibration it is possible to establish correspondences between the particle images. With at least two particle positions in image space the 3D position in object space is defined and can be calculated with a photogrammetric algorithm. To get the 3D particle trajectories in object space a tracking procedure based on image and object space based information is applied. The results of PTV processing are three-dimensional velocity fields, which can be used for hydrodynamic analysis. A processing scheme of PTV is shown in Fig. 5.

2.2.3. Comparison of flow measurement techniques

Table 2 summarizes some characteristics of the presented flow measurement techniques. Other overviews on the different methods are given in (Maas, 1992b) and (Virant, 1996). Compared to the measurement techniques obtaining pointwise information from one or a few probe locations, the temporal resolution of PTV can be considered as low. The major advantage of PTV is the simultaneous observation of a three-dimensional object volume, measuring not only all three components of the velocity vector but also providing trajectory information. Due to this fact PTV is the only technique, which offers the possibility to perform Lagrangian measurements.

Concerning the accuracy information shown in Table 2 the comparison of the potential of the different methods is hardly possible as the authors are using different measures to specify the quality of the results. For details about the potential of the different methods see (Jørgensen, 2002), (Heist/Castro, 1996), (Lai/He, 1989), (AIAA, 2003), (Bolinder, 1999), (Kompenhans et al., 1996) and (Maas et al., 1993).

Commercial systems for CTA, PWA, LDA, L2F and PIV are available on the market. The PTV method proposed in this thesis is successfully used for flow research at the Institute of Hydro-mechanics and Water Resources Management at ETH Zurich.

Table 2: Performance characteristics of the different flow measurement techniques

Method	Spatial resolution	Temporal resolution	Dimension of measurement	Accuracy potential	Results
CTA	low	very high	1-3	1-3% of the velocity scale	Vectors
PWA	low	high	1-3	~ 1% of the velocity scale, 5% for high turbulence	Vectors
LDA	low	very high	1-3		Vectors
L2F	low	high	1-3	signal to noise ratio ~ 0.3	Vectors
LIF	very high	very low	3	systematic errors ~1-2%, random errors of >5-10%	Vectors
PIV	very high	very low	2 (3)	< 1% of mean flow velocity	Vectors
PTV	high	low	3	lateral 1:4000, depth 1:2000 of the velocity vector	Trajectories

3. Photogrammetric aspects for 3D PTV

In this section the photogrammetric principles used by 3D Particle Tracking Velocimetry are described. First the fundamental mathematical model of the collinearity condition and its extensions are explained. A further section deals with the epipolar line intersection method to build up multi-camera correspondences in the case of a multi-media geometry.

3.1. Mathematical model

The fundamental mathematical model of photogrammetric 3D particle coordinate determination is the collinearity condition, which states that object point, camera projective centre and image point lie on a straight line (Fig. 6). This mathematical formulation, which contains three coordinates X_O, Y_O, Z_O of the projective centre and three angles ω, ϕ, κ describing the direction of the optical axis, applies to a pinhole camera model not regarding the influence of

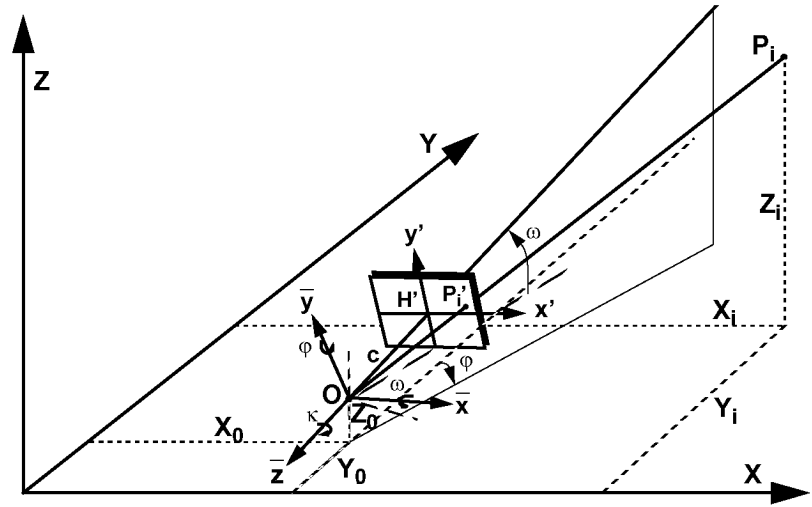


Fig. 6: Collinearity condition (camera model inverted for drawing purposes)

any distortions mainly introduced by the use of lenses. Considering the camera constant c and the principle point with its coordinates x_h, y_h leads to the following equations:

$$\begin{aligned} x'_i &= x_h - c \cdot \frac{a_{11} \cdot (X_i - X_0) + a_{21} \cdot (Y_i - Y_0) + a_{31} \cdot (Z_i - Z_0)}{a_{13} \cdot (X_i - X_0) + a_{23} \cdot (Y_i - Y_0) + a_{33} \cdot (Z_i - Z_0)} \\ y'_i &= y_h - c \cdot \frac{a_{12} \cdot (X_i - X_0) + a_{22} \cdot (Y_i - Y_0) + a_{32} \cdot (Z_i - Z_0)}{a_{13} \cdot (X_i - X_0) + a_{23} \cdot (Y_i - Y_0) + a_{33} \cdot (Z_i - Z_0)} \end{aligned} \quad (4)$$

where x'_i, y'_i are the image coordinates of the object point at the position X_i, Y_i, Z_i , the a_{ij} are the elements of the 3×3 rotation matrix derived from the three angles ω, ϕ, κ . To meet the physical realities the model has to be extended by introducing the following parameters to compensate the distortion of the lens and electronic effects. These parameters are determined within a calibration procedure. For digital close range applications a very common approach to

3.2. Handling of the mathematical model

model the lens distortion is given in (Brown, 1971). The radial symmetric lens distortion (k_1, k_2, k_3) and decentering distortion (p_1, p_2) is modelled in polynomial approach given by the following equations:

$$\bar{x}_i' = x_i' + dx_i \quad \bar{y}_i' = y_i' + dy_i$$

with:

$$dx_i = x_i' \cdot (k_1 r_i'^2 + k_2 r_i'^4 + k_3 r_i'^6) + p_1 \cdot (r_i'^2 + 2x_i'^2) + 2p_2 x_i' y_i' \quad (5)$$

$$dy_i = y_i' \cdot (k_1 r_i'^2 + k_2 r_i'^4 + k_3 r_i'^6) + p_2 \cdot (r_i'^2 + 2y_i'^2) + 2p_1 x_i' y_i'$$

$$\text{and:} \quad r_i'^2 = x_i'^2 + y_i'^2$$

In addition the influence of electronic effects from the digitalization and storage, mainly the unknown difference of the clock rates of camera and framegrabber may have to be compensated. These effects can be modeled by applying an affin transformation (El-Hakim, 1986):

$$\begin{aligned} \tilde{x}_i &= a_0 + a_1 \bar{x}_i' + a_2 \bar{y}_i' \\ \tilde{y}_i &= b_0 + b_1 \bar{x}_i' + b_2 \bar{y}_i' \end{aligned} \quad (6)$$

Due to linear dependencies of the six parameters ($a_0, b_0, a_1, b_1, a_2, b_2$) of the affin transformation with the parameters of the collinearity equation only two of these parameters are introduced as unknowns. The two remaining parameters are the scale factor a_1 in horizontal image coordinate direction and the shearing angle a_2 .

The collinearity condition (4) in combination of the additional parameters (5), (6) leads to the following functional model, which is suited to be linearized as observation equations in a least squares adjustment:

$$(x', y') = f(X_0, Y_0, Z_0, \omega, \phi, \kappa, c, x_h, y_h, k_1, k_2, k_3, p_1, p_2, a_1, a_2, X_i, Y_i, Z_i) \quad (7)$$

The 16 parameters describing the exterior and interior orientation, the lens distortion and affine transformation are introduced as unknowns in a calibration procedure. After their determination it is possible to apply the epipolar line intersection method to establish correspondences of the particle images from the different cameras.

3.2. Handling of the mathematical model

The mathematical model can be used in three different modes:

- Spatial resection: The parameters of the exterior orientation $X_0, Y_0, Z_0, \omega, \phi, \kappa$ and the camera model c, x_h, y_h including the additional parameters are determined in the calibration procedure. In 7.4.2. the calibration of an image acquisition system used for 3D PTV is described.
- Spatial intersection: After the calibration of the system and the establishment of multi-view correspondences 3D particle coordinates can be determined based on the orientation and camera model parameters.
- Bundle adjustment: Using multiple images of a scene, taken under different orientations, object point coordinates, camera orientation parameters and camera model parameters can

be determined simultaneously, based only on image space information and a minimum of one scale information in object space. This procedure has been used for the provision of reference values for the targets on the calibration bodies.

All three different modes are used when evaluating image sequences with 3D PTV.

3.3. Multimedia geometry

The motion of the particles is observed with cameras outside the flow through a glass plate. Therefore the rays have to pass through three different media, fluid, glass and air. Due to Snell's law the optical path is broken when refractive indices changes. Assuming homogeneity and isotropy of the different optical media and considering a plane parallel glass plate this effect can be modelled strictly (Fig. 7).

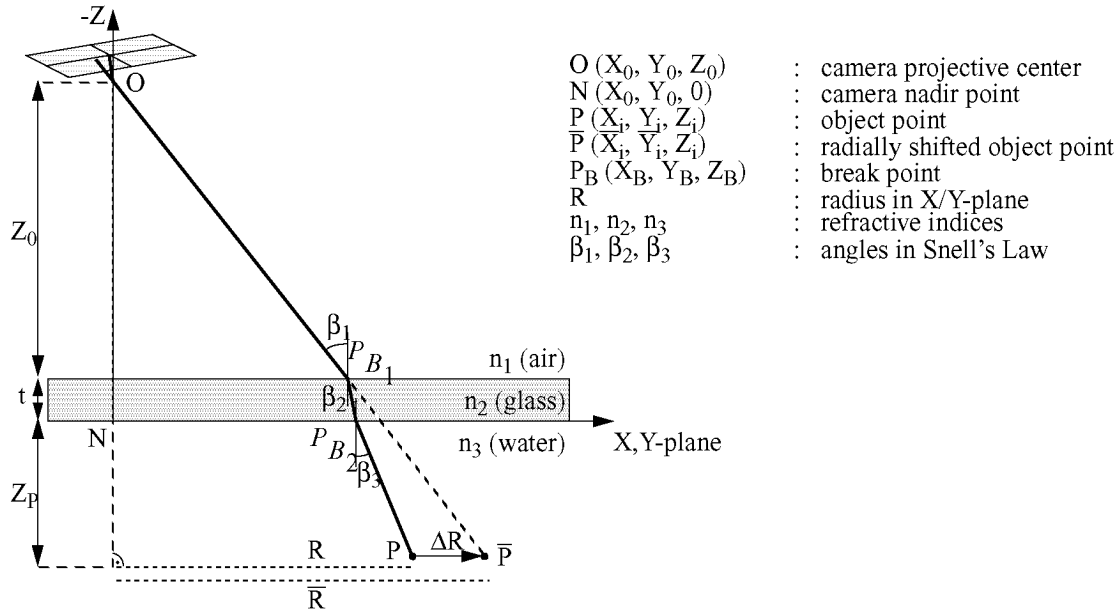


Fig. 7: Radial shift for compensation of multimedia geometry, taken from (Maas, 1996)

If the X-Y plane of the coordinate system is chosen parallel with the plane interface glass/water (or air/glass), some simplification are possible and only the radial shift ΔR has to be calculated to be able to use the collinearity condition equation (see in (Maas, 1996), p. 194). The radial shift is a function of the radial distance R of the object point P from the nadir point N of the camera, the thickness of the glass plate t , the depth Z_P in the fluid and the refractive indices n_i of the traversed media. Maas developed and implemented this approach for the PTV system at ETH (Maas, 1992b). In the PTV implementation for each camera discrete lookup tables with the radial shifts over the observed object volume are calculated and used to compensate the influence of the multimedia geometry.

Further details about the multimedia geometry (also beside these exactly modeled effects) and aspects regarding the implementation in the PTV software are described in (Maas, 1992b).

3.4. Epipolar line intersection technique

An important approach used for the PTV method is the establishment of multi-image correspondences by constraints in the epipolar geometry developed by Maas. The epipolar geometry is used to establish the correspondences automatically. The powerful technique is successfully used for PTV (Maas, 1990), (Maas, 1991a) and (Maas, 1992b) as well as for other applications

as surface reconstruction (Maas, 1991b) and deformation measurement (Dold/Maas, 1994). This method requires the knowledge of the interior and relative orientation as well as the additional parameters of the according images. Fig. 8 shows the epipolar geometry in a two camera arrangement. Using the coplanarity condition of the oriented image planes

$$\overrightarrow{O_1 O_2} \cdot (\overrightarrow{O_1 P'} \times \overrightarrow{O_2 P''}) = 0 \quad (8)$$

the epipolar line in image space can be determined. Proceeding from an image point of the first image the corresponding search area can be reduced to the epipolar line in the second image. In the strict mathematical formulation this line is straight, in the more general case with non-negligible lens distortion or multimedia geometry the epipolar line will be a slightly bent line, which can be approximated by a polygon (Maas, 1991a).

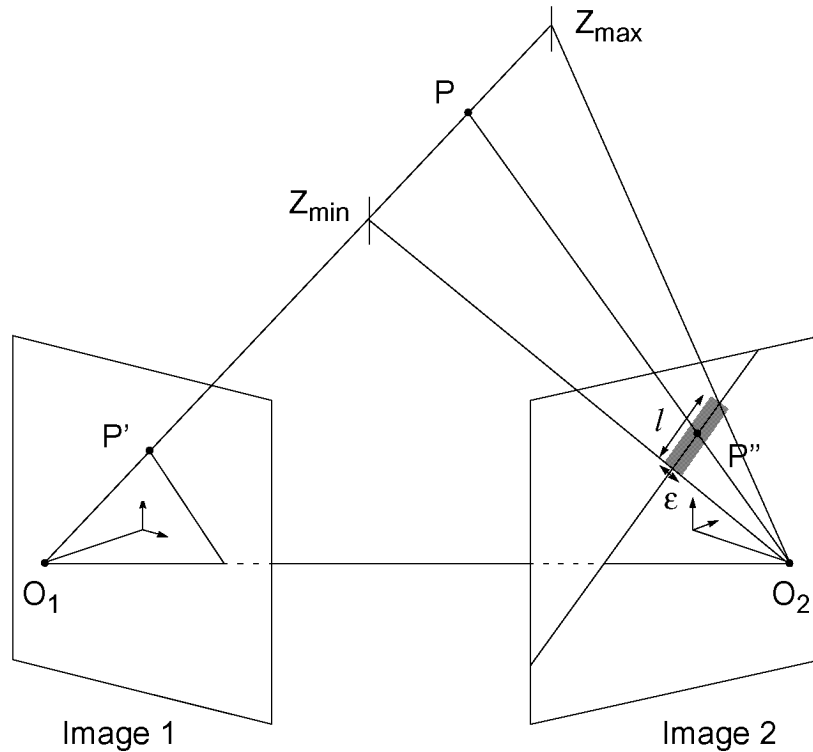


Fig. 8: Epipolar geometry in a two camera arrangement (left), example of intersecting epipolar line segments in a four camera arrangement (right)

In the case of real experiment data the search area has to be extended by a certain tolerance ϵ to the epipolar line, which becomes to a narrow bandshaped window in image space. The length l of the search area along the epipolar line can be restricted by the range of depth (Z_{min} , Z_{max}) in object space. The tolerance ϵ to the epipolar line is strongly influenced by the quality of the calibration results. Due to the large number of particles ambiguities occur as often two or more particles will be found in the epipolar search area. The use of a third or a fourth camera allows the calculation of intersections of the epipolar line segments in image space, which reduces the search area to the intersection points with a certain tolerance.

An example of an epipolar line intersection in a four camera arrangement is shown in Fig. 9. Starting from the first view, the possible candidates for the marked point (58) are searched along the epipolar line $l_{1,2}$ in the second image. For the candidates found in the second view

the epipolar lines $l_{2,3}$ are calculated and intersect with the epipolar line $l_{1,3}$, which reduces the search area of possible candidates to the intersection point with a certain tolerance. Remaining ambiguities may be solved by analysing the fourth view. The epipolar line intersection is implemented with a combinatorics algorithm to establish unambiguous quadruplets, triplets and pairs of corresponding particle images (Maas, 1992b).

Although the method can be extended to any arbitrary number of cameras, the use of more than four camera is usually neither necessary nor practical.

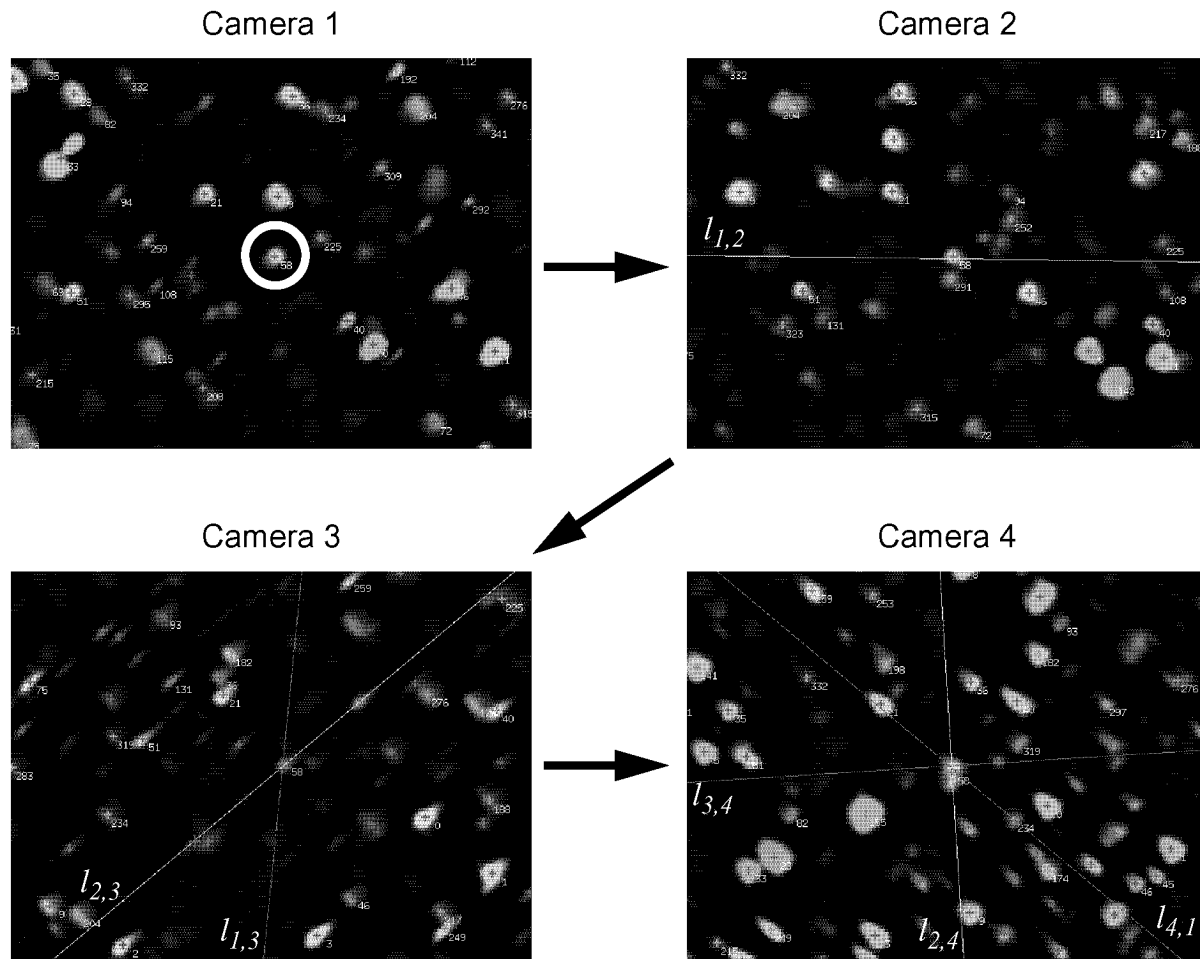


Fig. 9: Principle of the epipolar line intersection in a four camera arrangement

4. Hardware components of a 3D PTV system

In this section the technical aspects for a hardware setup and the potential of the method are discussed. The technique is based on the recording of synchronous image sequences of a flow visualized with small, neutrally buoyant particles. The hardware setup of a 3D PTV system consists of an image acquisition system with up to four cameras including a data storage device, an illumination facility and tracer particles to seed and visualize the flow. Whether high-grade components or off-the-shelf products come into operation is depending on the experiment requirements as well as on the available budget. The data acquisition system defines the achievable spatial and temporal resolution.

Because of the fast developments of the different hardware components the following sections can only give an incomplete snapshot of the available products on the market.

4.1. Visualization of the flow

To enable measurements in a transparent medium such in liquids or gas requires a visualization of the flow. In the case of PTV applications the flow to be investigated is seeded with discrete tracer particles, which should follow the motion of the fluid without disturbing it. A further important property is the visibility of the tracer particles.

The flow-following properties are mainly influenced by the size and the density of the particles. The difference between the density of the fluid and the particles should be kept small to avoid vertical drift velocity. In the case of flows in fluids this can be achieved quite easily, but it is hardly possible for flows in gases. In general slip and delay can be reduced by the use of smaller particles, which again decreases the visibility.

Regarding the automated image coordinate measurement by using a grey value-weighted centre of gravity the particles have to cover at least 2×2 pixel in image space to be located with subpixel accuracy. But again the tracer particles must not appear too large in image space. If a high spatial resolution is requested the problem of overlapping particles has to be considered. The number of overlapping particles grows linearly with the particle image size and approximately with the square of the number of particles per image. The size of the particles used in PTV applications is in the order of a few up to some hundred μm depending on the experiment.

In some cases hydrogen/oxygen bubbles are used as tracers to visualize the flow, which can be produced by an aeration unit or electrolysis (e.g. in (Schimpf et al., 2002), where the investigation of bubble columns is described). An experiment with two different kinds of particles is described in chapter 7.4. A selection of possible particles can be found in (Maas, 1992b), details about the light scattering properties are given in (Engelmann, 2000).

4.2. Illumination

A decisive component of a PTV setup with a strong influence on the image quality is the illumination facility. Different light sources can be employed for a suitable illumination:

- Argon ionic lasers
- Diode lasers
- Halogen lamps
- Halogen short arc lamps
- Light diodes

The illumination facility should provide a high and homogenous light intensity overall the whole observation volume. The wavelength of the emitted light has to be appropriate to the spectral sensitivity of the sensors used for the image sequence acquisition.

Laser light sources provide monochromatic light with a high intensity, but are difficult or even dangerous to deal with. Lasers are expensive in comparison to the other mentioned light sources.

Halogen lamps are easy to handle (e.g. very flexible in combination with fibre optics) and deliver homogenous illumination at very low costs. A disadvantage is the rather low light intensity with a strong blue component, which run contrary to the high spectral intensity of CCD sensors in the red wave band. Halogen short arc lamps show more or less the same properties as halogen lamps but provide higher light intensity and their handling is more difficult.

Diodes are easy to deal with and deliver homogeneous light at very low costs. A disadvantage is the poor light intensity.

For the recent PTV experiments performed at ETH a continuous 20-Watt Argon Ion Laser was used as illumination facility.

4.3. Sensors

There is a great variety of image sensors on the market, which could be successfully applied for the image sequence acquisition for PTV purposes. Decisive properties are the geometrical and temporal resolution. Further aspects are data storage as well as the costs.

In the following some of these properties of imaging devices are described and discussed regarding their applicability for PTV.

4.3.1. Video norm

Reading out from a standard video CCD (Charged Coupled Device) sensor is regulated by a video norm that defines the timing and the level of the transmission. There are two different norms (both strongly related to an interlacing technique):

- CCIR (Comité Consultatif International des Radio Communications) European norm with 625 lines per frame. The vertical reading (field) frequency is 50 Hz.
- RS170, a standard, which was defined by the EIA (Electronics Industries Association) and is used in USA. One image frame consists of 525 lines, vertical reading frequency is 59.9 Hz.

The analogue signal delivered by the video cameras can be recorded on analogue videotapes by a video recorder and digitized off-line afterwards. The loss of quality caused by the intermediate storage of the image data on video tape can be avoided by on-line digitization with the use of framegrabbers. The resolution of the currently used data acquisition system for PTV is in the order of 640 x 480 and 768 x 576 pixels.

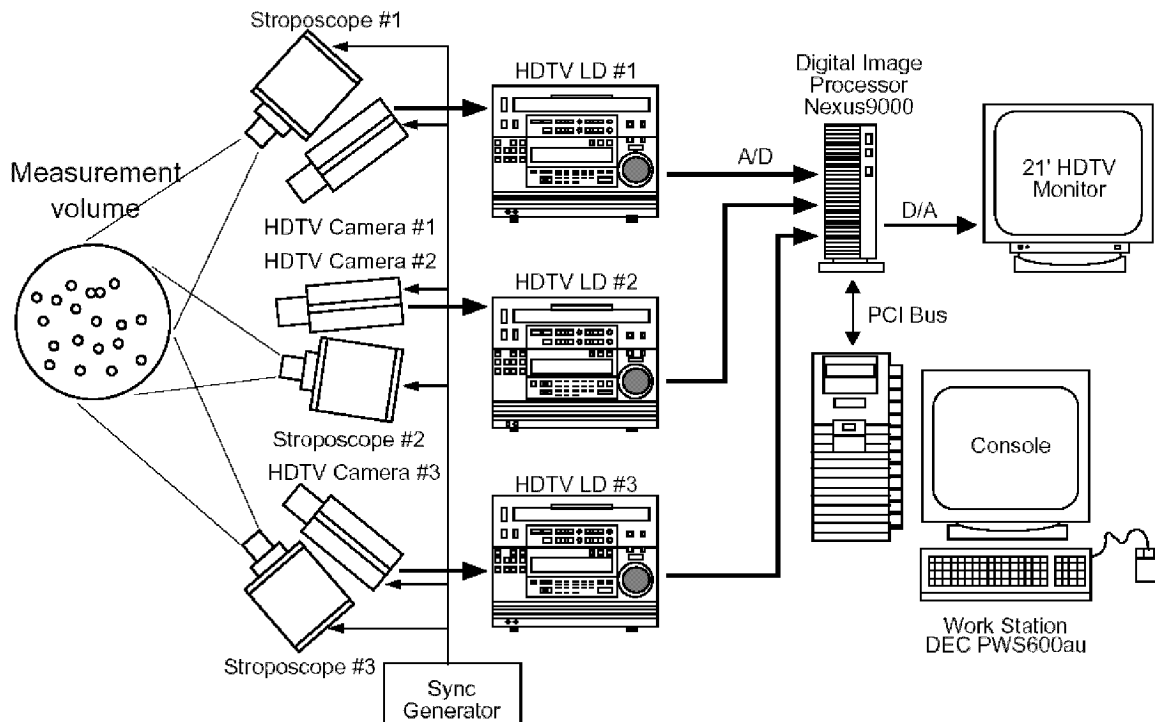


Fig. 10: HDPTV system with three High Definition TV cameras, laser disk recorders, digital image processor, taken from (Suzuki et al., 2000)

4.3.2. Image acquisition with High Definition TV cameras

A possibility to increase the system's image resolution is achieved by the use of high definition TV cameras. A 3D PTV using High-definition CCD-cameras was built up at the University of Tokyo at the Department of Mechanical Engineering. As mentioned above, standard video cameras deliver images with 0.5 megapixels and less. High-definition CCD-cameras provide images around 2 megapixels. An existing system originally developed by Nishino et al. (Nishino et al., 1989) and later improved by Sata and Kasagi (Sata/Kasagi, 1992) consists of three Sony XCH-1125 TV cameras and three laser disk recorders (Sony HDL-5800). Their present image system provides image sequences with a resolution of 1920 x 1024 pixels (the system is described in (Suzuki et al., 1999)).

The 3D HDPTV system with its hardware components is shown in Fig. 10. Stroboscopes synchronized with the TV signal are employed for illumination. Images captured by each camera are recorded onto the laser disk recorder at 30 frames/s. The recorded images are then A/D converted and transferred to a workstation. The higher resolution is thought to lead to a higher number of particle trajectories to be trackable in a velocity field. Compared to standard CCD cameras the costs for the high-definition system can be considered as rather high. According to Suzuki the costs for the system, which was built up in the year 1996, amount to 1 million US \$. Some further remarks about this system, the data processing and its performance can be found in section 5.4.

4.3.3. IEEE-1394 technology (Firewire)

The high performance serial bus IEEE-1394, also called Firewire, offers a possible way for on-line image sequence storage. The output of the camera is directly delivered in different image formats (greyscale, coloured, uncompressed and compressed). Due to the direct output no framegrabbers are needed. Normal VGA resolution (640 x 480 pixels) at a frame rate of 30 Hz can be captured in progressive scan mode. XGA (1024 x 768 pixels) and SXGA (1280 x 960 pixels) resolution is also available at smaller frame rates, which will increase soon considering the fast developments in imaging technology. Synchronization is possible by an external trigger. The given maximum bandwidth of is the limiting factor when temporal and geometrical resolution is concerned. IEEE-1394 sensors were not used for PTV at ETH yet.

4.3.4. Integration modes

The conventional CCD sensors are designed for use in the interlacing scanning systems of video and TV. For these systems two alternative integration modes are used:

- field integration mode uses the double integration of two adjacent lines, giving low vertical resolution but high dynamic resolution.
- frame integration mode uses the integration of each odd line after integrating each even line, giving high vertical resolution but low dynamic resolution.

Due to the time delay between the acquisition of odd and even fields the image contents appears blurred if fast moving object are recorded. The best way to get rid of such interlacing effects is to use progressive scan cameras. Quite simply, progressive scan means that the picture information is accumulated simultaneously and the charges from all the pixels are transferred to one or two horizontal registers. The result is a non-interlace image with full vertical and horizontal resolution captured in a single rapid shutter event.

Today's progressive scan cameras are available at reasonable costs and should be applied for PTV image acquisition to provide good image quality at full frame resolution. Especially in the case of recording small moving objects the progressive scan readout can be regarded as the most suitable choice. Nevertheless a considerable problem has been identified by the image sequence acquisition with the progressive scan cameras JAI CV-M10 used in the experiments described in 7.3.3. At a recording rate of 60 Hz the signal from camera to frame grabber is transmitted through two different cables. As a negative effects this results in different signal magnitudes for even and odd lines. As no further experience with other types of progressive scan cameras were made, it is not possible to identify the mentioned effect as a general problem of the sensors of this architecture.

4.3.5. Fill factor and light sensitivity

The fill factor of a sensor is the fraction of the sensor area occupied by the photodetector and ranges in general form 20 % to 90 %. Because the sensitive area of a CCD sensor is only a fraction of its total area, on-chip lenses can be used to concentrate the light of the optical image into the sensor area of the pixel and thus increase sensitivity.

For example CCD chips from SONY use such microscopic lenses to redirect light from the inactive areas back to the active pixels. The Sony Hyper HAD® sensor structure has an on chip lens (OCL) located over each pixel. The Exwave HAD takes the Hyper HAD sensor technology a step further (AudioVideoSupply, 2003). The OCL of the Exwave HAD CCD is a nearly gap-less structure, eliminating the ineffective areas between the microlenses. This enables the whole accumulated layer to receive the maximum amount of light.

4.3.6. Cameras with CMOS technology

An alternative type of sensors besides CCD cameras is offered by the CMOS technology (Complementary Metal Oxide Semiconductor). In the recent years remarkable progress was made in the development of this sensor technique. Some of the advantages of CMOS sensors over the common CCD sensors are blooming resistance, tuneable response, region of interest (ROI) selective readout flexibility as well as low noise and low power consumption for high pixel rates.

Available cameras (Silicon Imaging's MegaCamera) on the market provide full frame resolution of 2048 x 1536 pixels at 30 Hz frame rate. Another camera, the Phantom v5.0 offers a maximum recording speed of 1000 pictures per second using the sensor's full 1024 x 1024 pixel array. Frame rates are continuously variable from 30 to 1000 pictures per second. An integral image memory is capable to record 4096 images in full format (for example 40 seconds at 100 Hz). Higher frame rates at reduced image sizes may also be selected using the Phantom camera control software.

The architecture of the sensors is flexible and allows an arbitrary arrangement of the pixels on the chip, which could also increase the geometrical resolution (e.g. which staggered pixel positions).

CMOS cameras allow the execution of processing functions within the camera, such that the amount of data to be transferred to the system's memory or disk can be drastically reduced. Relevant operations like filtering, blob detection, centroid computations etc. could thus be performed on-board, leaving only pixel coordinates of the blob centers to be transferred.

This may be useful for PTV applications as with the realtime-detection of the particle image coordinates the storage of the image sequences could be avoided. However today's CMOS cameras are not yet capable to detect and extract the image coordinates of 1000 or more particles at reasonable frame rates. Therefore and due to the significantly higher costs compared to CCD cameras no CMOS sensors were used for PTV applications at ETH yet. In consideration of the technical developments in the future CMOS sensors might be a valuable alternative to the currently used CCD cameras.

4.3.7. Synchronization

To be able to determine the 3D position of a moving particle it has to be imaged by at least two cameras at the same time. Therefore the image acquisition has to be synchronized. The synchronization of a multi-camera setup can be realized in different ways.

A quite simple method to get synchronized image sequences acquired by three monochrome cameras operating in combination with a single RGB-framegrabber. Each camera can be treated as one of the three colour channels. One camera is defined as master and the two others as slaves. The image data of all three cameras is then stored in one image sequence of RGB images, which can be divided in monochrome images afterwards.

In the case of an intermediate storage of synchronized image sequences on analogue video-tapes a time code added to the images enables to read corresponding images.

The synchronization of four progressive scan cameras with two framegrabbers is described in (Stürer et al., 1999b) and (Stürer et al., 2000). In this setup the cameras are also synchronized by a master-and-slave mode to relieve the framegrabbers (Matrox genesis) from timing tasks, which were critical at high frame rates. One problem is to start the two framegrabbers simultaneously. For this purpose, the two framegrabbers run in a trigger mode and need a TTL pulse that indicates when to grab the next image of the cameras. To provide a constant TTL pulse, a

synchronization unit was built that was connected to the v-sync of the cameras giving a TTL pulse at the chosen frame rate of the cameras. The operator can start TTL pulse and with it the two frame grabbers simultaneously begin to grab. The image data is stored in real time on hard disc via two RAID controllers (RAID stands for Redundant Array of Inexpensive or sometimes "Independent" Disks). This procedure has the advantage that a degradation of the images is avoided and it facilitates a long measurement time. The system was tested for a measuring time of 2 minutes, but even longer measurement times should be possible.

Only when the motion of the particles is slow compared to the frame rate of the imaging devices it might be sufficient if the images of the different cameras are acquired by a multiplexed system. This was the case in the micro-gravity experiment described in chapter 7.4.

4.4. System calibration

An essential requirement for a successful application of the PTV method is the knowledge of the exterior orientation parameters as well as the interior orientation parameters, lens distortion and effects of the A/D conversion. The mentioned parameters and the handling of the mathematical model is described in section 3. The actual calibration uses a reference body with known control points, which is placed into the object volume and is imaged once by all cameras of the system. With the known 3D coordinates of the control points on the reference body and the measured image coordinates the parameters describing each camera can be determined. Depending on the experiment a suitable reference body has to be provided considering among others the accuracy of the reference points, their visibility and coverage over the entire observed object volume. As an example of such a reference body used for PTV see Fig. 52. For the different experiments, which were performed in the recent years several reference bodies of different sizes were produced at ETH. Details about the used reference bodies can be found in (Maas, 1992b), (Becker et al., 1995), (Stüer, 1999) and (Willneff/Maas, 2000).

4.5. Hardware of the 3D PTV system at ETH

The system currently used at the ETH Zurich was upgraded from offline to online image digitization. In the previous system, the image sequences were firstly recorded on analogue videotapes and digitized afterwards, while in the new system two frame grabbers (Matrox Genesis) are used to provide online digitization and storage. The development of the hardware setup can be nicely traced comparing the systems described in (Maas, 1992b), Virant (Virant, 1996), Stüer (Stüer, 1999) and the most recently in (Lüthi, 2002). The length of the recorded digital image sequences is nowadays restricted by the storage device capabilities. The data rate for a 60 Hz full-frame camera with a resolution of 640 x 480 pixels is about 19 MB/sec, and hence in an experiment, which lasts for 1 minute four cameras deliver a total amount of about 4.5 GB image data. Some details about the recently used hardware setup and changes are given in section 7.3.3. A possible hardware design is shown in Fig. 11.

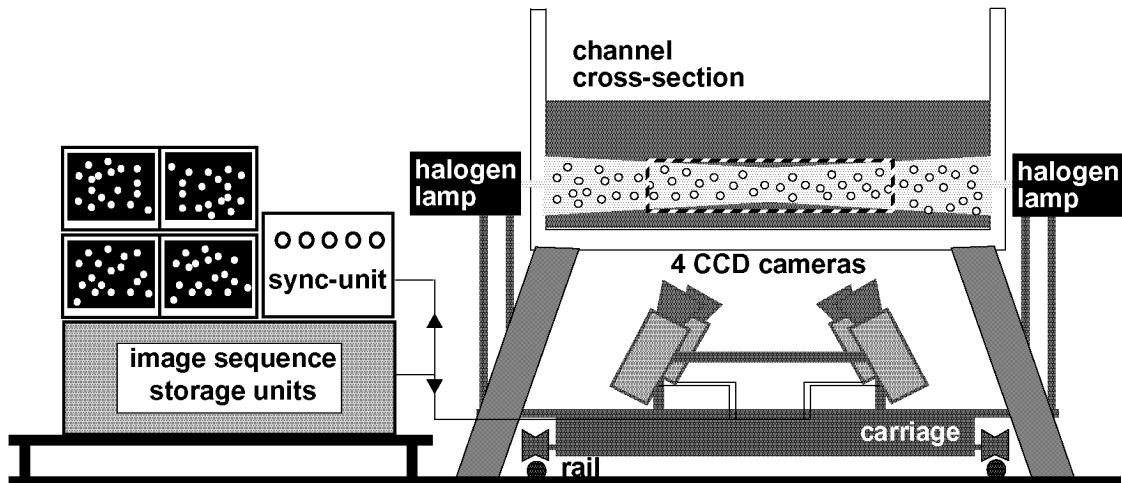


Fig. 11: Hardware setup for channel cross section experiments, adapted from (Maas, 1992b)

4.6. Potential of 3D PTV

With an image format of 768×576 pixels, the method allows for the determination of velocity vectors of more than 1000 particles per time instant using a four camera system. The relative accuracies of the vector components are approximately 1:4000 (standard deviation of X and Y coordinates over field of view); the accuracy of the depth component Z is typically by a factor of two to three worse than the components perpendicular to the main viewing direction. These figures are valid under controlled conditions; suboptimal illumination conditions, complex flows, temperature gradients or image noise may lead to a severe degradation of the potential. The length of the trajectories depends on the seeding density: With a lower number of particles in the observation volume the probability of ‘loosing’ particles due to unsolved ambiguities in the detection, the establishment of correspondences or in the tracking procedure decreases. In practice, particles could be tracked over several hundred frames when the number of particles in the observation volume was kept small (Virant, 1996).

5. Overview on particle tracking methods

A particle moving in 3D object space can be imaged as a 2D path in the image space of an observing camera. If corresponding particle images were found in at least two cameras the 3D particle position can be determined. If in addition the temporal assignment is possible, the trajectory can be reconstructed. Fig. 12 shows the trajectory of a particle in an object volume over four time steps and its according 2D paths in image space recorded with a two camera arrangement. The PTV system used at ETH works with up to four cameras to provide better spatial resolution. The goal of the tracking procedure is to select the correct link for the same particle from one time step to the next.

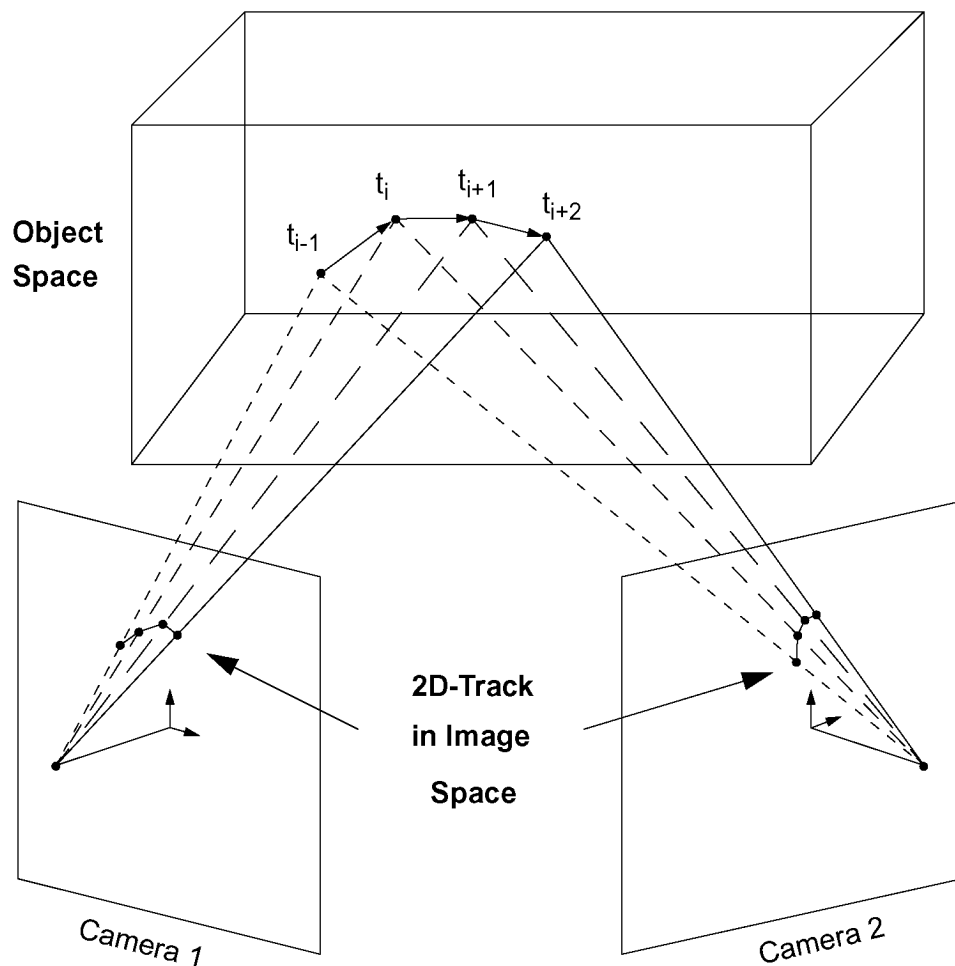


Fig. 12: Particle trajectory in image and object space recorded with a two camera arrangement

5.1. Coordinate based spatio-temporal assignment

The developed image and object space based tracking technique for spatio-temporal matching uses different criteria to find corresponding particle positions in object space as well as in image space. The following criteria can be used for a reliable and effective assignment (Papantoniou/Maas, 1990):

- The velocity of a particle is limited in all three components of the motion vector.
- The Lagrangian acceleration of a particle (the difference of two consecutive velocity vectors of one particle) is limited.
- In cases of ambiguities the assignment with the smallest Lagrangian acceleration is the most probable one.

The first criterion defines a three-dimensional search volume, whose size depends on the minimum and the maximum velocity in all three coordinate directions. The limitation of the Lagrangian acceleration defines a conic search area. These criteria are formulated in object space, but can easily be transferred to image space.

From three consecutive time steps the difference of the magnitude and direction of predicted and found particle position can be calculated. In the case of ambiguities a quality function is used to get the final assignment as proposed in the third criteria. A particle and its possible link candidates in the following two time steps fulfilling the velocity and acceleration criteria are shown in Fig. 13.

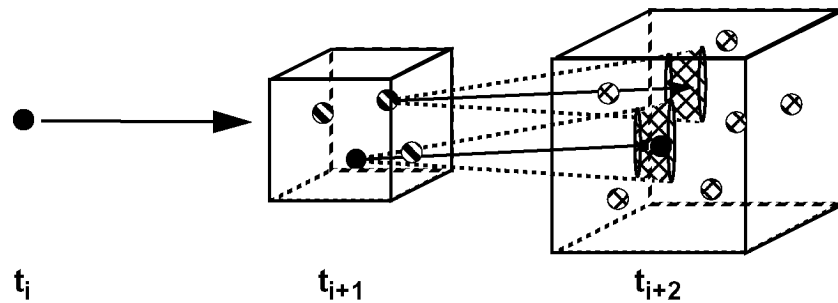


Fig. 13: Particle motion and search volume in object space, taken from (Stüer et al., 1999a)

5.2. Algorithmic aspects for spatio-temporal matching for 3D PTV

The two most important processing steps of 3D PTV - the establishment of spatial and of temporal correspondences between particle images in synchronous image sequences of multiple CCD cameras - which were strictly separated in the existing implementations, have been unified (see in (Willneff/Grün, 2002) and (Willneff, 2002)). In former implementations the trajectories of the particles are reconstructed in two different ways:

- The particle positions are determined for each single time step; tracking is performed afterwards in 3D space. In the previous implementation at ETH Zurich multi-camera correspondences are established by epipolar line intersection techniques in a first step, before the trajectory reconstruction is performed in 3D space (see in (Malik et al., 1993) (Papantoniou/Maas, 1990) and (Papantoniou/Dracos, 1989)). A similar procedure is used by Kasagi and Nishino in the 3D PTV system of the University of Tokyo (see in (Kasagi/Nishino, 1990), (Nishino et al., 1989) and (Nishino/Kasagi, 1989)).

- Other methods first track the particles in image space. Then the spatial correspondences between the 2D trajectories are established (e.g. (Engelmann, 2000), (Ge/Cha, 2000), (Guenzennec et al., 1994) and (Netzsch/Jähne, 1993)).

In the following sections image space based and object space based tracking methods are described and examples of the according approaches are given. Based on the previous system at ETH a new spatio-temporal matching algorithm for 3D PTV was developed, implemented and tested. The principles of the method are described in section 6.

5.3. Image space based tracking techniques

This technique firstly tracks the particles in image space and thus provides the temporal matching leading to 2D tracks in image space of each camera separately. The spatial correspondences between the 2D tracks are established after that in a separate processing step to generate trajectories in object space. Fig. 14 shows the scheme of an image space based tracking method with its main processing steps.

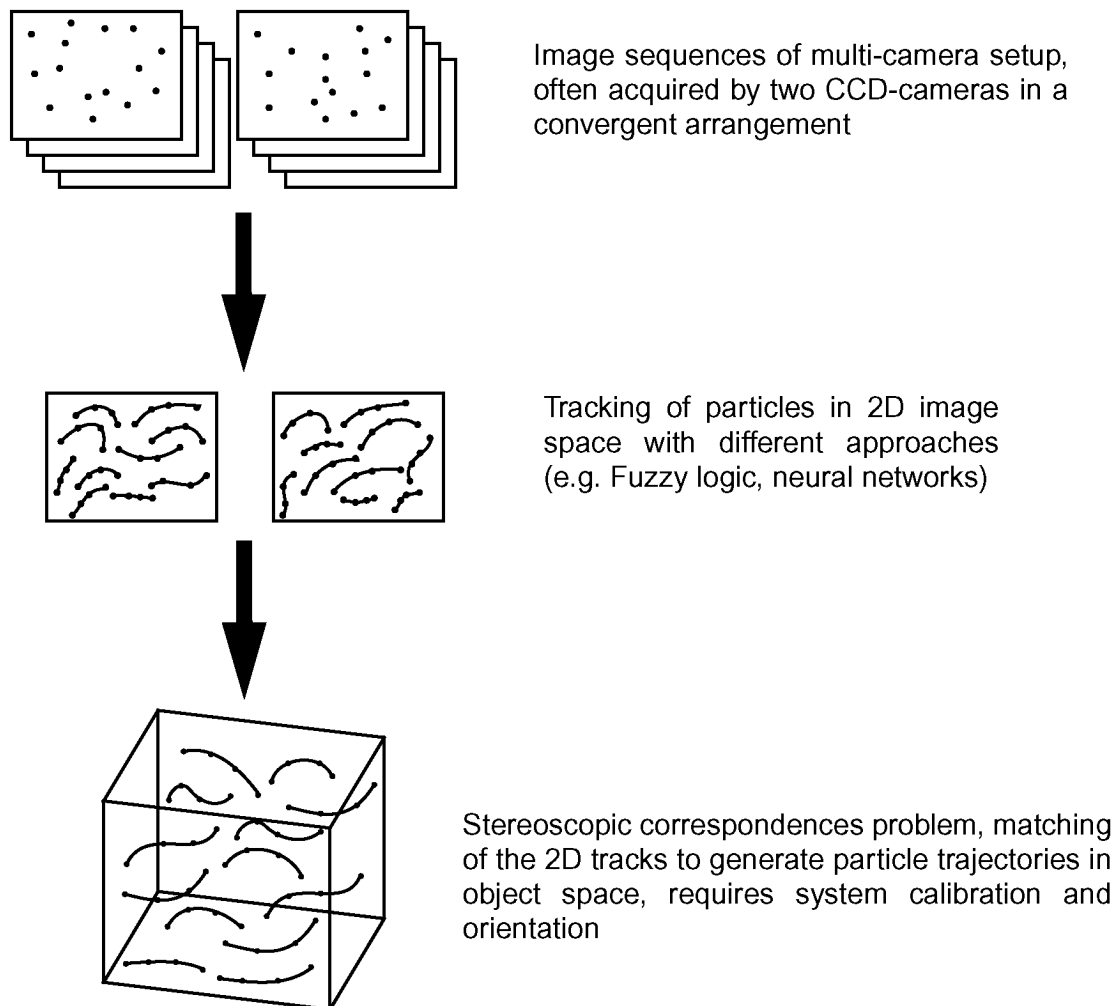


Fig. 14: Main processing steps of an image space based tracking method

A operable system applying this tracking method is described in (Engelmann, 1998) and (Engelmann, 2000), where the image acquisition system consists of two CCD cameras. In his

Ph.D. thesis (Engelmann, 2000) Engelmann gives a detailed view on the method and describes two different hardware setups, which were successfully used for the data acquisition for PTV. Two experiments were carried out at the circular Heidelberg wind-wave facility and at the newly constructed AEOLOTRON circular wind-wave facility. More details about the Heidelberg wind-wave facilities can be found in (Hering, 1996) and (Schmundt et al., 1995).

For the first experiment a two camera setup equipped with Pulnix TM 6701 AN cameras was used to acquire image sequences with 60 Hz and a resolution of 648 x 484 pixels. In a second experiment two Sony XC-73CE (providing a resolution of 752 x 582 pixels) with a frame rate of 30 Hz recorded the hydrogen bubble velocimetry distribution. The temporal resolution was considered to be sufficient to determine the motion of the bubbles.

Depending on the particle velocity and exposure time the particles appear as streaks. A first step to obtain the 2D trajectories in image space is a segmentation of the streak lines performed in each image. After the segmentation of the streak lines the temporal correspondence problem from one time step to next has to be solved. Wierzimok and Hering proposed a tracking method via interlaced images (Wierzimok/Hering, 1993). The integration time of the two fields of one image has a certain temporal overlap depending on the used camera and shutter mode. In the case of the Pulnix TM-640 the overlap was 50 % of the integration time. The temporal overlap is supposed to be a feature for the identification of objects in the consecutive images. Further details about this tracking approach via interlaced images can be found in (Hering, 1996). At low particle density a dilation operation is sufficient criterion for the correspondence match, but ambiguities will occur at a certain concentration. A set of Fuzzy variables was implemented to solve the ambiguities with a confidence measure (Hering, 1996). Five particle characteristic properties are taken as Fuzzy variables to determine a confidence measure for the solution of the temporal correspondence problem:

- The distance of the current streak from the streak in the previous image
- The distance from the current streak from its estimated position
- The difference of the current velocity of the streak from the velocity in the previous image
- The grey-value difference of the streak in the current image from the previous
- The difference of the streak area in the current image from the previous.

Fuzzy-logic lookup tables resulting in a confidence measure for each possible correspondence then link these five values. The candidate of the largest confidence measure is taken as corresponding.

A linear or a second order model is used for the position estimation of the streaks.

The same approach extended to three dimensions is applied in the actual PTV implementation at ETH (see in section 6.4.). The simple estimators are considered to be sufficient in most cases, nevertheless a more sophisticated estimator, which can be used is proposed in (Jähne, 1997) applying Kalman-filtering as a recursive linear optimal estimator. To reconstruct particle trajectories in object space the found temporal correspondences have to be matched in the stereoscopic views. Mainly three different constraints proved to be important for the stereo correlation:

- Ordering constraint: Temporal order, each trajectory consists of a list of subsequent, timely ordered streaks. For each streak a corresponding streak in the second image is required, otherwise the trajectory is split up in two or more trajectories.
- Geometric constraint: Epipolar constraint, corresponding trajectories are found within the epipolar window of a certain tolerance.

- Object property constraint: The relation of correlating to non-correlating streaks of two trajectories must not exceed a threshold. Two trajectories correspond to each other if the distance between the streaks varies only within the epipolar window

The epipolar constraint requires a calibration procedure to determine the orientation parameters of the two camera system and is considered to be one of the strongest constraints to solve the stereoscopic correspondences. Also for the PTV implementation at ETH the use of the epipolar geometry is a fundamental. The epipolar line intersection method (see in 3.4.) extended up to four cameras is very important for the solution of the multi-ocular correspondences in the PTV implementation at ETH. Again comparing the two implementations the multimedia geometry is strictly modeled in both approaches (see in 3.3.). Regarding the performance of the tracking method Engelmann does not provide according values in his thesis as later proposed in 7.1.

An alternative method applying neural networks for the tracking of particles is proposed in (Ge/Cha, 2000). Their stereoscopic particle tracking system consists of two non-interlaced Sony-8500 cameras with a resolution of 782 x 582 pixels for the observation of three-dimensional flow fields. Again tracking is performed in image space first. After the determination of the 2D particle positions in each frame their displacements are extracted in image space. To increase the spatial resolution they apply both Hopfield and stochastic neural networks for the tracking procedure. Based on a search of all possible tracks over four or five consecutive frames the potential tracks are extracted. A global energy value is then assigned to each valid track. As stated, neural networks are well suited to find the solution producing the lowest energy in an optimization problem. The extracted 2D tracks are stereoscopically matched to generate 3D tracks thereby representing the 3D velocity field. As a performance estimation the authors of (Ge/Cha, 2000) report that almost 600 particles could be tracked.

A further PTV system using image space based tracking is proposed in (Guenzennec et al., 1994) who tested a system with a mirror alignment for the acquisition of stereoscopic images. The system works with one single camera, the mirror arrangement located in front of the camera lens leads to two different viewing directions for the left and right part of the image. The stereo angle can be varied by different arrangements of the mirrors. After a pre-processing of the images, the PTV algorithm determines the particle tracks from sequences of five frames in each of the two views using the concept of path coherence. Then a stereo matching technique searches for stereo matched pairs of particle tracks in the two views.

5.4. Object space based tracking techniques

An object space based tracking technique tries to solve the correspondences in one instant of time to determine the three-dimensional particle position first. The temporal matches are searched afterwards in the 3D object space. Fig. 15 shows the scheme of an object space based tracking method with its main processing steps.

The consequent application of the method of intersection of epipolar lines allows the establishment of multi-image correspondences and the determination of 3D particle positions in object space (developed and implemented by Maas, see in (Maas, 1992b), briefly described in 3.4.). The obtained point cloud for every single time step serves as input data for the object space based tracking technique. The tracking procedure is described in more detail in (Papantoniou/Dracos, 1989) and (Malik et al., 1993). Each n-tupel of images is treated without considering temporal coherences with previous or subsequent time steps. The list of 3D coordinates is the only information, which is used by the tracking algorithm. Remaining ambiguities, which cannot be solved by the epipolar line intersection method lead to missing 3D particle positions over one or more time steps. Despite the high potential of the method this is the main disadvan-

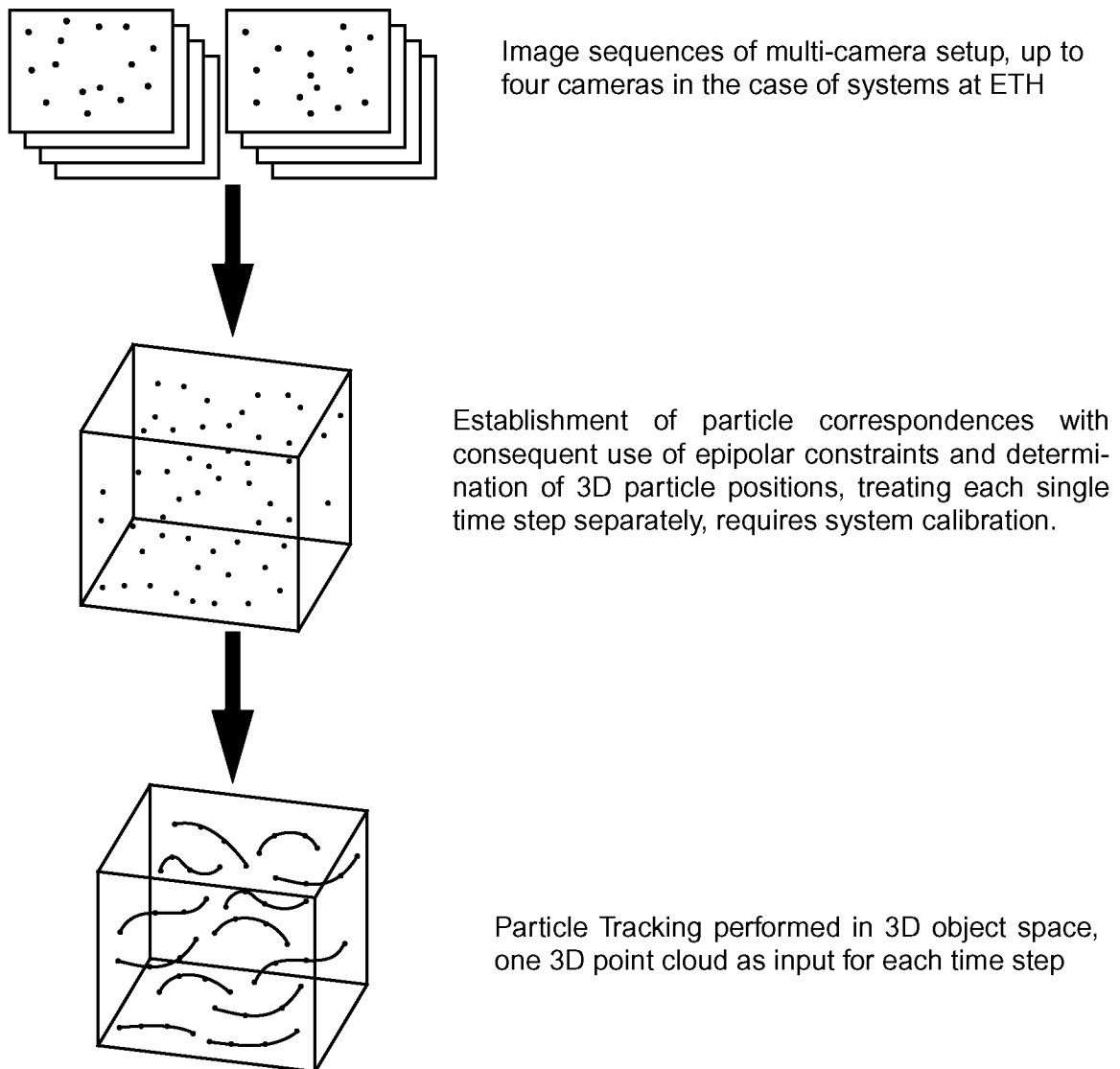


Fig. 15: Main processing steps of an object space based tracking method

tage, causing a gap in the particle trajectory, which probably can be closed by interpolation if concerning just one time step.

An operable system exists at ETH since many years and has been successfully used for various applications. A sample of publications about the projects of the recent years dealing with 3D PTV are (Becker et al., 1995), (Dupont et al., 1999), (Lüthi, 2002), (Maas et al., 1997), (Stürer, 1999) and (Virant, 1996).

A similar method was developed at the University of Tokyo at the Department of Mechanical Engineering. The 3D PTV system originally developed by Nishino and Kasagi (Nishino et al., 1989), (Nishino/Kasagi, 1989), Kasagi and Sata (Kasagi/Sata, 1992) and Sata and Kasagi (Sata/Kasagi, 1992) was used for studies in liquid flow measurements and was modified by Sata et al. (Sata et al., 1994) for airflow measurements. After the reconstruction of the particle positions of each time step the tracking is performed in object space. Sata and Kasagi evaluated the 3D particle tracking algorithm over multiple time steps by using a modelled Lagrangian

time spectra of velocity fluctuations. They also found that the size of the search region could be significantly reduced, if the turbulence characteristics time scale is sufficiently larger than the imaging frequency. In 1993 Ninomiya and Kasagi (Ninomiya/Kasagi, 1993) showed that more than 600 velocity vectors could be obtained by tracking over four time steps using a standard NTSC camera setup.

The recently used system is described in (Suzuki et al., 1999) and (Suzuki et al., 2000) consists of three high-definition CCD cameras. The hardware setup is briefly described in 4.3.2., the image acquisition system is shown in Fig. 10. Due to the significantly higher resolution of the imaging device Suzuki, Kenoya and Kasagi expected to obtain 6-7 times more particle trajectories compared to the former NTSC system. In a single-phase flow experiment an average of 1200 velocity vectors could be obtained, which is less than expected in advance. Compared to Virant (Virant, 1996), who yielded 1300 simultaneous velocity vectors from image sequences acquired with 512 x 512 pixels resolution, this number can be considered as rather low. In the arrangement used by Suzuki, Kenoya and Kasagi also particles outside the measurement volume were illuminated, so that the yield of velocity vectors is significantly decreased unlike the estimate owing to the increase of overlapping particle images. They claim to obtain more instantaneous velocity vectors when using semitransparent solid particles and only one single stroboscope to illuminate the measurement volume.

From an algorithmic point of view the research group of the Department of Mechanical Engineering at the University of Tokyo does not report of recent developments of the particle tracking method.

6. 3D PTV based on image and object space information

Based on the previous implementation at ETH a more consequent exploitation of the available information was thought to lead to improvements of the PTV method. In the previous implementation at ETH Zurich the establishment of multi-camera correspondences is performed by epipolar line intersection technique treating each single time step separately ((Papantoniou/Dracos, 1989), (Maas et al., 1993) and (Malik et al., 1993)). The tracking procedure is performed in object space exclusively using the 3D point cloud of each time step. A combined spatial and temporal assignment is supposed to lead to a higher tracking efficiency.

6.1. Spatio-temporal consistency in multiocular image sequences

In the late eighties and early nineties multiocular systems for the navigation of autonomous robots and vehicles were developed. At INRIA in France Ayache and Lustman developed a system with three cameras allowing the assignment of line segments from image triplets for each time instant of an image sequence (Ayache/Lustman, 1987). Navab and Zhang performed further developments at INRIA trying to combine the proposed stereo matching algorithm with a monocular line tracking approach (Navab/Zhang, 1992). Navab and Zhang realized that each of these processes may work faster and more reliably if they could borrow dynamically some information from each other. They proposed an unified iterative algorithm for both temporal tracking of stereo pairs of line segments and camera system ego-motion estimation. The dynamic cooperation between stereo matching and temporal matching processes was applied to image sequences acquired with a calibrated vision system, which was mounted on a mobile vehicle. The approach was found to be more reliable and less time consuming than using a classical stereo reconstruction for each single time step.

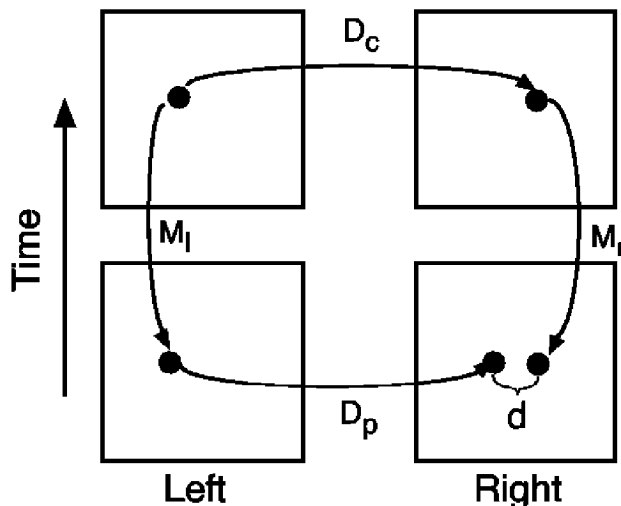


Fig. 16: Spatio-temporal "loop" check, taken from (Bolles/Woodfill 1993)

A spatio-temporal technique for checking the consistency of stereo range results and integrating them over time was presented in (Bolles/Woodfill 1993) and (Baker/Bolles, 1994). The ultimate goal of this research was to develop passive range sensing technique that provide the spatial and depth resolutions required to detect small navigation obstacles. The experimental data was obtained by mounting a pair of cameras on a vehicle (HMMWV). The cameras were manually aligned with approximately parallel axes and recorded image sequences on VHS videotape as the vehicle was driven on and off road. As the vehicle was bouncing along over rocks and ditches it was not possible to

maintain a precise calibration. Therefore the matching algorithm could rely on precise epipolar geometry, yet it could constrain the searches to a small number of lines relative to the predicted epipolar line. The basic approach of the system was to perform conventional stereo disparity estimation in the two views (“left-right check”) and optical flow estimation from present to past (“forward-backward check”). The stereo estimates are corroborated by performing a reverse right-to-left stereo match and verifying that the left-to-right result is its inverse. The optical flow estimates similarly validated by estimating the past-to-present flow. The principle of the spatio-temporal “loop” check is shown in Fig. 16. The two optical flow estimates M_l and M_r for each pixel in both cameras and the spatio-temporal transitivity of two stereo estimates from the current frame D_c and the past frame D_p can be checked to ensure that a four sided “loop” of matches is consistent. The spatio-temporal transitivity check is considered as consistent if the distance d between the matches $M_r(D_c(P))$ and $D_p(M_l(P))$ is within one pixel.

D’Apuzzo proposed a algorithm to track corresponding points from multiple views through image sequences and to compute their 3D trajectories (D’Apuzzo, 2002). The multi-image matching process is based on the adaptive least squares method (LSM) with additional geometrical constraints of the matched point to lie on the epipolar line (Grün, 1985). Both, the spatial correspondences between the images of the different views as well as the temporal correspondences between subsequent frames are computed using the LSM algorithm (Fig. 17).

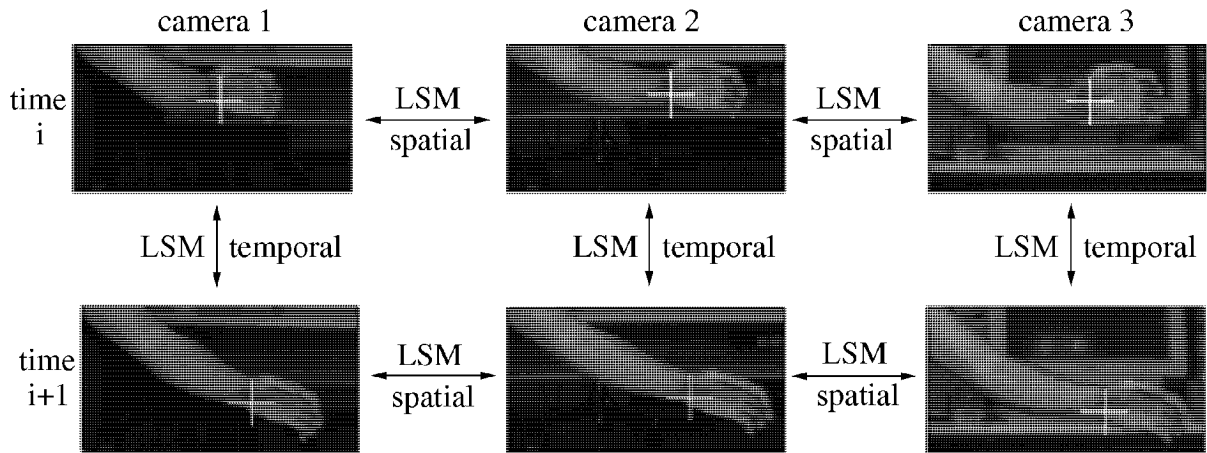


Fig. 17: LSM tracking: temporal and spatial correspondences established with LSM, taken from (D’Apuzzo, 2002)

The process starts matching corresponding points from the different views of the cameras. After predicting the position in the next frame and the search of the position with the best cross-correlation, the correspondence is established by least squares matching (temporal LSM). The position of the tracked point at time $i+1$ is linearly predicted from the two previous time steps $i-1$ and i . The best value of cross-correlation between the image at time i and the image at time $i+1$ is found by scanning a search box around the predicted position. LSM is applied at that position and the result is considered to be the exact position of the tracked point in the new frame. This procedure is performed in parallel for the different images. To check the results, spatial LSM is computed at the positions resulting from the temporal LSM. If the differences between the two results do not exceed a certain threshold the point is tracked and the process continues to the next time step. The 3D coordinates of the tracked points for each time step are computed by forward intersection and its trajectory, velocity and acceleration is determined. The method can be used to track well-defined points on the human body.

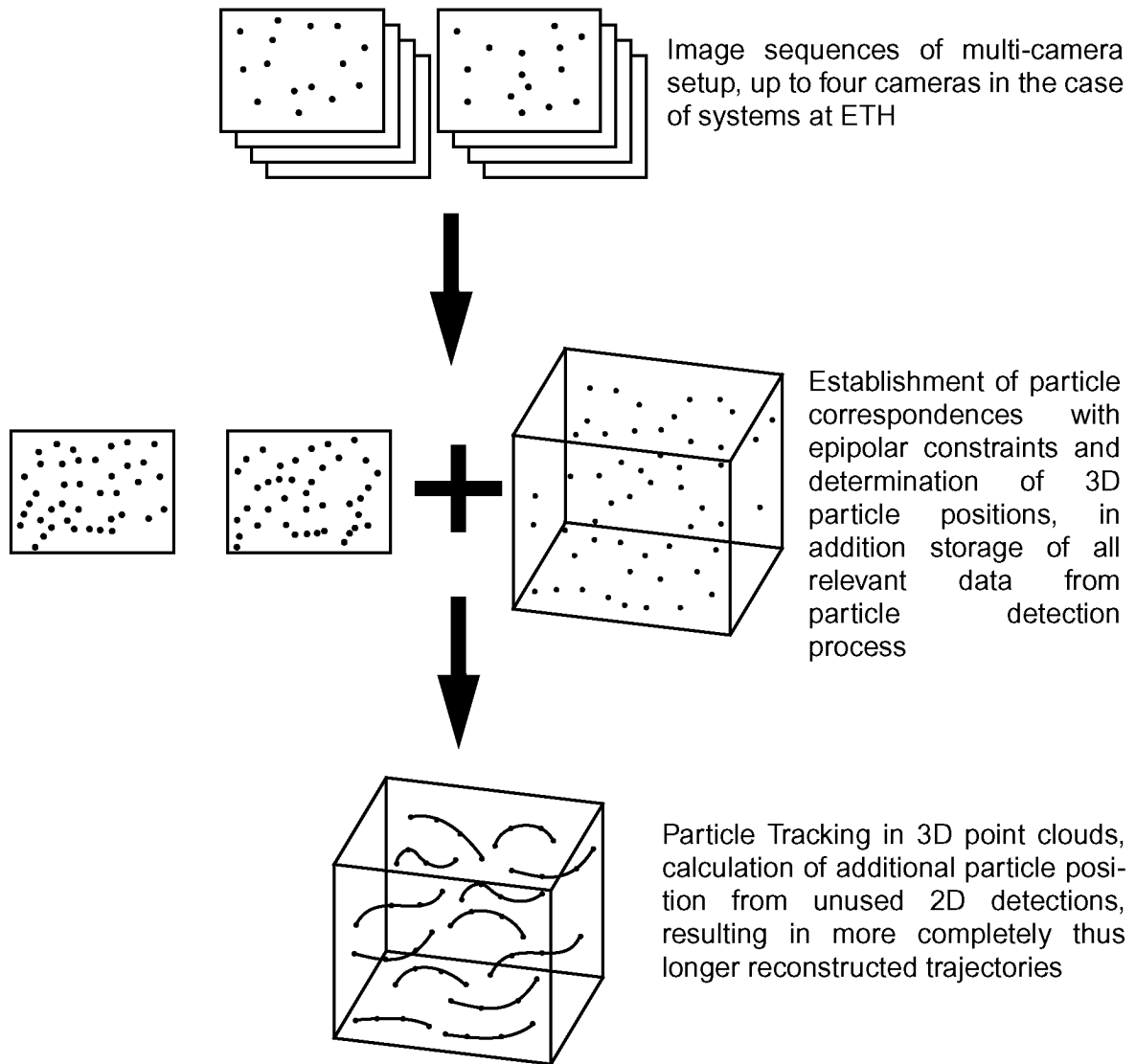


Fig. 18: Particle tracking based on image and object space information

6.2. Spatio-temporal matching algorithm for 3D PTV

Our spatio-temporal matching algorithm uses the information extracted from image and object space simultaneously. The processing scheme of the tracking technique based on image and object space information is shown in Fig. 18. Compared to the previous system only the software solution is changed, the hardware requirements for the data acquisition remain the same.

Although the number of ambiguities can be reduced drastically by the use of 3 or 4 cameras in a suitable configuration, they cannot be solved completely in case only one time step is considered. Some detected particle locations still remain unmatched (obviously not all detections in image space can be matched, e.g. when a particle is visible only in one image). Assuming a 4-camera setup a particle at best can be detected in four images, which delivers 5 redundant observations (4×2 image coordinate observations minus 3 object space coordinate unknowns).

The number of image coordinate observations should therefore be sufficient for the determination of the according particle position if only the ambiguity in the correspondences could be

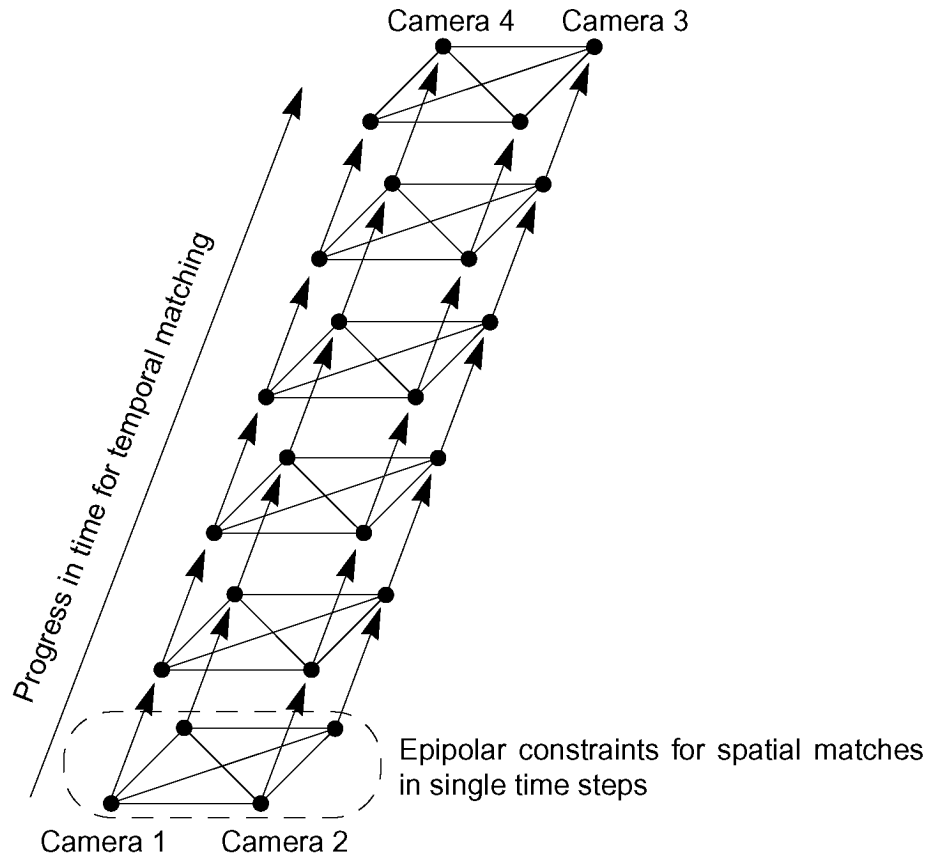


Fig. 19: Redundant spatio-temporal connections in the synchronized image sequences of four cameras, courtesy by (Grün et al., 1996)

solved reliably. Along the epipolar line segments in the different views too many possible candidates are found especially when the particle density is high or/and the depth range of the object volume is rather large.

If a particle can be tracked over some consecutive time steps a quite reliable prediction of the particle position in the next time step can be made. In the case of two images this reduces the search space from an epipolar line segment to a single 2D search position - with a certain added tolerance - and can be determined by back-projection of the respective predicted particle position. Compared to the approach treating every time step separately this decreases the number of possible candidates causing less unresolvable ambiguities.

Fig. 19 shows the different possible matches in space and time, which can be used to reconstruct the motion of a particle recorded by four cameras. The different previous tracking approaches only use either the temporal or the spatial matching, while the enhanced method benefits from the use of both. Compared to the approach proposed in (Bolles/Woodfill 1993) and (Baker/Bolles, 1994) not only a pair of cameras (Fig. 16) is used for the image acquisition. Baker, Bolles and Woodfill performed a spatio-temporal “loop” check in image space to find consistent matches from stereo pairs.

The principle of spatio-temporal consistency is also used for the enhanced PTV approach. Starting from initial tracks from particle positions established by applying the epipolar line intersection method, the PTV approach predicts the particle position in 3D space for the next

time step. As the camera orientation data is available from a system calibration the according search positions can be found by back-projecting the predicted 3D coordinates into the image space of all views. The search in image space either leads to 3D particle positions or to formerly unmatched image particle detections, which can be used to calculate additional particle positions. In contradiction to (Baker/Bolles, 1994) the spatio-temporal “loop” check is not performed in image but in object space. The consistency check of the particle motion could be extended from a simple geometrical model (as applied in the current PTV implementation, see 6.4.) to a model also considering physical properties (Papantoniou/Dracos, 1989).

The main issue of the new algorithm is the handling of redundant tracking information. Not only the 3D particle coordinates of the single time step but also the detections in image space are used to establish the temporal correspondences. In addition to the 3D point clouds used by the object space based tracking technique the new developed method handles also the image space based information. The redundant image coordinate observations combined with the prediction for the next particle position allow the establishment of spatio-temporal connections even when the velocity field has a high density or the movement of the tracer particles is fast.

After the particle detection, the establishment of the correspondences and 3D particle position determination the data collection for the tracking algorithm can be divided in the following steps:

- The particle detection delivers a list of 2D image locations determined by a grey value-weighted center of gravity with subpixel accuracy including additional features like size and intensity of the according particle detection.
- The application of the epipolar line intersection method leads to corresponding particle detections at one time instant. The particle detections used in a correspondence are labelled with the according correspondence number. Unused particle detections remain unlabelled in this status of the processing.
- The matched particle detections belonging to one correspondence are then used for the calculation of the 3D particle position in object space. The 3D coordinates are derived by a forward intersection. They are forming the initial 3D point cloud before the tracking is performed.

All this data is generated by the previous implementation as well, but only the 3D point clouds of each time step is used for the former tracking procedure. For the proposed approach the image and object space information is collected throughout the whole sequence and provides the input for the enhanced spatio-temporal matching algorithm for PTV. The tracking procedure using image and object space based information in combination with a kinematic motion modelling is described in 6.4.

6.3. Alternative criteria for temporal assignment in image sequences

To improve the assignment of particle images some characteristic attributes as size, shape and brightness might help to increase the reliability of the tracking procedure. But experience showed that these parameters depend less on the actual features of the particles itself as on the illumination conditions varying significantly for the different viewing directions of the observing cameras, (Racca/Dewey, 1988) and (Maas, 1992b). This leads to rather low correlation between the parameters of the particle image regarding one time step acquired with different cameras. Due to this fact these parameters cannot further contribute to a reliable assignment of corresponding particle images.

Within the image sequence of one single camera it can be assumed that higher correlations are existent, which is supposed to allow an improved assignment (Maas, 1992b).

Trying to use the parameters of a particle image as additional criteria, the following methods can be considered:

- area based matching
- feature based matching

The first method would try to match each single particle image with a certain patch size into the image space of the consecutive image. This method for the assignment seemed to be inefficient for the search of corresponding particles. Applying area based matching of so-called investigation areas in the PIV technique (see in section 2.2.2.4.) is suitable because only a thin light sheet is observed.

The underlying mathematical model of the area based matching approach requires continuous, non-transparent and non-reflective objects. For PTV a three-dimensional object volume is observed, therefore particles from different depth ranges and possibly contrary motion directions or speed will affect an area based matching approach. A volume seeded with particles is a multi-layered object where occlusions of particle images are likely, which both makes an successful use of area based matching hardly applicable or even impossible.

In the context of the three-dimensional reconstruction of the particle positions not only the exact image coordinates but also other features are determined. For this reason it is obvious to use these data, which is already available for a feature based matching. The determined particle features are:

- the number of pixels belonging to a particle
- the dimension in x- and y-direction in pixels
- the sum of grey values of all the pixel belonging to a particle.

The quality of the images has an influence on the parameters for the particle detection, which have to be adjusted to reasonable values to detect as many particles as possible but avoiding mismatches. The images used for PTV show the particles as bright spots on a more or less dark background. The pixels belonging to a particle image are segmented with a simple threshold algorithm and the exact image coordinate is determined with a grey value-weighted center of gravity of segmented region. To avoid detection errors (e.g. caused by noise) a particle image has also to fulfil the properties such as a minimal and maximal size in x- and y-direction as well as a minimum sum of the grey values belonging to a particle. The choice of the threshold is made empirical, but is essential, because it influences directly all the mentioned particle features. With a higher threshold pixels, which belong to a particle image will be neglected and therefore do not contribute to the position determination nor to the features of the according particle.

A former investigation has shown higher correlation between corresponding particle parameters in consecutive images in sequences of single cameras compared to the images of different cameras (Maas, 1992b). Particularly the sum of the grey values seemed to be a suitable supporting feature, because of the lower influence of this parameter on the discretisation effects of the imaging system. Tests have shown that in spite of higher correlation between the sum of grey values of corresponding particles the contribution to an assignment is little. Insignificant differences of neighbouring particle images might be an explanation for that. Especially particles, which are also close in object space will appear quite similar in image space because of their more or less same physical attributes and illumination conditions. Particles, which are close only in image space will probably appear different but can be excluded from the assignment because of their distance in object space.

A typical particle image has a size of 2×2 to 7×7 pixels. Especially for smaller targets in motion the influence of discretisation effects is considerable. As size may change from 2×2 to 3×3 the assignment using the dimensions in x - and y will be rather obstructed or impossible than made more reliable. Also with the use of an area based matching problems of that kind would occur, particularly considering the mostly rounded particle images and reasonable choice of matching parameters.

The epipolar constraints in combination with a kinematic model already gives a very strong criteria for the spatio-temporal assignment. Therefore and due to the considerations about the particle attributes within an image sequence acquired by one camera, no significant improvement was expected by the use of the additional criteria mentioned above and thus is not implemented in the new spatio-temporal matching algorithm for 3D PTV.

The used criteria for the spatio-temporal assignment are the three-dimensional particle positions in object space, the velocity and the acceleration from one time step to the consecutive one. This concept is similar to the approach proposed in (Papantoniou/Maas, 1990), except that no assumptions on the correlation of neighbouring particle motion are used for the spatio-temporal assignment.

6.4. Tracking procedure using kinematic motion modelling

Several approaches can be employed for the kinematic modelling of the particle motion. A quite familiar model for tracking applications is the time-dependent polynomial of order two (constant velocity) or three (constant acceleration). The latter leads to the following differential equation:

$$\ddot{\vec{x}}(t) = 0 \quad (9)$$

where $\vec{x}(t)$ indicates the position at time t . Through the integration of this equation and representing the acceleration $\ddot{\vec{x}}(t)$ by $\vec{a}(t)$ and velocity $\dot{\vec{x}}(t)$ by $\vec{u}(t)$ one obtains:

$$\begin{aligned} a(t) &= \text{const} \\ v(t) &= a(t_0) \cdot (t - t_0) \\ x(t) &= \frac{1}{2} a(t_0) \cdot (t - t_0)^2 + v(t_0) \cdot (t - t_0) + x(t_0) \end{aligned} \quad (10)$$

where t_0 is the starting time of an object's path of movement. The model can be adapted to the alpha-beta-gamma model, which is proposed for tracking applications in (Fraser/Shao, 2001). This method requires the determination of the so-called tracking index leading to the gain coefficients α , β and γ for position, velocity and acceleration. Kalman Filtering is also a suitable method for the filtering and prediction of moving objects, but requires a time-expensive computation of the covariance matrix for the filter gain coefficients (Hering, 1996).

A reliable extrapolation of a particle position with a more sophisticated model would require a certain number of positions from previous time steps. This is only the case if the particle was already tracked for some time steps, where the simpler prediction combined with a given search volume already succeeded to establish the links between the particle positions. Taking in account that particle positions might be noisy (especially in the viewing directions of the cameras, see in 4.6.) the use of a higher kinematic motion model would rather lead to disadvantages than to an improvement. Considering the number of particles to be observed and resulting computational costs the implementation was kept simple and a second order prediction is used.

Due to the discrete temporal resolution of the image acquisition system a transition from the continuous formulation to a discrete one is necessary:

- From a 3D particle position $\bar{x}_p(t_i)$ at time step t_i a position $\bar{x}_p(t_{i+1})$ for consecutive time step t_{i+1} is predicted under the assumption of a piecewise constant particle velocity $\bar{u}_p(t_i)$, eq. (11). A simple linear extrapolation is possible if the particle of step t_i already has a valid link to the previous time step t_{i-1} , otherwise the position from t_i itself is used as search position. The temporal resolution Δt is given by the frame rate of the sensors used for the image sequence acquisition. Each particle is treated separately.

$$\begin{aligned}\bar{x}_p(t_{i+1}) &= \bar{x}_p(t_i) + \bar{u}_p(t_i) \cdot \Delta t \\ &= 2 \cdot \bar{x}_p(t_i) - \bar{x}_p(t_{i-1}) \\ \text{with } \bar{u}_p(t_i) &= \frac{\bar{x}_p(t_i) - \bar{x}_p(t_{i-1})}{\Delta t}\end{aligned}\tag{11}$$

- Assumptions on the correlation of neighbouring particle motion as proposed in (Papantoniou/Maas, 1990) are not used for the prediction of the particle position of the next time step.
- The search of suitable candidates is performed in image space. This requires the backprojection of the three-dimensional search position from object space to image space of all cameras, which can easily be done when camera orientations and multimedia geometry are known.
- The search is also performed in the image space of the cameras where the particle of step t_i could not initially be found or matched (e.g. due to overlapping particle in one or more views). Based on a list of possible candidates a search position $\bar{x}_p(t_{i+2})$ for time step t_{i+2} is predicted. If a valid link to the previous time step t_{i-1} exists the predicted position $\bar{x}_p(t_{i+2})$ is calculated under the assumption of constant particle acceleration (model of second order, eq. (12)), otherwise again a linear extrapolation is used.

$$\begin{aligned}\bar{x}_p(t_{i+2}) &= \bar{x}_p(t_{i+1}) + \bar{u}_p(t_{i+1}) \cdot \Delta t + \frac{1}{2} \cdot \bar{a}_p(t_{i+1}) \cdot \Delta t^2 \\ &= \frac{1}{2} \cdot (5 \cdot \bar{x}_p(t_{i+1}) - 4 \cdot \bar{x}_p(t_i) + \bar{x}_p(t_{i-1})) \\ \text{with } \bar{a}_p(t_{i+1}) &= \frac{\bar{u}_p(t_{i+1}) - \bar{u}_p(t_i)}{\Delta t}\end{aligned}\tag{12}$$

- For each found path a quality criterion is calculated. The parameters for the quality measure are the acceleration and the direction change of the particle, concerning the time steps t_i , t_{i+1} and t_{i+2} . The quality measure of a found path might be determined by an extended model that considers also the feature correlation of the particle image attributes (as size, shape and brightness, described in 6.3.), an information, which is not used in the implementation presented here.
- Conflicting particle connections are avoided by the quality criteria.
- If a particle from time step t_i is already linked to the previous time step t_{i-1} and can be connected to a particle of time step t_{i+1} , but no candidate in step t_{i+2} is found, the quality

factor is calculated from the time steps t_{i-1} , t_i and t_{i+1} . In the tracking procedure the particle links are created between the time steps t_i and t_{i+1} . Therefore the ‘last’ particle position t_{i+1} of a trajectory should also be connected with a link, but the establishment to this last particle position does not require information from time step t_{i+2} .

- If still no link could be established with the already calculated 3D particle positions, the remaining unmatched particle detections in image space from time step t_{i+1} around the predicted location are used to determine an additional particle position (again the reconstructed path has to fulfil the quality criterion).
- The tracking can be performed in progressive as well as regressive way. This offers the possibility to extend a trajectory not only in forward but also in backward direction.

Fig. 20 shows the processing scheme of the tracking procedure. With this tracking procedure the reconstruction of more complete trajectories is possible. Additional particle positions are calculated from formerly unused detections in image space.

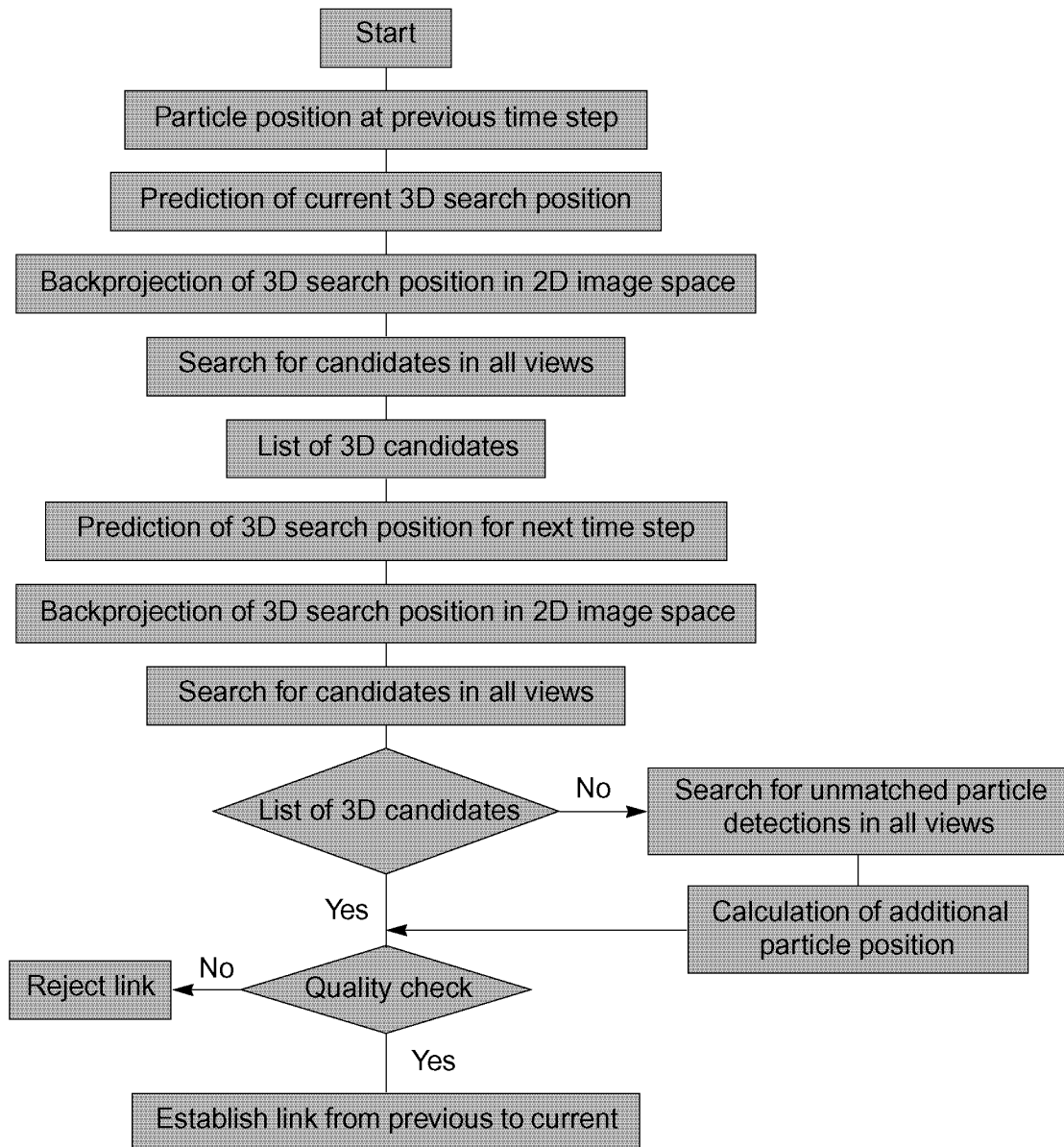


Fig. 20: Processing scheme of the tracking procedure

To distinguish the different tracking procedures the enhanced approach applied in only forward direction is called ‘Enhanced (forward only)’, applied in forward and backward direction it is called ‘Enhanced (directional)’. The object space based tracking method, which tracks only the particles determined by the epipolar line intersection is called ‘Previous’.

6.5. Exploitation of redundant information for ambiguity reduction

The number of unsolved ambiguities resulting from the epipolar line intersection technique can be decreased if the temporal context is considered. In the case of ambiguities particle trajectories are often interrupted for only one or a few time steps. With the new algorithm these gaps can be bridged reliably and even the continuation of a trajectory is possible when the redundant information is exploited in a correct way.

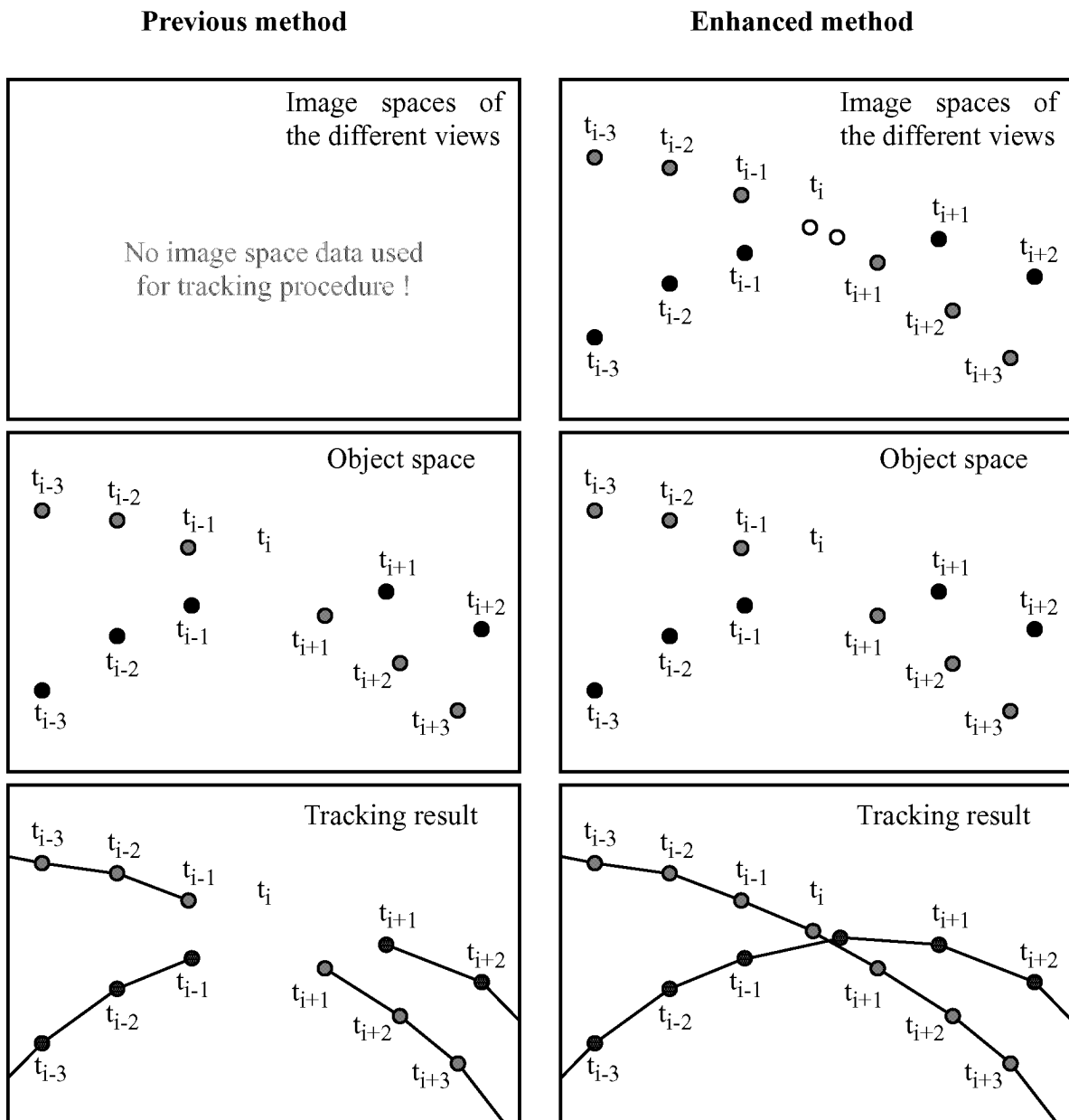


Fig. 21: Comparison of the use of available input data for the tracking procedure and results derived with the previous and the enhanced method.

Fig. 21 shows the differences in the use of object and image based information by the tracking algorithms. With the object space based tracking method (left) no particle position in time step t_i can be calculated due to ambiguities in the epipolar line intersection. The available data used for the image/object space based tracking (shown right) are 3D particle positions (marked with filled circles) as well as image coordinates (unmatched particle detections are marked with unfilled circles). The result of the enhanced tracking algorithm closes gaps by additionally calculated particle positions from unmatched image coordinates. The goal of the enhanced algorithm is to yield longer trajectories. The length of trajectories can be increased by:

- Bridging a gap of a single time step by an additionally calculated particle position to connect two fragments of a trajectory
- Bridging a gap of variable length between two or more fragments of a trajectory
- Continuing a trajectory in forward or/and backward direction with additionally calculated particles
- A combination of the mentioned cases

Fragmented particle trajectories can be reconstructed more completely. With the enhanced method the existing gaps between the two or more trajectory fragments should be bridged and connected to one trajectory with increased length. This is possible by the knowledge of the motion from former time steps allowing a suitable extrapolation of the particle position and the use of yet unused image-space based information. Extrapolation is only used for prediction purposes. The calculation of the particle positions to close gaps is strictly based on image space observations (at least the 2D positions in image space from two different views). It is obvious that the influence of measurement errors is increasing when a particle position is calculated from fewer observations with a lower redundancy. But if the camera arrangement is suitable, the loss of quality is not substantial and still acceptable compared to an interruption of the particle trajectory.

Considering the structure of tracking results the following effects can be expected:

- The number of short trajectories will decrease
- The number of long trajectories will increase
- The average length of a trajectory will increase
- The total length of all trajectories will increase
- The total number of trajectories will decrease due the connection of trajectory segments

These effects should be visible in histograms showing the distribution of particle trajectories of specific lengths (or length classes). The qualitative change of the trajectory length distribution, which is expected for the PTV results is shown in Fig. 22. The distribution of the trajectory lengths yielded with the previous method reaches its maximum earlier than the enhanced approach, which corresponds to more and shorter trajectories. The distribution graph yielded with the enhanced approach is more flat and decreases slower with increasing trajectory length. As the total number of trajectories is expected to be decreased (due connecting of fragments to long trajectories) the integrated area under the enhanced graph might be of a smaller size. In the case of actual experiments the temporal resolution is limited by the frame rate of the image acquisition leading to a discrete distribution function of the trajectory length or specific length classes. The shape and relation of two distribution functions yielded with the different tracking algorithms will depend on the analysed data set, but should show up with the expected tendencies. A discussion about the yielded results of the reconstruction of more complete trajectories and some examples from simulated and real experiment data can be found in chapter 7.5. It has to be considered that all presented histograms are displayed in logarithmic scale.

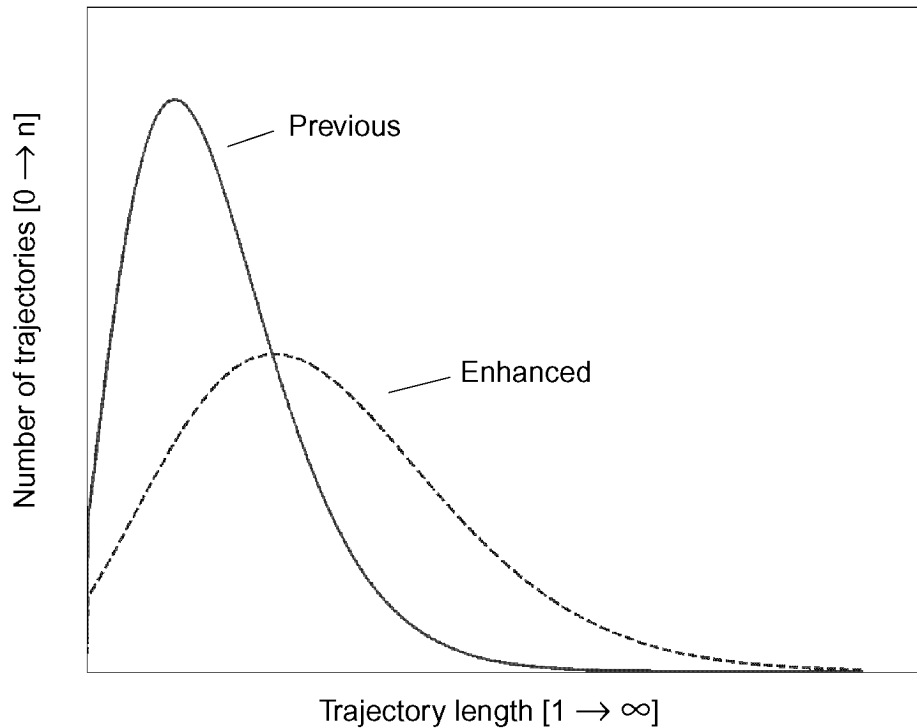


Fig. 22: Qualitative histogram of the expected trajectory length distribution yielded with the previous and enhanced PTV approach

6.6. Non-algorithmic limitations of trajectory lengths

The goal of the PTV method is to reconstruct as many trajectories as long as possible. Besides the limitations of the performance of the implementation the motion of the particles itself can reduce the traceability of a particle. This is the case when a particle leaves the observation volume.

To obtain as few ambiguities in the epipolar line intersection method as possible the object volume should be observed commonly by all available cameras. This is valid only for a certain percentage of the object volume. But even outside of the volume of full coverage particle trajectories can be reconstructed if the spatio-temporal connections can be solved. Based on the principles of the PTV method a particle moving in object space can only be tracked if it is in the field of view of at least two cameras. As the particle position is determined by forward intersection the 2D location in two image spaces is required. A particle moving from inside the observation volume to its border will sequentially disappear from the different field of view of the cameras until it will be completely vanished.

These conditions will change from experiment to experiment, but in any case it can be assumed that particles intrude and leave the observed volume during the sequence thus leading to the end of the particle trajectory.

6.7. Parameter settings for PTV processing

For the actual processing of PTV data several parameters must be adjusted to yield reasonable results. The setting of these parameters requires empirical knowledge as well as a-priori information about the flow field, which is under investigation.

The parameters concern different aspects as:

- Shape and size of the observation volume
- Quality of the calibration and orientation
- Image quality
- Number of particles
- Motion of the particles

The shape and size of the observation volume is roughly known by the experiment setup itself, but is also limited by the depth of focus of the cameras. Concerning the epipolar line intersection technique (as described in 3.4.) a larger depth range of the observed object space leads to an increased number of ambiguities due to the longer epipolar segments to be examined.

The quality of the calibration and orientation of the cameras has a strong impact on the different processing steps. The direct influence on the accuracy of the three-dimensional particle coordinates determined by forward intersection is more or less obvious. But it also affects the establishment of the particle correspondences and thus contributes to the tracking results.

An accurate calibration allows to use a smaller tolerance to the epipolar line segments and thus a smaller number of found particle candidates have to be considered in the establishment of the multi-ocular correspondences. This results in a reduction of the number of occurring ambiguities, which is beneficial for both the previous as well as the enhanced tracking approach.

An insufficient calibration makes less impact on the number of linked particles determined with the enhanced method than with the previous approach. This can be explained as follows: The previous approach has to establish particle correspondences by the exclusive use of epipolar constraints, leading to more ambiguities the lower the calibration quality is. The enhanced method however considers the particle motion in object space, too. Compared to the previous method, it is therefore capable to resolve a larger number of ambiguities. In any case the calibration has to be carried out carefully as it is an absolute prerequisite for a successful 3D PTV application.

The image quality is mainly influenced by the illumination facility as well as the seeding particles to visualize the flow. For automated particle detection the image sequences should provide high contrast between background and particles. For the particle detection a threshold to segment the background is used. The image coordinates are determined with a grey value weighted center of gravity.

For the tracking procedure several parameters for the particle motion have to be adjusted. A limitation for the particle motion the minimum and maximum velocity in all three coordinate directions is specified, the quality estimation of a particle link requires a value for the maximum valid acceleration and divergence angle.

For the actual application of 3D PTV a step by step advice is given in the appendix of this thesis. Detailed background about the system calibration and automated particle detection can be found in (Maas, 1992b).

7. Tests of the spatio-temporal matching algorithm

The developed spatio-temporal matching algorithm for 3D PTV was tested with simulated data as well as with data from real experiments. Eight different data sets were used for the performance tests.

All data sets were processed with the tracking approaches ‘Previous’, ‘Enhanced (forward only)’ and ‘Enhanced (bidirectional)’. The tracking methods ‘Previous’, ‘Enhanced (forward only)’ and ‘Enhanced (bidirectional)’ were developed by the author and work as described in chapter 6. These approaches are based on object and image space based information. The method ‘Previous’ tracks only the particles, which 3D position could be determined by the epipolar line intersection. ‘Enhanced (forward only)’ and ‘Enhanced (bidirectional)’ are able to determine additional particle positions by using formerly unmatched particle detections. Performing the method in forward and backward direction yields most complete particle trajectories.

In addition two of the eight data sets (see 7.3.3.7. and 7.3.3.8.) were also evaluated with the tracking method ‘TrackingHS’, which was originally developed by Papantoniou, Dracos and Malik (Malik et al., 1993) and later modified by Stürer (Stürer, 1999). In comparison to the former approach Stürer’s tracking approach does no longer support the principles of group velocities and minimum energy considerations as proposed in (Papantoniou/Dracos, 1989). For the two data sets, which were also processed with this method, the tracking rate was rather low and it was expected that better results might be yielded with the approach ‘TrackingHS’.

On the one hand the tests are performed to compare the potential of the different methods, on the other hand these tests should prove the operability of the developed software implementation concerning each single functionality.

7.1. Definition of performance characteristics

To be able to evaluate the performance of the PTV methods some performance characteristics are defined. As obvious performance characteristics can serve the number of particles p_{3D} and the number of linked particles l_{3D} per time step. To get rid off temporal variations within the image sequences a simple way to compare the performance of the previous and the enhanced method is the average number of established links over all time steps. The number of linked particles l_{3D} is probably the most important value for performance evaluation concerning the spatial resolution.

But not only absolute values can be used for the performance evaluation. The ratio between the number of established links l_{3D} and particles p_{3D} gives the tracking efficiency eff_{3D} of the method which is applied:

$$eff_{3D} = \frac{l_{3D}}{p_{3D}} \quad (13)$$

Due to the fact that the enhanced method has the capability to create additional particle links $l_{3D}(add)$, the relative efficiency $eff_{3D}(rel)$ should also be related to the number of particles $p_{3D}(prev)$ derived with the previous method to achieve a better comparability:

$$eff_{3D}(rel) = \frac{l_{3D}(prev) + l_{3D}(add)}{p_{3D}(prev)} = \frac{l_{3D}(enh)}{p_{3D}(prev)} \quad (14)$$

The ratio between the number of additional links $l_{3D}(add)$ and links $l_{3D}(prev)$ established with the previous method was used to quantify the gain g_{3D} of the enhanced method:

$$g_{3D} = \frac{l_{3D}(enh) - l_{3D}(prev)}{l_{3D}(prev)} = \frac{l_{3D}(add)}{l_{3D}(prev)} \quad (15)$$

The total number of all reconstructed trajectories N_{traj} can be instructive however it is also decisive to consider the length l_{traj} of the trajectory as well. A trajectory of a particle might be interrupted twice resulting in three trajectory sections while an enhanced algorithm may be able to reconstruct just *one* complete trajectory without gap. Another possible way to assess tracking results is the average length avl_{traj} of all the particles trajectories which could be reconstructed by the different approaches:

$$avl_{traj} = \frac{\sum l_{traj}}{N_{traj}} \quad (16)$$

Considering the total number of all trajectories and their corresponding length it is possible to derive the total number of established links L_{traj} of all trajectories:

$$L_{traj} = avl_{traj} \cdot N_{traj} = \sum l_{traj} \quad (17)$$

This total number of links L_{traj} of all trajectories can also be calculated as the sum of all established links throughout the whole sequence.

A summary of the performance characteristics for comparison of the previous and the enhanced method will be given in the related sections where the processing of the different data sets is described and in section 7.5.4.

The analysis of the histograms (as described in 6.5.) showing the distribution of trajectories of different lengths or specific length classes is also useful to compare the tracking results of the different approaches.

7.2. Tests using simulated data

The input data for 3D PTV are multi-ocular synchronous image sequences supplemented with additional information to model the sensors. These additional informations consist of specifications from the hardware components and parameters describing the interior and exterior orientation of the cameras. To perform tests with simulated data it is also necessary to simulate a more or less reasonable flow field and a realistic hardware design including the specifications and configuration of the image acquisition system.

7.2.1. Generation of simulated image sequences

In a first step a three-dimensional flow field with a random particle distribution in a chosen object volume is generated. For each single time step a set of three-dimensional particle coor-

ordinates is created, which then can be reprojected to the image planes of the corresponding cameras. To model the sensors commercial standard video cameras are assumed.

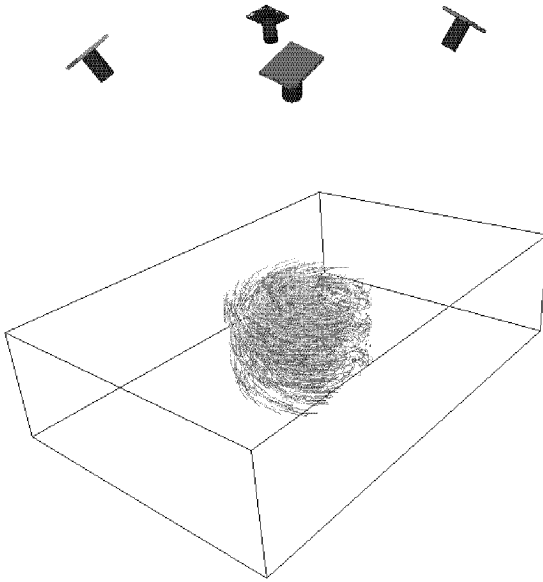


Fig. 23: Simulated configuration showing a four camera setup and the observed object volume with vortex flow

Without restrictions to the general validity the assumed lenses are considered as distortionfree and the image size is set to 640×480 pixels with a pixel size of $10 \times 10 \mu\text{m}^2$. The focal distance is chosen to 11.0 mm, which leads in combination with an average object distance of 200 mm to good image coverage. The considered values of the different parameters are according to existing operable 3D PTV hardware designs and today's camera techniques. The parameters of the exterior orientation are chosen in that way that the camera configuration leads to well-defined intersections of the optical rays and are similar to a hardware setup typically used for 3D PTV. The configuration is shown in Fig. 23.

To define the interior orientation of the cameras the principal point is assumed to be in the exact center of the image sensor (for sensor model see section 3.1.). Additional parameters modelling the distortion of the lens or electronic effects (shearing δ , scale in s_x) are not used. As mentioned above this can be done without restrictions to the general validity and not using those parameters just simplifies the generation of the simulated image data. The images are generated by reprojection of the 3D particle coordinate to 2D image space. After the choice of some describing features like size and brightness the synthetic image is modified that the particles appear as bright spots on a dark noiseless background.

The resulting image sequence data is processed with the 3D PTV software in the same way as the data acquired during real experiments. The data generated for the simulation tests can be varied in manifold ways regarding the camera setup, the number and motion of particles as well as the length of the sequence. The reconstructed particle trajectories can then be compared with the initially defined velocity field, which is known unlike real experiments. The tracking results were investigated regarding the completeness of the reconstructed trajectories, not concerning the accuracy of the reconstructed particle positions.

7.2.2. Simulation of a vortex flow field

To test the performance of the developed algorithm a vortex flow field is simulated. The particles move circularly around a common axis parallel to the z-direction of the object coordinate system. In addition the particles move along this axis, the z-component of the motion vector is a random value out of a given interval and changes individually for each particle during the progression of the sequence. The vortex flow field is shown in Fig. 24. The visualization shows a selection of the reconstructed trajectories resulting from the PTV processing, not the simulated reference trajectories.

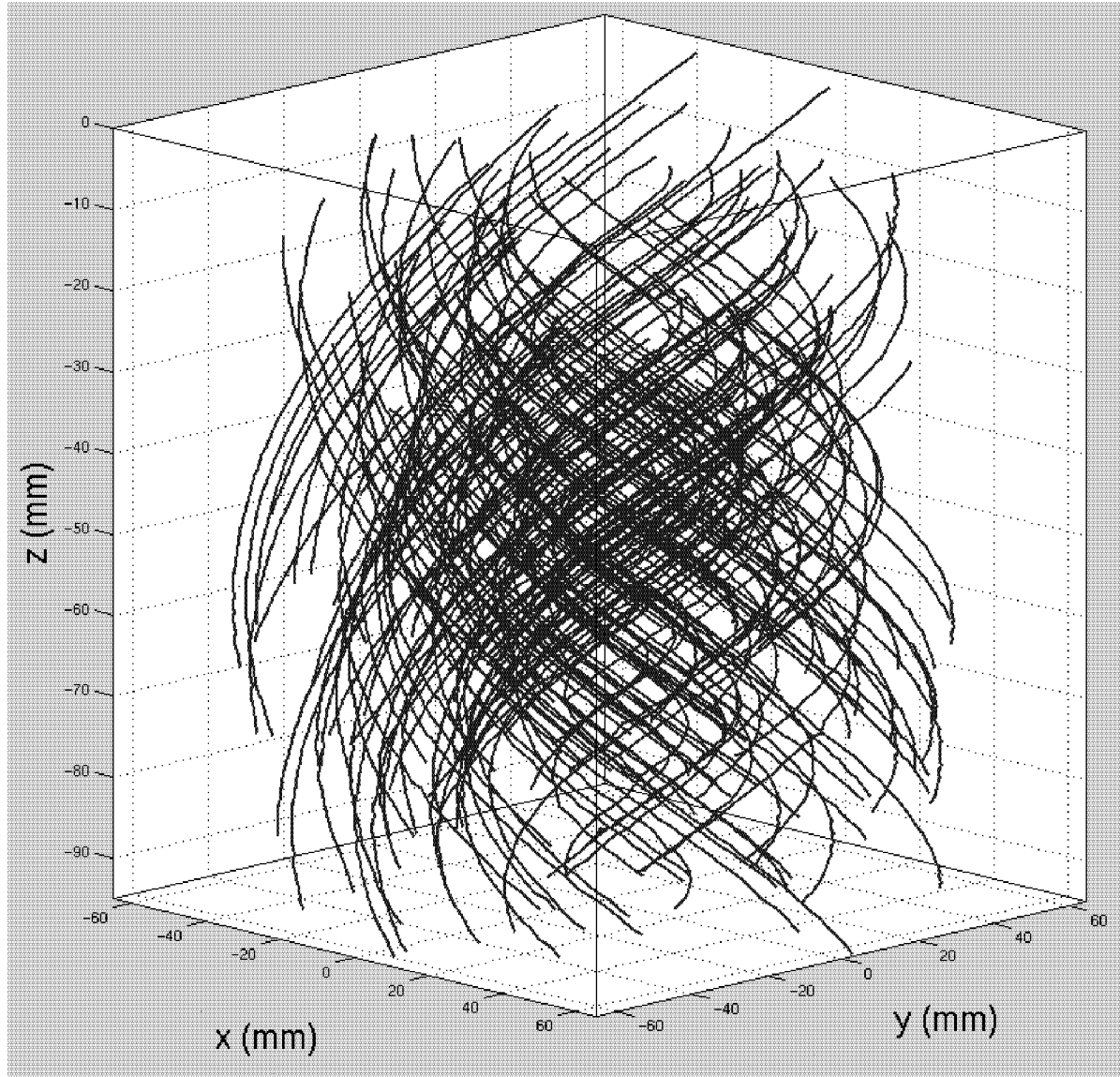


Fig. 24: Vortex flow field, showing a selection (ca. 200) of the particles, which could be tracked over the complete sequence of 51 frames

The size of a particle image is set to 3×3 pixel. The sum of grey values is individual for each particle but remains the same in each view of the cameras and is kept constant during the sequence. To simplify the generation of the sequences the backprojection of the image coordinates is performed only with integer pixel accuracy, which leads to some deviations between the simulated and reconstructed 3D positions. Depending on the simulated motion and seeding density particles can leave the object volume or overlap each other in image space. Even when four cameras are used not all ambiguities in the correspondences can be solved by the geometric constraints of the epipolar line. Therefore not all particle positions can be reconstructed per time step not to mention be tracked over the time. A particle image of the simulated vortex flow is shown in Fig. 25.

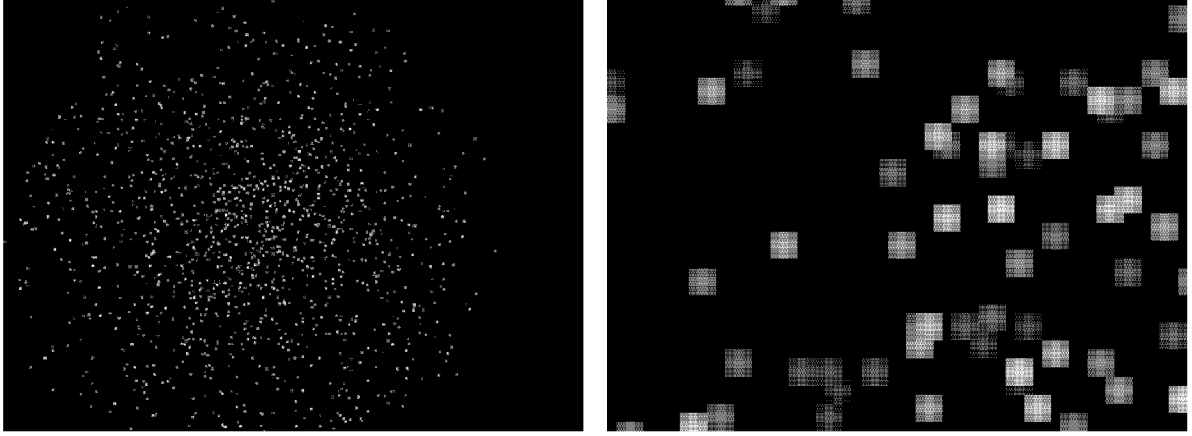


Fig. 25: Particle image of simulated vortex flow (left), detail view (right)

Due to overlapping particle images not all - less than 1350 particles per image - can be detected in image space. Therefore and due to ambiguities in the epipolar line intersection method even less particles can be reconstructed in object space. From the 1500 simulated particles around ~ 1250 per time step can be reconstructed in 3D. An important parameter for the performance of the tracking method is the number of linked particles but also the number of blunders. The number of linked particles can be specified easily, unlike the number of mismatches. Setting the tracking parameters empirically the acceptable movements of a particle are defined. The analysis of the results concerning wrong tracks can only be qualitative. Using a suitable 3D-viewer helps to review the reconstructed particle trajectories.

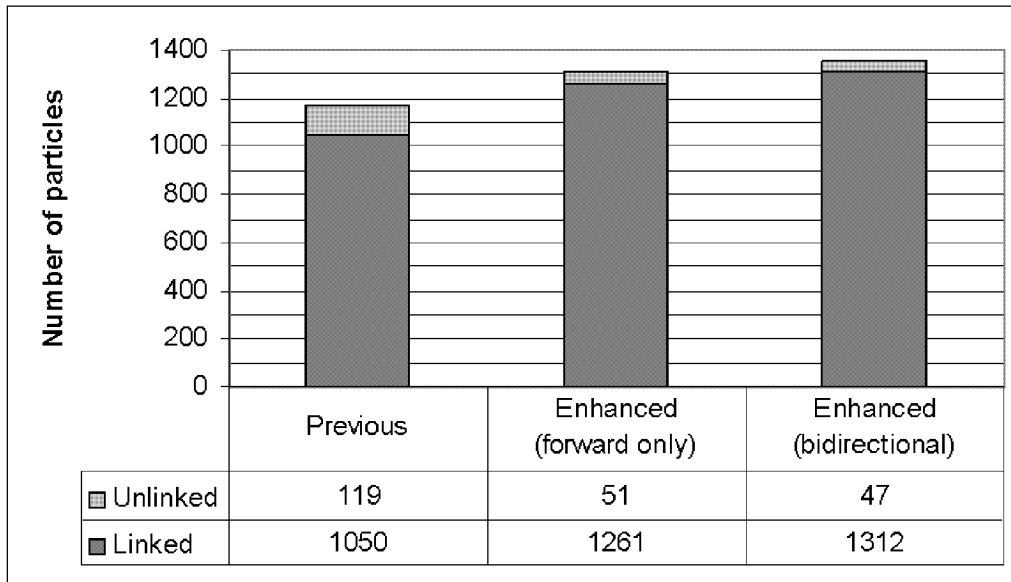


Fig. 26: Average number of particles and links over 51 time steps determined with the previous and enhanced PTV approach applied to the data set 'simulated vortex'

With suitable tracking parameters around 1050 (previous) and 1300 (enhanced) particles per time step can be tracked from one time step to the next. As a result one will get a velocity field with a high spatial resolution with a low number of mismatched particles. The application of an only object space based tracking method leads to a considerably lower number of established connections. Both the total number of reconstructed particle positions as well as the

tracking efficiency could be increased with the enhanced method. In the case of this data set the neighbouring particle motions are highly correlated. The tracking approach, which was originally developed by Papantoniou, Dracos and Malik (Malik et al., 1993) might therefore yield a higher tracking rate than the results obtained with the ‘Previous’ method (see at the beginning of this chapter). Even when applied only in forward direction, more links are established with the enhanced method than particle positions could be determined by the epipolar line intersection.

Tests with this particular data set show the advantages of the combined use of object and image spaced based information for the spatio-temporal matching. Further tests with data sets acquired during real experiments are performed to prove the operability of the method for the practical use in different flow measurement tasks.

Table 3: Performance characteristics N_{traj} , avl_{traj} and L_{traj} of the data set ‘simulated vortex’

Tracking method	Number of trajectories N_{traj}	Average trajectory length avl_{traj}	Total number of all established links L_{traj}
Previous	5’616	10.3	57’781
Enhanced (forward only)	2’710	24.2	65’564
Enhanced (bidirectional)	2’665	25.6	68’165

The sequence length was 51 time steps, as the number of particles is known and was set to 1500, in total 76500 links exist over the 51 time steps. As shown in Table 3 the average trajectory length avl_{traj} could be increased by factor ~ 2.5 . By connecting parts of trajectories the number of trajectories could be decreased to reconstruct longer trajectories. As expected not all particle positions and even more obvious not all links could be recovered from the image sequences. Nevertheless a high percentage of almost 90 % of all existing simulated links could be obtained.

As mentioned in 6.5. the distribution of the lengths of the reconstructed trajectories should differ considering the results yielded with the previous and the enhanced method. As shown in Fig. 27 the expected effects are clearly visible. In the classes of the shorter trajectories (particles tracked less than 25 time steps) the previous method generates more trajectories, but is inferior compared to the enhanced approach when the reconstruction of longer trajectories is considered. It must be noted that the axis of the number of trajectories is displayed in logarithmic scale.

The number of long trajectories decreases exponentially with the trajectory length and starting from a certain sequence length no particle might be tracked over the whole number of time steps. In other words, the maximum trajectory length will be less than the sequence length, which is equal to zero values in the frequency distribution of the trajectory lengths. In the case of the data set ‘simulated vortex’ the evaluated sequence had a limited length of 51 time steps.

Remarkable is the number of particles, which could be tracked over all time steps. With the previous method 53 particles could be tracked completely, while with the enhanced method

404 complete trajectories could be obtained. This is almost a third of all particles, which were simulated.

Despite the expected continuous decrease in the frequency distribution concerning longer trajectories in this case the class with the longest trajectories shows up with a higher frequency than preceding classes. Only 51 time steps are evaluated and all particles, which might have been tracked throughout the whole sequence are gathered in the last class of the longest trajectories. This explains the increase of the trajectory frequency at the end of the sequence. This effect not only occurs in the case of the simulated data but also in the two real experiment data sets ‘Trinocular’ (7.3.1.) and ‘forward facing step’ (7.3.2.) where only a limited number of time steps was available for the performance tests of the tracking algorithms. For the evaluation of the other data sets longer sequences were available, so that the main advantage of the enhanced method to be able to reconstruct longer trajectories should be even more visible in the trajectory length distribution.

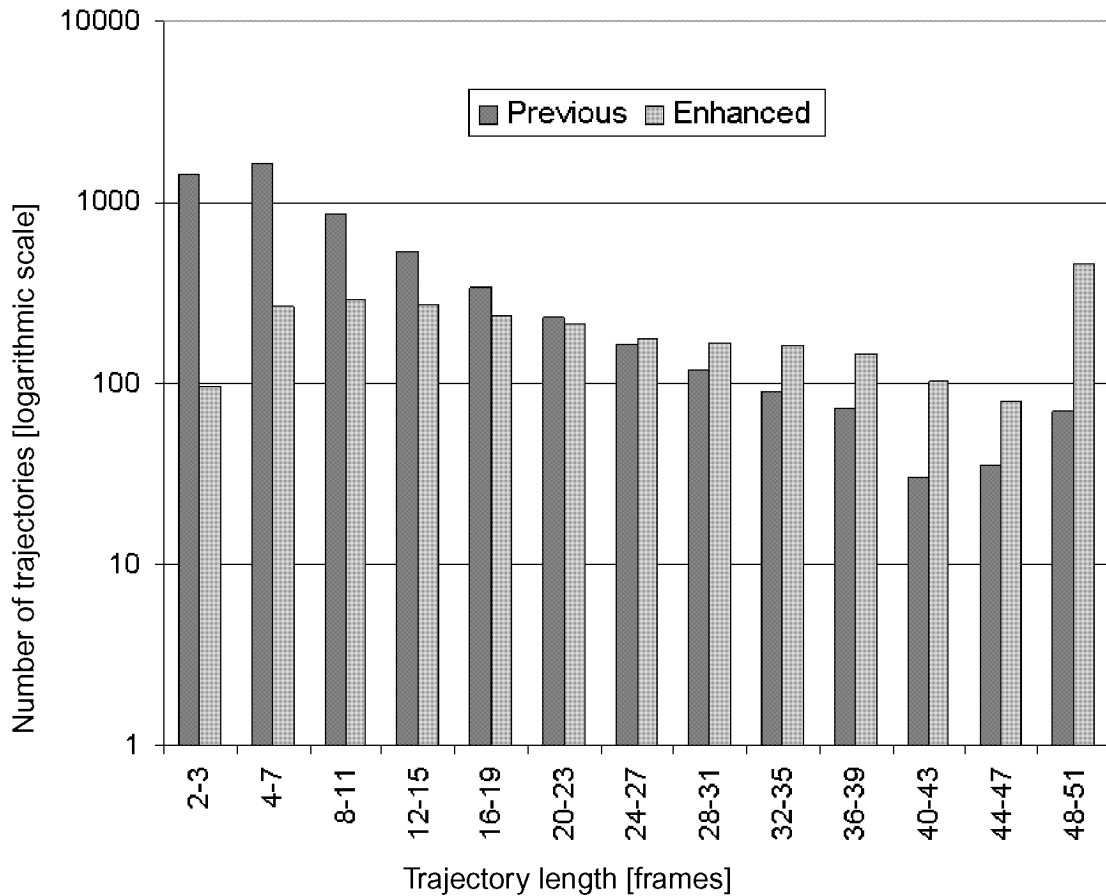


Fig. 27: Histogram of the trajectory lengths obtained with previous and enhanced PTV approach applied to the data set ‘simulated vortex’

7.3. Tests using real data

As PTV should be applied in real experiments, the method’s capability has to be tested with respective data sets. The performance of the method is influenced by many factors as the image quality, seeding density, particle velocity conditions in the flow, calibration and more. With just simulated data sets a thorough testing is not possible. For this reason various data sets from

different experiments were investigated in this section. In addition in chapter 7.4. the processing of the MASER 8 data set, which was acquired under micro-gravity conditions is described in detail. The data sets differ in many aspects as particle density, flow field character and hardware setup thus providing a good basis to prove the applicability of the developed method. For two of the experiments only a limited number of image data was available for the tests, but anyway could contribute to the performance evaluation of the tracking method.

7.3.1. Data set 'Trinocular'

This data set was obtained at the 24 m open channel flume of the ETH for the investigation of open channel flows. A three camera setup was used to record the flow field of this experiment. The cameras were mounted in a stereoscopic arrangement with their axes intersecting at about 50 degrees. A 3 Watt argon-ion laser was used to illuminate observation of 10 x 10 x 1.5 cm. The cameras and the illumination facility were mounted on a carriage system driven by a stepper motor running along the channel. Further details about the experiment can be found in (Papantoniou/Dracos, 1990) and (Papantoniou/Maas, 1990), a description of the water channel is given in (Bertschler, 1985).

The data set was acquired with the first PTV hardware setup at ETH; nevertheless it is suitable to test the performance of the tracking methods. The images acquired by Aqua-TV HR480 cameras with 1/2" frame transfer integration. Since video disks or image sequence memory were not available the video data was intermediately stored on three analogue video recorders and were digitized afterwards to a resolution of 512 x 512 pixels at a frame rate of 25 Hz.

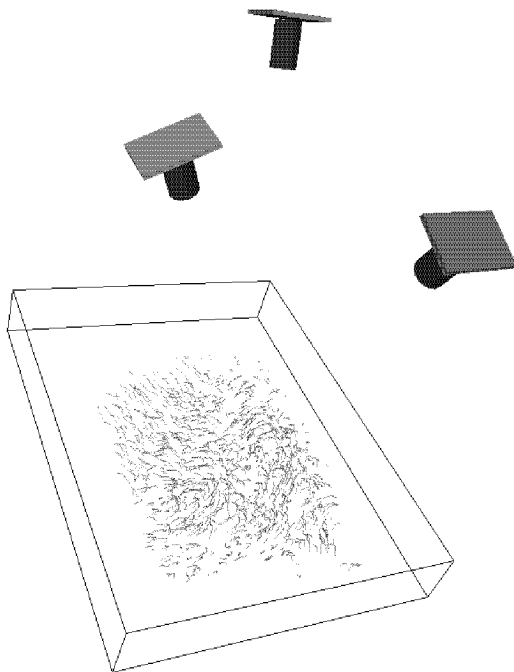


Fig. 28: Configuration with three cameras

To be able to read corresponding images from the videotapes, a synthetic binary pattern, which codes a sequential image number, is added to the video signal of all three cameras. Despite the intermediate storage causing deterioration of the signal the quality of the image sequence was high. The number of time steps used for the tests was 31. The camera arrangement for this experiment is shown in Fig. 28, the optical axes of the cameras are convergent forming a tetrahedron, which leads to well-defined intersections of the epipolar lines. The calibration accuracy were quite high, nevertheless the epipolar intersection led to a certain number of ambiguities, which might partly have been solved by a four camera setup. Making use of the spatio-temporal context these ambiguities could be solved even when only three cameras are used for the image acquisition. The reconstructed velocity field is shown in Fig. 29. As shown in Fig. 30 the number of

links was increased by almost 40 % while at the same time the number of unlinked particles was reduced. In other words, regarding this data set it was possible to establish more links with the enhanced method than 3D particle positions with the previous approach.

The increased tracking efficiency also has a strong influence on the length of the reconstructed trajectories. The average trajectory length $av l_{traj}$ could be increased by factor ~ 2 (see Table 4).

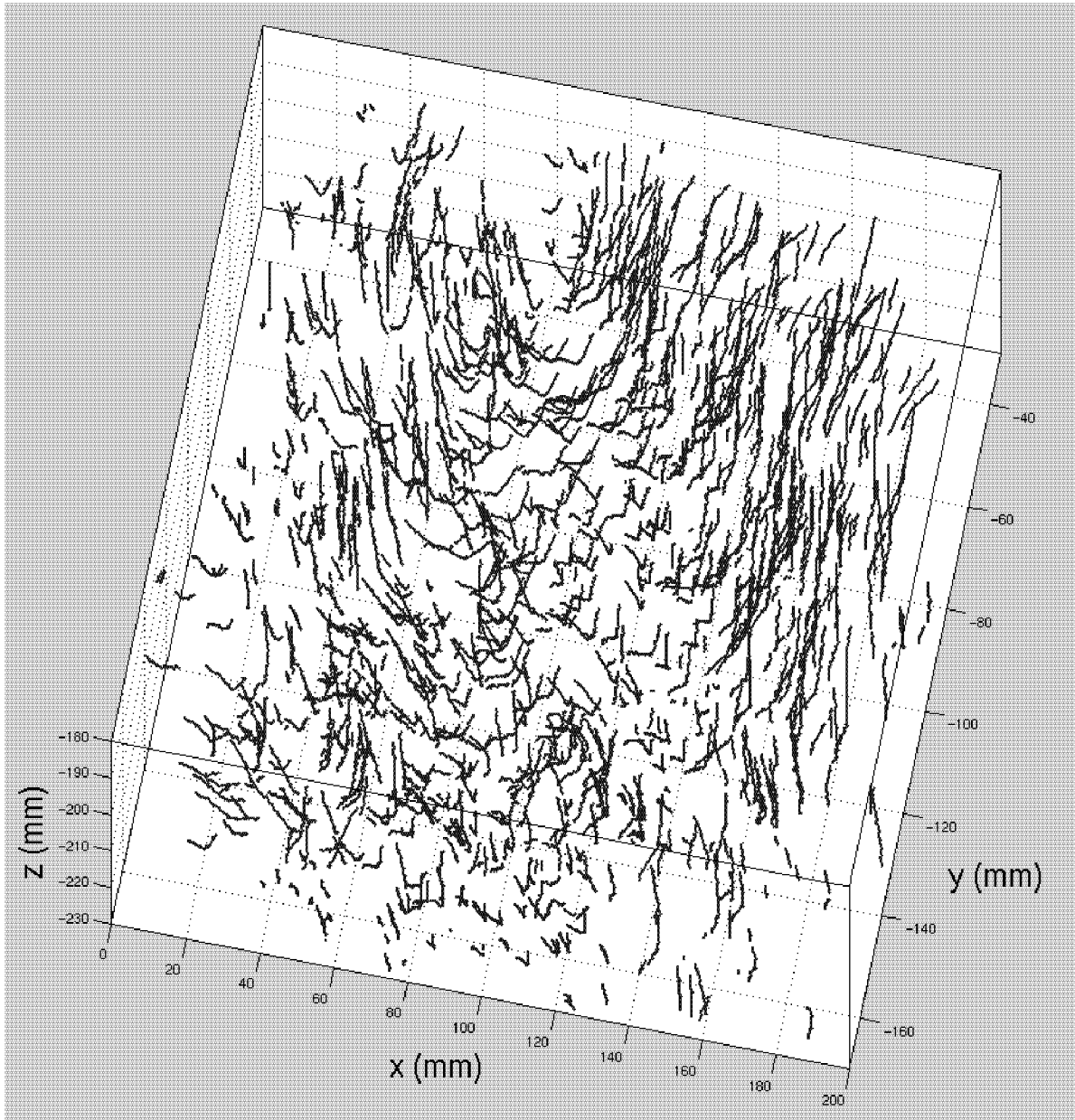


Fig. 29: Velocity field 'Trinocular', showing all trajectories tracked longer than 4 frames

As the available image sequence of this experiment is limited to 31 frames both tracking approaches could track a certain number of the particle throughout the complete sequence. The previous method was able to track 82 particles over the entire sequence while with the enhanced method 204 complete trajectories were obtained. The number of trajectories longer than 15 frames could be increased from 294 to 590.

Table 4: Performance characteristics N_{traj} , avl_{traj} and L_{traj} of the data set ‘Trinocular’

Tracking method	Number of trajectories N_{traj}	Average trajectory length avl_{traj}	Total number of all established links L_{traj}
Previous	2’240	7.7	17’243
Enhanced (forward only)	1’569	13.4	20’949
Enhanced (bidirectional)	1’567	14.3	22’391

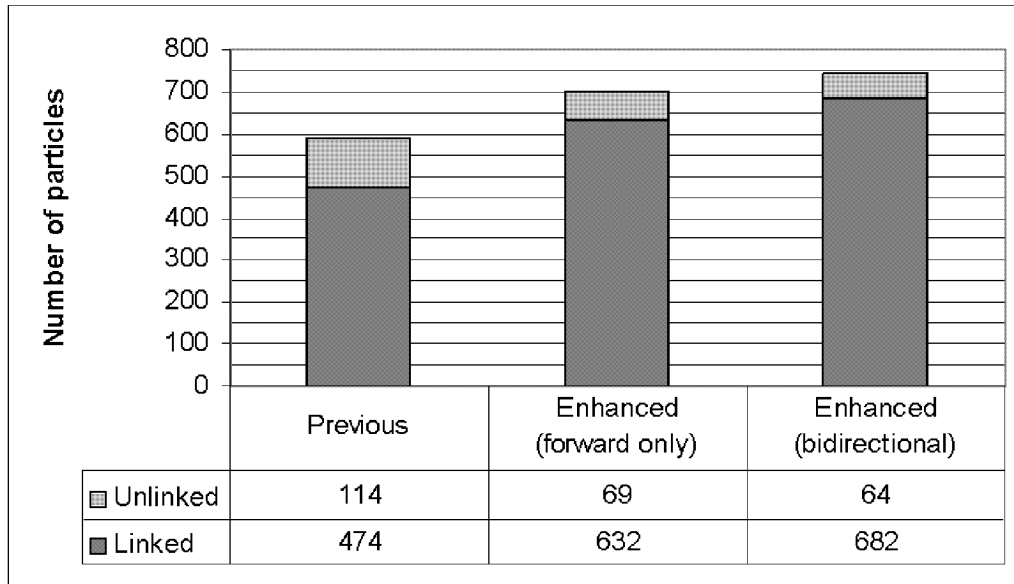


Fig. 30: Average number of particles and links over 31 time steps determined with the previous and enhanced PTV approach applied to the data set ‘Trinocular’

The frequency distribution of the trajectories (Fig. 31) shows that the enhanced approach is significantly superior in the reconstruction of longer trajectories (longer than 12 time steps) compared the previous method. Except of the already explained gathering effect due to limited sequence length the characteristic of the frequency distribution is in good coherence to the expected improvements (as mentioned in 6.5.) and the results of the evaluation of the simulated data set described in section 7.2.2.

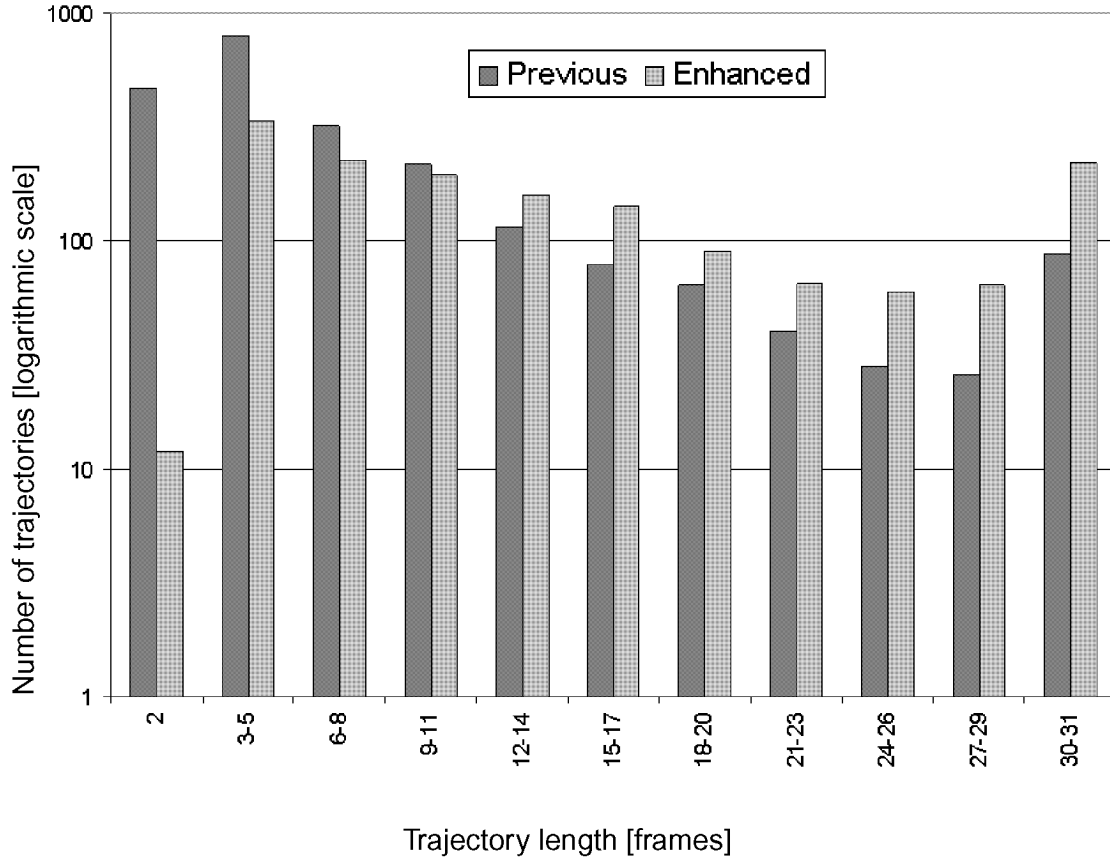


Fig. 31: Histogram of the trajectory lengths obtained with previous and enhanced PTV approach applied to the data set ‘Trinocular’

7.3.2. Data set ‘Forward facing step’

In the framework of ‘Investigations of separation on a forward facing step’ data sets were acquired at ETH. Stürer performed the research work (Stürer, 1999). As the data set described in 7.3.1. the measurement was conducted in the open water channel, for details about the experiment facility see (Virant, 1996) and (Bertschler, 1985). A regulated radial pump pumps water in a closed circuit and the throughput is controlled by a magneto-inductive flow-meter. The cross section of the test area was 560 mm x 80 mm and the entry length was long enough to get a fully developed laminar parabolic flow field in the observation area. The height of the step was 20 mm over the whole span. This gave a channel height to step height aspect ratio of 4:1. The flow field was still laminar with an unsteady recirculation zone in front and on the step. The observation volume was 80 mm x 100 mm x 30 mm and placed at a fixed position in the middle of the channel and on top of the forward facing step. Particles enter and leave the observation volume and for this reason it is obvious that particle cannot be tracked for infinite time.

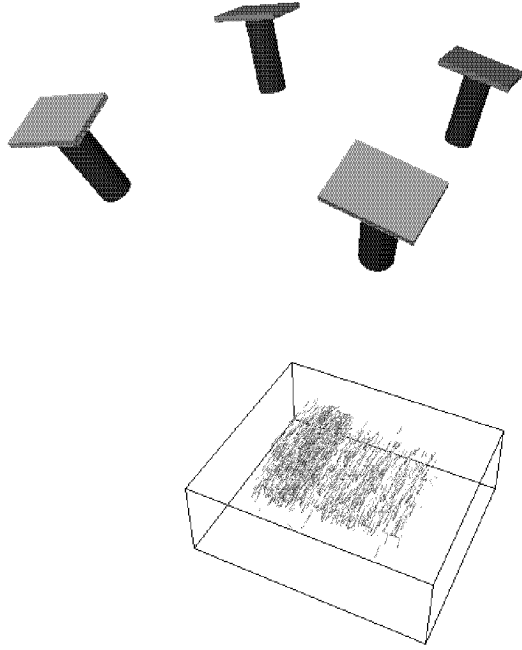


Fig. 32: Four camera arrangement used for observation of flow separation at a forward facing step

The flow to be investigated was seeded with flow markers with a diameter of 40 - 63 μm . The observation volume is illuminated by two 400-Watt halogen-short-arc lamps, which have a high output efficiency of polychromatic light. The motion of the flow markers are continuously recorded by four CCD cameras (RS170, Jai CV-M10, progressive scan) with a spatial resolution of 640 x 480 pixels and a temporal resolution of 30 Hz. The chipsize of these CCD cameras is 1/2". The cameras are synchronized by a master and slave setup and operating in shutter mode so that the short exposure time avoids a streaky imaging of the moving particles.

The images of the four cameras are digitized and losslessly compressed by two frame-grabbers (Matrox Genesis) and stored in real-time on hard disc via two RAID controllers. This procedure has the advantage that the degradation of the

images is minimized and it facilitates a long measurement time (the reliability of the system was tested for a measuring time of 2 minutes, even longer measurement times should be possible). The four-camera arrangement of this experiment is shown in Fig. 32. The distribution of the particles of the flow was quite inhomogeneous and the seeding density can be considered as rather high, additionally some disturbances occurred due to scratches and stains on the bottom of the channel leading to some mismatches in the establishment of correspondences. The reconstructed velocity field is shown in Fig. 33. The forward facing step itself is not included in this visualization. The number of particles was around 1400; the number of established links was more than 800 with the previous method reaching more than 1000 links with the enhanced method. The results concerning the number of particles and links are shown in Fig. 34.

Table 5: Performance characteristics N_{traj} , avl_{traj} and L_{traj} of the data set ‘forward facing step’

Tracking method	Number of trajectories N_{traj}	Average trajectory length avl_{traj}	Total number of all established links L_{traj}
Previous	1915	5.2	9'971
Enhanced (forward only)	1818	6.2	11'316
Enhanced (bidirectional)	1814	6.6	11'975

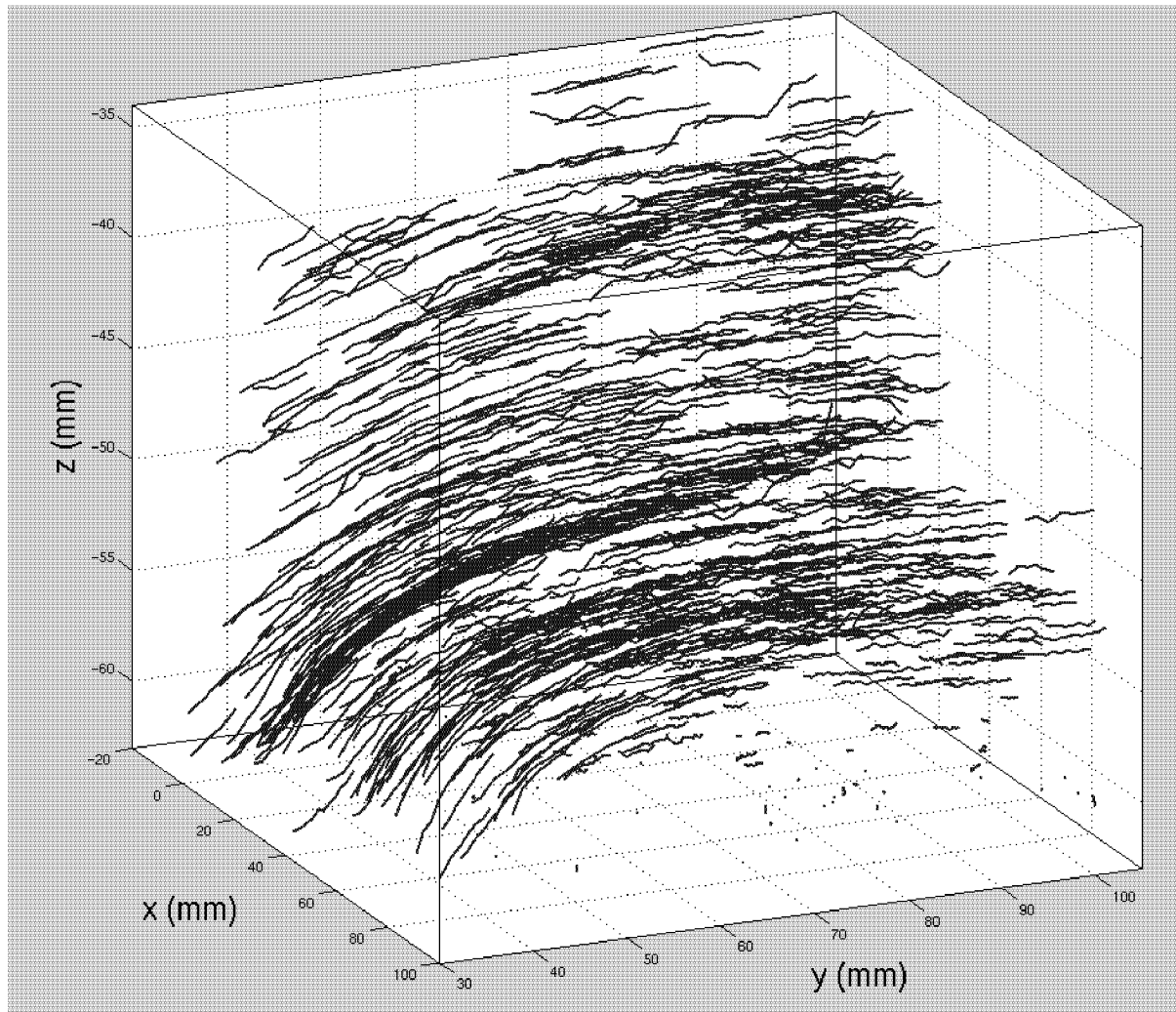


Fig. 33: Velocity field forward facing step, showing the trajectories longer than 5 frames

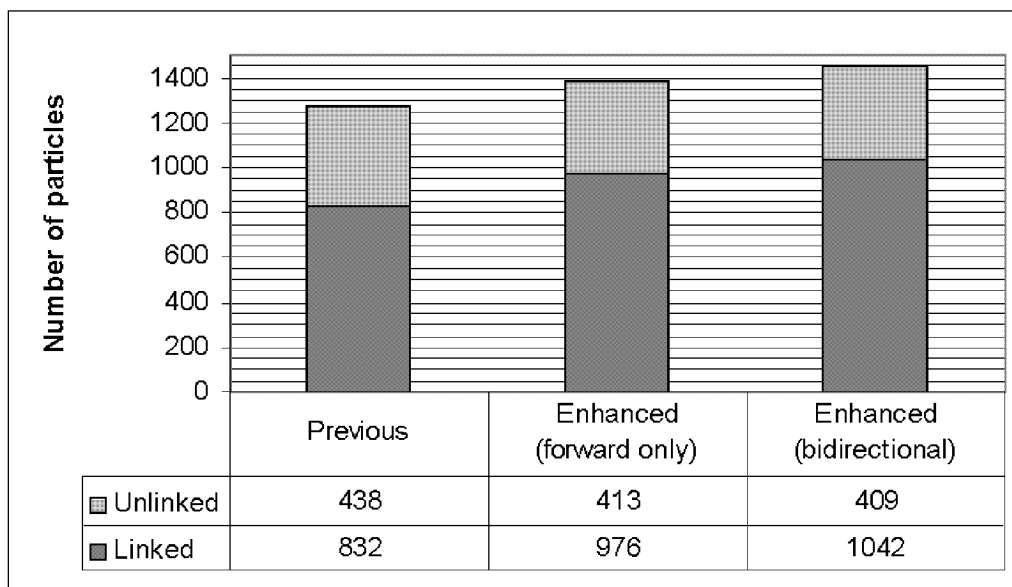


Fig. 34: Average number of particles and links over 11 time steps determined with the previous and enhanced PTV approach applied to the data set 'forward facing'

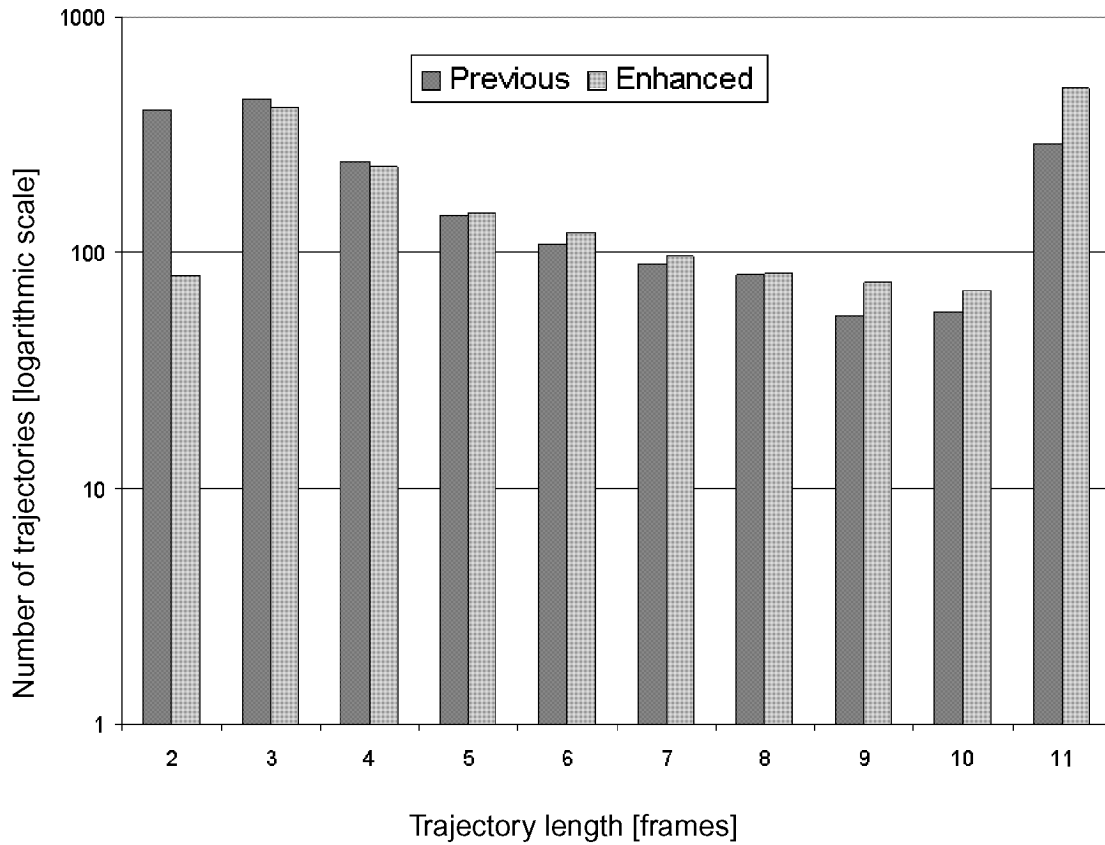


Fig. 35: Histogram of the trajectory lengths obtained with previous and enhanced PTV approach applied to the data set ‘forward facing step’

The tracking efficiency for both tracking approaches was rather low, which is maybe caused by the high particle density and the disturbances mentioned above.

The average trajectory length avl_{traj} could not be increased as significantly as in the other presented data sets, which simply may be caused by the limited number of time steps (Table 5). For this experiment a sequence of only 11 time steps was available for the performance tests. Therefore the number of particles that could be tracked over the complete sequence is rather high. The previous method delivered 286 complete trajectories compared to 499 with the enhanced approach.

The frequency distribution of the trajectory lengths in Fig. 35 shows advantages of the enhanced method starting from a trajectory length of 4 time steps. Due to the fact that only a limited sequence of 11 time steps was available for the evaluation the frequency distribution again increases at the end of the sequence.

7.3.3. Data sets for investigation of velocity derivatives

Within the research work for the investigation of velocity derivatives in turbulent flows a series of data sets were acquired at ETH. Lüthi and Burr performed the research work. The experiment and the discussion of the results can be found in (Lüthi et al., 2001). A full description about the research work is given in the Ph.D. thesis of Lüthi (Lüthi, 2002). The motivation for this research work was to make use of the essentially Lagrangian method of 3D PTV to elucidate some mechanisms of turbulence that previous Eulerian approaches could not access. The

results of the 3D PTV measurements were used to derive the field of velocity derivatives, which remained inaccessible until recently.

In the following sections the experimental setup designed to generate a turbulent flow by electromagnetic forcing will be described, some brief considerations about flow characteristics as Lagrangian length scale and Kolmogorov time are given.

In the sections 7.3.3.6., 7.3.3.7. and 7.3.3.8. the evaluation of the three different data sets ‘copper sulphate’, ‘1.0’ and ‘2.5’ performed for this research work are described.

7.3.3.1. Turbulent flow generation by electromagnetic forcing

In the experiment turbulent flows with velocity derivatives measurable through 3D PTV should be produced. It was decided to use a setup where the flow domain is a rectangular box with the flow forced electromagnetically from two opposite walls. The forcing is accomplished through the Lorentz forces f_l . Two 4 by 4 arrays of cylindrical rare earth sintered strong permanent magnets (RECOMA 28, 42 mm in diameter, strength 1 Tesla) were mounted on the two opposite side walls of the tank. The flow was produced as schematically shown in Fig. 36.

The magnets were arranged in such a way that positive and negative magnetic fluxes alternate, forming a chessboard pattern. Copper plates placed in front of each array serve as electrodes. The tank is filled with an aqueous copper sulphate (CuSO_4) test fluid. A DC electric current of

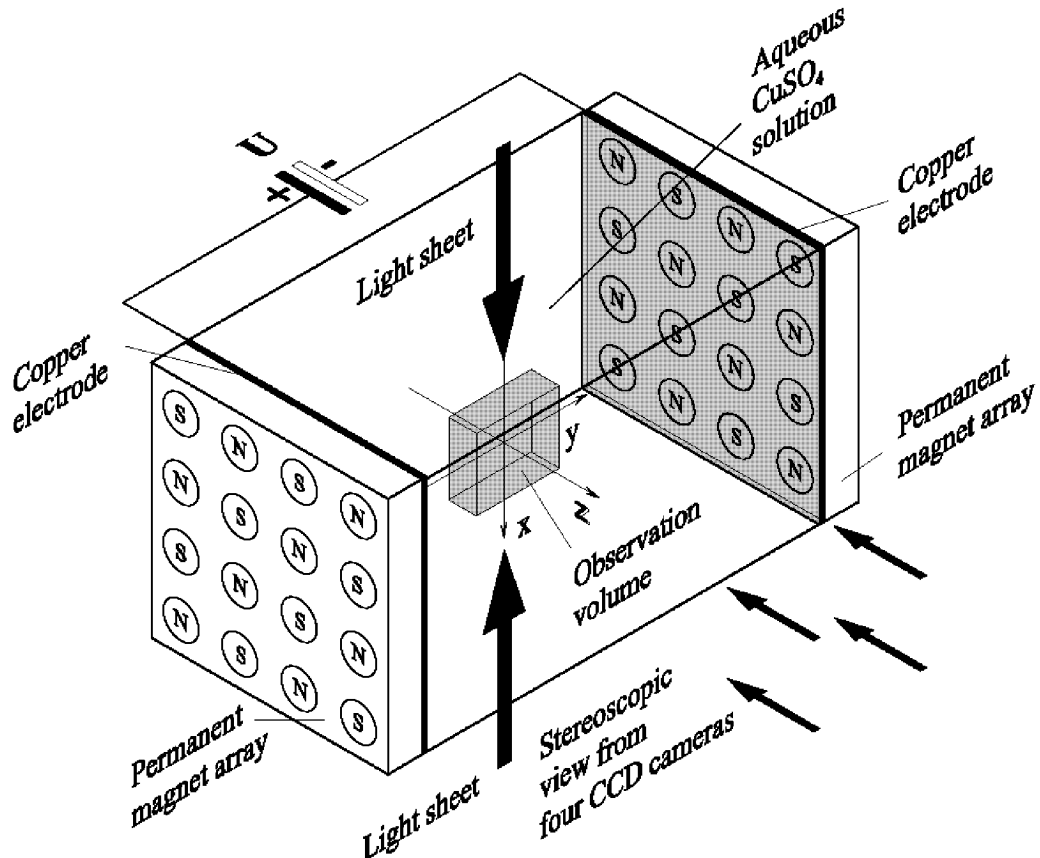


Fig. 36: Schematic of the experimental facility and coordinate system (x,y,z), taken from (Lüthi, 2002). Electromagnetic forcing from two opposite walls produces swirls over each magnet. At short distances of the walls the flow becomes three dimensional and towards the observation volume fully turbulent. The flow is recorded by four CCD cameras at recording rates of first 30Hz and - in a later stage - at 60Hz.

up to 7 A was applied and from the interaction of the current density, j , with the magnetic field B , Lorentz forces, f_l , are induced, according to:

$$f_l = j \times B \quad (18)$$

The forcing produces a non-oscillating swirling motion in the proximity of each magnet. Within a few seconds these circulations cause a three dimensional time dependent flow region with a front that quickly propagates towards the center resulting in a turbulent velocity field with zero mean flow and fluctuations, \bar{u}_i in the order of $O(0.01\text{m/s})$, occupying the entire volume of the tank. From observation of the experiment it becomes clear that in the proximity of the copper plates the flow is more intense, while less isotropic than in the observation volume, which is located in the center of the tank. Not the whole area between the copper plates was observed. The cameras were focused on the central part of the water tank. The experiments were conducted in two different setups.

7.3.3.2. Length scale and Kolmogorov time

To clarify the terminology used below some equations and scale definitions important for the performance evaluation of the tracking approaches are given here.

For a reliable Lagrangian analysis of an observed flow field a certain minimum trajectory length is required. This minimum trajectory length (in time steps or travel distance) is depending on the temporal resolution of the image acquisition and the characteristics of the observed flow itself and can be estimated by a-priori known specifications or derived from measurements results. Particle trajectories, which are longer than the relevant so-called Kolmogorov scales are the key prerequisite for a Lagrangian flow analysis (see in (Kolmogorov, 1941a), (Kolmogorov, 1941b) and (Frisch, 1995)). From a simple numerical model for the Lorentz force field, eq. (18), the total Lorentz forces over the magnets can be estimated to be ~ 0.03 N. Since ϵ is defined as the mean dissipation of energy per unit mass and time, the following expression can be used to estimate ϵ of the entire flow:

$$\epsilon \sim \frac{N \cdot \langle u_M \rangle}{vol \cdot \rho} \quad (19)$$

With the mean velocity $\langle u_M \rangle$ of the particles, the volume of the water tank vol and the density of fluid ρ the dissipation ϵ can be calculated. The equations (20) allow the estimation of the Kolmogorov scale η and the Kolmogorov time τ_η if the dynamic viscosity ν of the copper sulphate fluid is known:

$$\eta = \left(\frac{\nu^3}{\epsilon} \right)^{\frac{1}{4}} \quad \tau_\eta = \left(\frac{\nu}{\epsilon} \right)^{\frac{1}{2}} \quad (20)$$

The knowledge of the Kolmogorov scale η respectively the Kolmogorov time τ_η helps to evaluate the quality and significance of the tracking results yielded with the different tracking methods. They define the minimum trajectory length, which is required to be sufficient for a Lagrangian analysis. As the number of too short trajectories might be high a reliable performance evaluation requires the knowledge or at least of an estimation of these relevant scales. For the detailed determination of the Kolmogorov scale η and the Kolmogorov time τ_η for the experiments ‘copper sulphate’, ‘1.0’ and ‘2.5’ see (Lüthi, 2002). For the experiments ‘copper sulphate’ and ‘1.0’ τ_η was derived from the measured velocity field to 10 respectively to 14 frames. As τ_η was not determined from the measurement results for the data set ‘2.5’ only an

estimation of around 8 frames can be given here. According to these values the number of suitable trajectories can be calculated, serving as performance meter of the applied tracking approaches.

7.3.3.3. Setup for the experiment ‘copper sulphate’

In a first experiment a quasi-isotropic turbulent was produced inside a $320 \times 320 \times 170 \text{ mm}^3$ water tank. The hardware configuration for this experiment is shown in Fig. 37. The turbulent flow produced for the experiment ‘copper sulphate’ was forced with a DC current of 7 A. The flow was seeded with polystyrene particles with a diameter of $40 - 60 \text{ }\mu\text{m}$. The seeding density of the detected particles is around $50 \text{ particles/cm}^3$, which corresponds to a mean particle distance of $\sim 2.7 \text{ mm}$. The volume observed by the four cameras was located in the central part of the tank and had a size of around $20 \times 20 \times 20 \text{ mm}^3$.

The calibration target was a regular array of 7×9 points with a grid distance of 2 mm resulting in a size of $14 \times 18 \text{ mm}^2$. To provide full coverage over the observed object volume the plane calibration target was recorded in three different z-positions directly measured with a micrometer.

The tolerance to the epipolar line was set to $20 \text{ }\mu\text{m}$. In addition the depth range of the illuminated and therefore observed object volume can be considered as large. The rather large dimension in viewing direction leads to longer epipolar line segments along, which possible candidates are searched for. As the lenses provide only limited depth of focus this again results in suboptimal particle images in regions further away from the focused object distance. All this led to a high number of ambiguities in the epipolar line intersection method and to many unmatched particle detections.

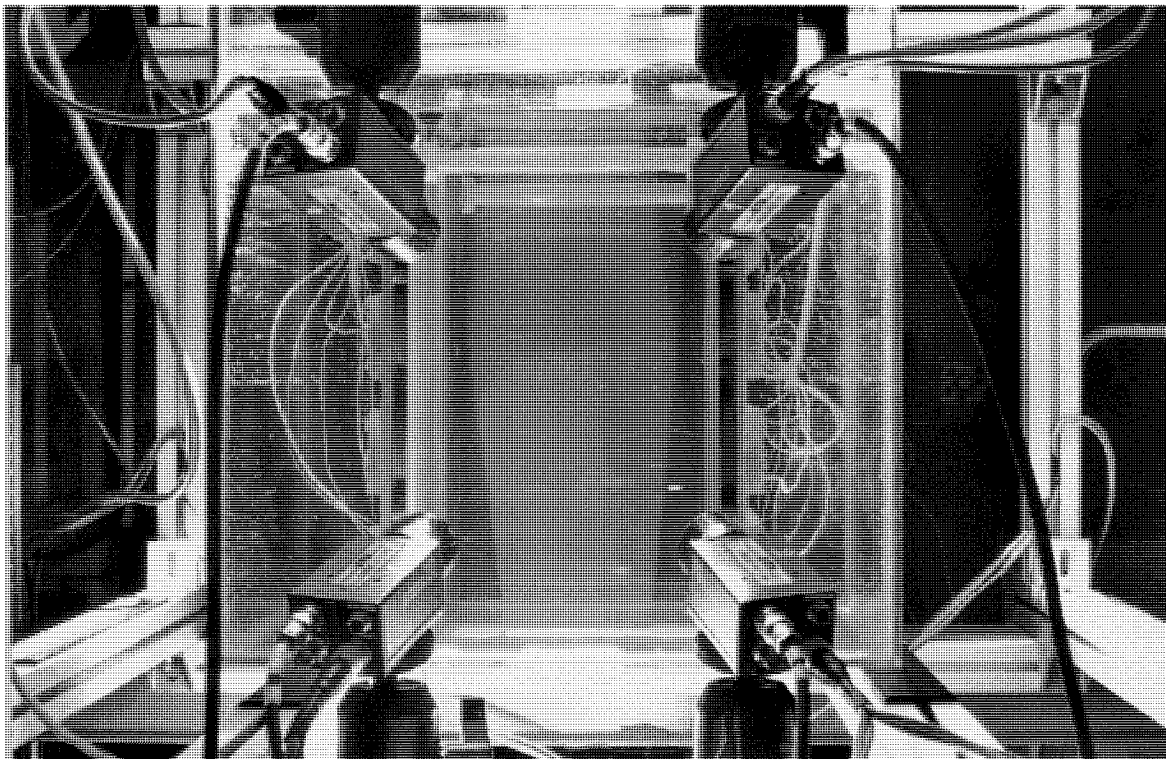


Fig. 37: Hardware configuration for the first experiment flow in ‘copper sulphate’ fluid

7.3.3.4. Setup for the experiments ‘1.0’ and ‘2.5’

Two further experiments were performed with a optimized experimental setup (the modifications are described in 7.3.3.5.). For both experiments ‘1.0’ and ‘2.5’ the flows again were produced electromagnetically but in a much smaller volume of $120 \times 120 \times 140 \text{ mm}^3$. The test fluid can be handled in much easier fashion considering filtering and the contamination with disturbing oxygen bubbles. From the estimated and later measured Kolmogorov time τ_η it became desirable to have a flow with comparable velocities but smaller time scales to increase recording time compared to the first experiment. Fig. 38 shows the hardware configuration for the data acquisition of the smaller object volume.

As the particles used in the first experiment appeared slightly too large in image space only particles with a diameter of $40 \text{ }\mu\text{m}$ were used to visualize the flow. For a better spatial resolution the seeding density was increased to $75 \text{ particles/cm}^3$, which corresponds to a typical particle distance of $\sim 2.3 \text{ mm}$. For the experiments ‘1.0’ and ‘2.5’ the four cameras observed a volume with a size of around $20 \times 20 \times 30 \text{ mm}^3$.

A reference body with 36 points distributed in a volume of $18 \times 15 \times 7 \text{ mm}^3$ was used for the calibration. Actually the reference body was produced for a former project described in (Stürer et al., 1999a) and has larger dimensions than the values mentioned above. Due to the smaller volume, which was observed in these experiments only a part of the reference information was used to perform the calibration.

Fig. 39 shows an example of a sequence image acquired for the experiment ‘2.5’. For the data sets ‘1.0’ and ‘2.5’ the experiment setup was identical, but the observed velocity field was generated with different electric currents resulting in a slower or faster motion of the tracer particles and changed turbulence conditions. The flow produced for the experiment ‘1.0’ and ‘2.5’ were forced with a DC current of 1.0 A respectively 2.5 A .

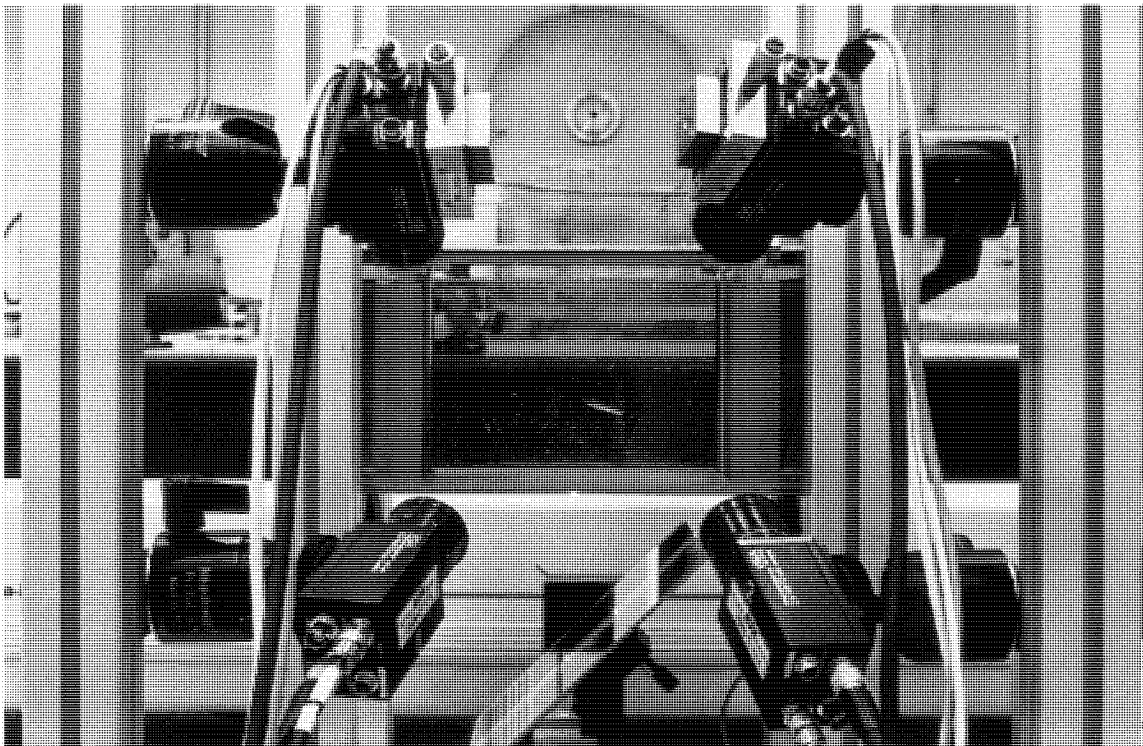


Fig. 38: Hardware configuration used for the data acquisition for the experiments ‘1.0’ and ‘2.5’

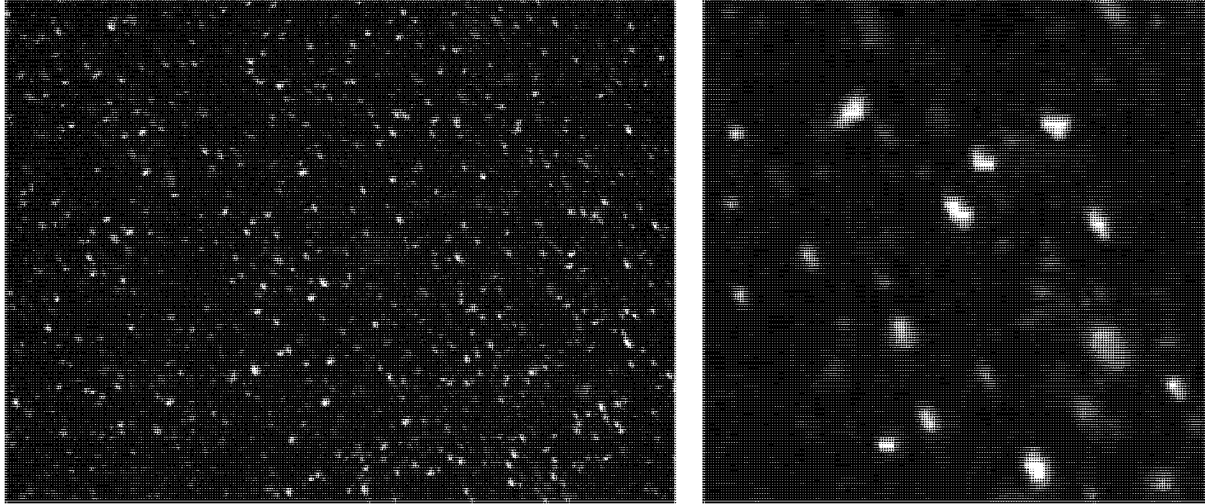


Fig. 39: Example of a sequence image from data series '2.5' (left), detailed view (right)

7.3.3.5. Optimization of the experimental setup

The turbulent flows in the aqueous copper sulphate test fluid were recorded by the same Jai CV-M10 cameras as used for the image acquisition for the experiment described in section 7.3.2., again providing a resolution of 480 x 640 pixels. The cameras were equipped with Rodenstock macro lenses. For the first experiment 'copper sulphate' the synchronized images were stored on two PCs, Pentium 200 MHz, SCSI, with 30 frames/s. Each PC has a Matrox Genesis frame grabber card (GEN/F64/8/STD) from which a RAID controller simultaneously writes the images to three hard disks. In total 1800 frames referring to 60 s can be recorded. During the 60 s the data rate is 36 MB/s. The observation volume was illuminated by two 400-Watt metal halide lamps. The high power of the metal halide lamps produces a significant amount of heat leading to unwanted thermal forcing in the observation volume.

The second experiment setup used for the acquisition of the data sets '1.0' and '2.5' differed from the first with respect to three items:

- The experiment was placed in a smaller tank
- The images were recorded with a frame rate of 60 Hz
- The illumination facility was replaced

The reasons for the development of a 60 Hz cameras system was the promise of an improved traceability of particles and an increased number of frames per Kolmogorov time τ_η as compared to the first experiment 'copper sulphate'. Based on the existing 30 Hz setup the new system has been custom developed by *BS Engineering*. The storing of the image sequences has been identified as problematic as even the elaborate technique with RAID controllers produces internal overflows. In collaboration with *BS Engineering* the system was changed in that way that the images are stored in two PCs 4 GB RAM memories. The system is now capable to record sequences of 100 s at a data rate of 72 MB/s, which corresponds to 6000 frames, as compared to 1800 frames of the former setup. For the illumination of the second experiment a continuous 20 Watt Argon Ion Laser was used, the light source offers an improved ease of handling and provides less thermal energy to the observation volume that the flow is no longer influenced by buoyant forcing.

As Lüthi showed in (Lüthi, 2002) the overall performance improved not only in quality but also in the amount of statistical data available.

7.3.3.6. Experiment ‘copper sulphate’

For this experiment a sequence over 200 frames was available to test the PTV approaches. The electromagnetically generated flow field was turbulent with swirling motion and vortexes. The obtained flow is shown in Fig. 40, for visualization purpose only the trajectories longer than 50 frames are displayed. Neither with the previous nor with the enhanced tracking method it was possible to track a particle over the entire sequence of 200 frames.

As shown in Fig. 41 the number of links could be increased by 54 %. The average trajectory length avl_{traj} could be increased by more than factor ~ 2 , which were obviously yielded by the connection of trajectory fragments as the total number of tracks was reduced significantly (see in Table 6). The longest trajectory obtained with the previous method was tracked over 65 frames while the enhanced approach could track a particle over 110 time steps. As the image sequences processed and discussed above only had a limited length, the recording time of this data set was long enough (as no particle could be tracked over the entire sequence) to show the

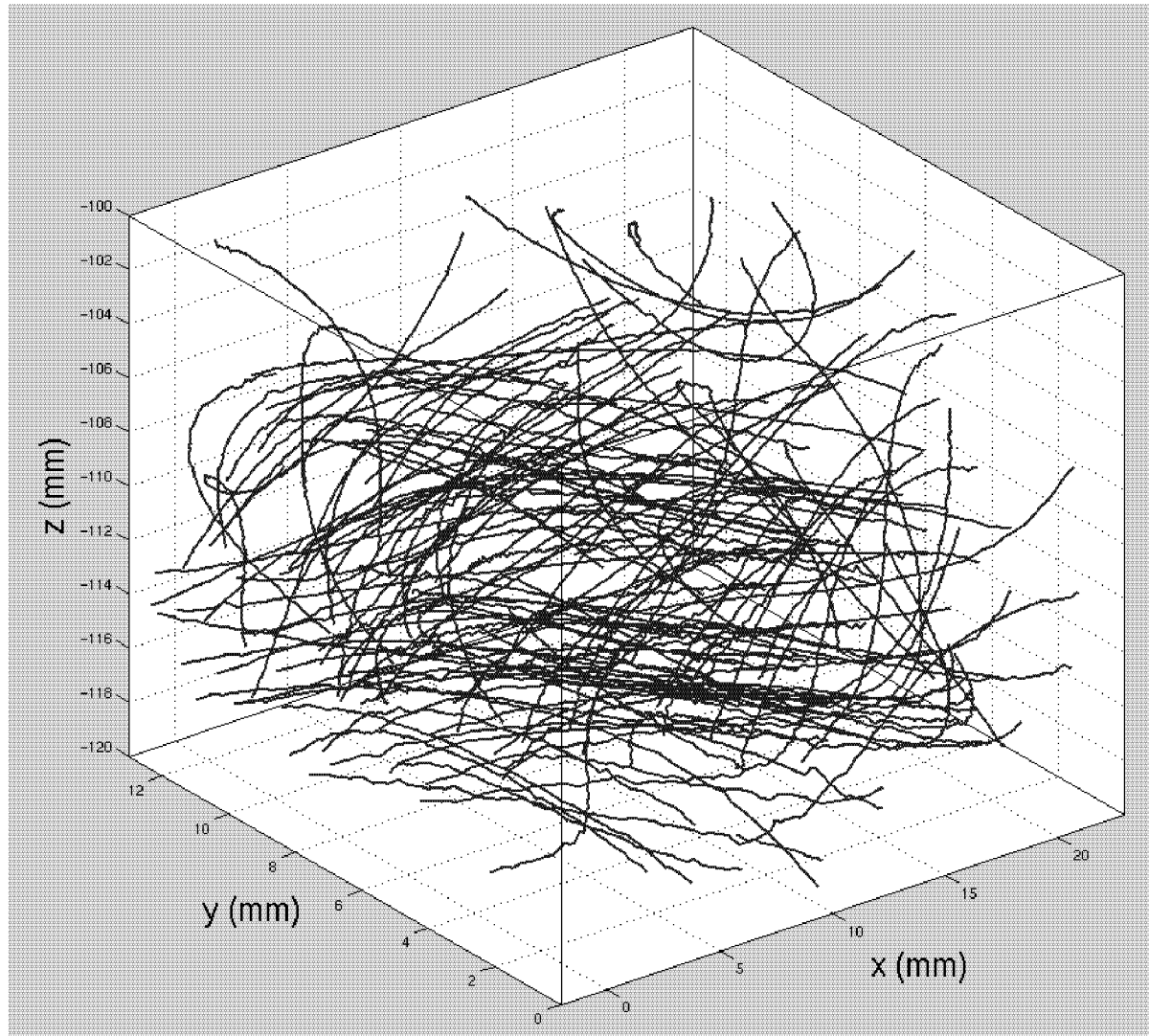


Fig. 40: Velocity field ‘copper sulphate’, showing the trajectories longer than 50 frames

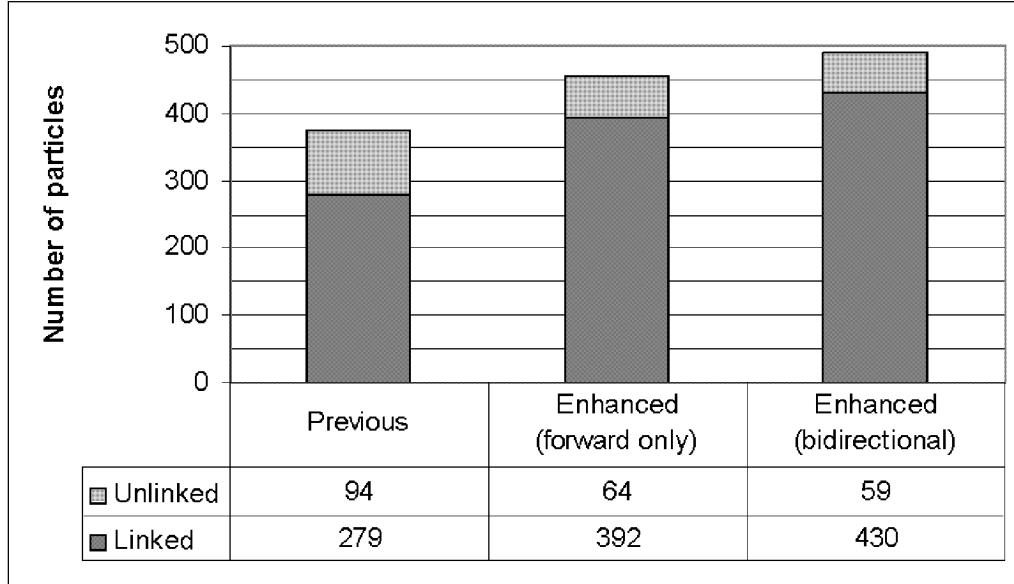


Fig. 41: Average number of particles and links over 200 time steps determined with the previous and enhanced PTV approach applied to the data set ‘copper sulphate’

expected frequency distribution without the increase of the frequency in the class of the longest trajectories. With increasing trajectory length the frequency of trajectory of that specific length decreases.

Table 6: Performance characteristics N_{traj} , avl_{traj} and L_{traj} of the data set ‘copper sulphate’

Tracking method	Number of trajectories N_{traj}	Average trajectory length avl_{traj}	Total number of all established links L_{traj}
Previous	6'283	8.3	51'945
Enhanced (forward only)	3'690	18.1	66'811
Enhanced (bidirectional)	3'596	20.7	74'294

Fig. 42 clearly shows this effect and the advantages of the enhanced method compared to the previous tracking approach. For a better visualization, the histogram of the trajectory lengths (Fig. 42) does not include all trajectory length classes (sequence length 200 frames), as only one single particle could be tracked longer than 90 time steps. The histogram is in good coherence to the expectations stated in section 6.5.; the capability to reconstruct long trajectories is significantly improved. Starting from a trajectory length of 15 frames the enhanced method is superior compared to the previous approach. Regarding to Lagrangian analysis the Kolmogorov time τ_η was determined to a minimum length of 10 frames for this flow field and is marked with a black dashed line in Fig. 42.

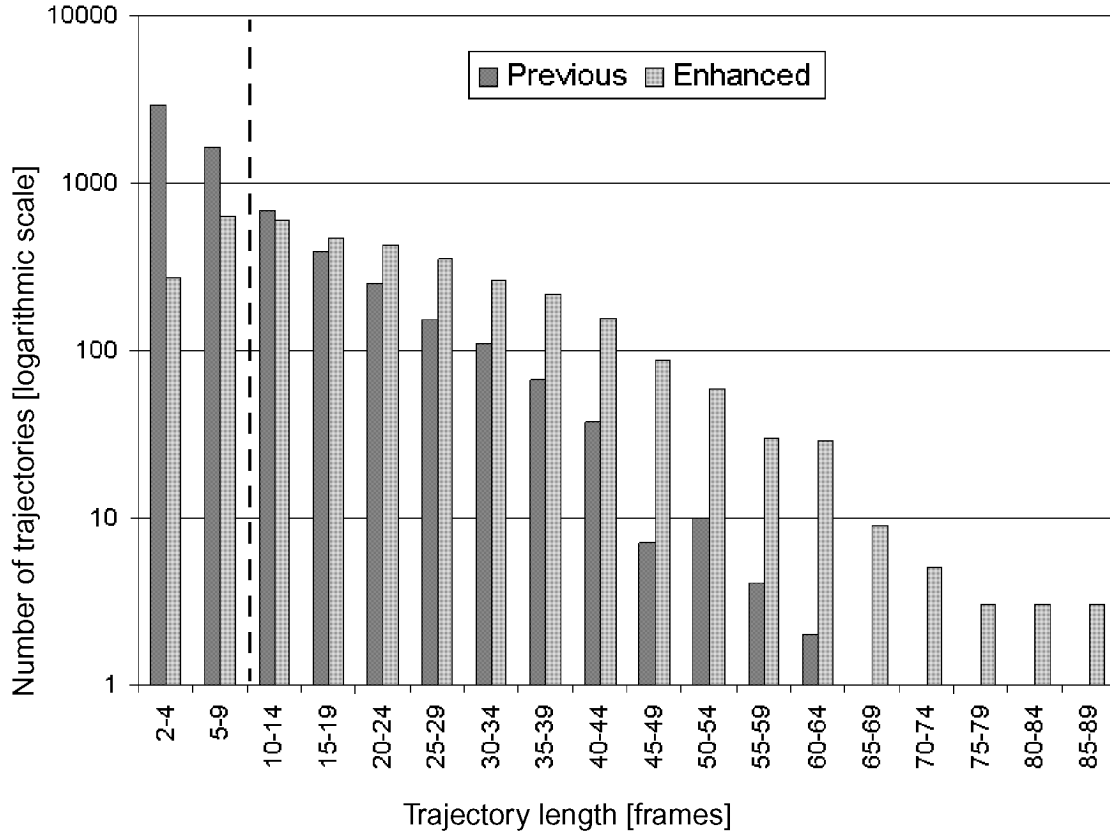


Fig. 42: Histogram of the trajectory lengths obtained with previous and enhanced PTV approach applied to the data set ‘copper sulphate’, the dashed line marks the minimum trajectory length for Lagrangian analysis determined to 10 frames from the dissipation of the measured flow field

7.3.3.7. Experiment ‘1.0’

For this experiment an image sequence of 500 time steps captured with the new 60 Hz system was available. Again the turbulent flow field contained vortexes and swirling motions. The obtained flow is shown in Fig. 43, for visualization purpose only the trajectories longer than 75 frames are displayed. As mentioned at the beginning of the chapter this data set was also processed with the tracking method ‘TrackingHS’, which yielded a slightly higher tracking rate than the approach ‘Previous’. As shown in Fig. 44 the number of links could be increased by 39 % compared to the ‘TrackingHS’. Despite this improvement the tracking efficiency itself was rather low applying all applied approaches, slightly improved with the enhanced method. Nevertheless the average trajectory length avl_{traj} could be increased by around factor ~ 2 . The longest trajectory obtained with the previous method was 135 respective 140 frames with ‘TrackingHS’, while the enhanced approach could track a particle over 164 time steps. For a better visualization, the histogram of the trajectory lengths (Fig. 45) does not include all trajectory length classes (up to 500 frames), as only one particle could be tracked for 164 time steps. Regarding to Lagrangian analysis the Kolmogorov time τ_η was determined to a minimum length of 14 frames for this flow field and is marked with a black dashed line. For this data set the enhanced method is superior in all specific length classes, which can contribute for a Lagrangian analysis.

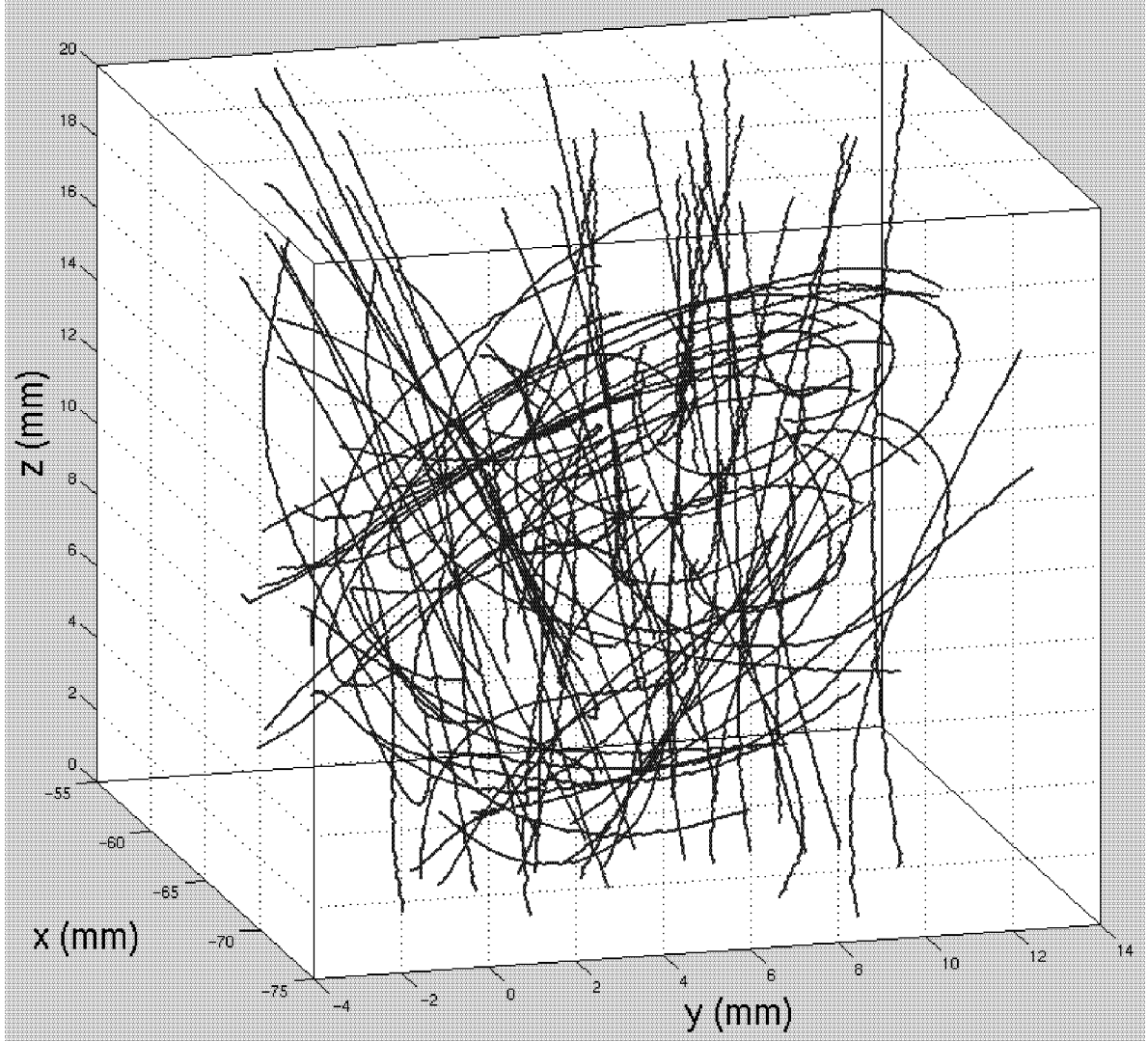


Fig. 43: Velocity field data set '1.0', showing the trajectories longer than 75 frames

Table 7: Performance characteristics N_{traj} , avl_{traj} and L_{traj} of the data set '1.0'

Tracking method	Number of trajectories N_{traj}	Average trajectory length avl_{traj}	Total number of all established links L_{traj}
TrackingHS	30'552	5.1	155'437
Previous	23'950	5.9	141'335
Enhanced (forward only)	18'888	9.4	177'127
Enhanced (bidirectional)	18'305	10.5	192'458

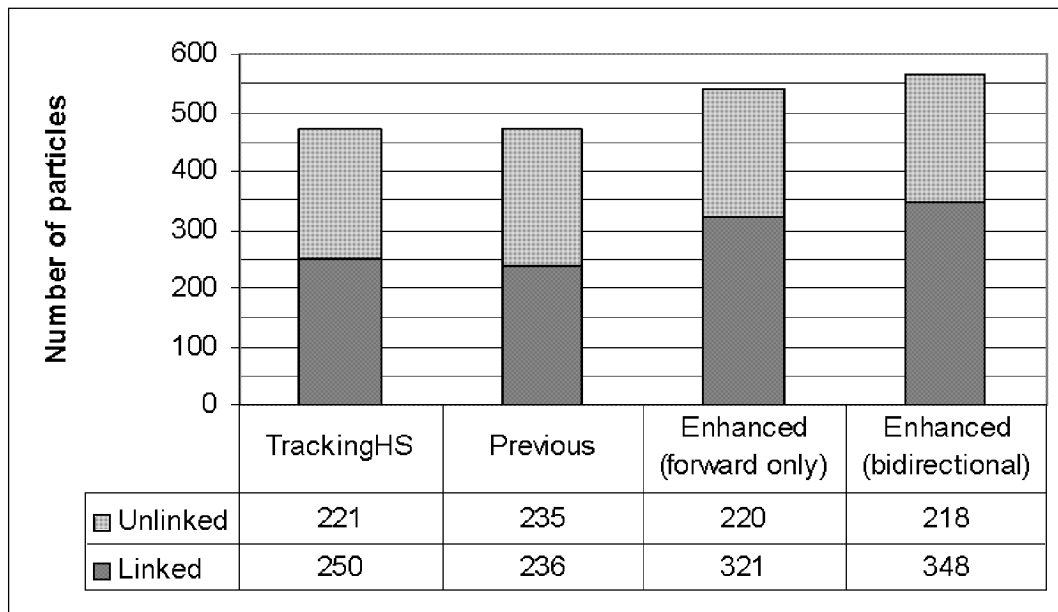


Fig. 44: Average number of particles and links over 500 time steps determined with the different PTV approaches applied to the data set '1.0'

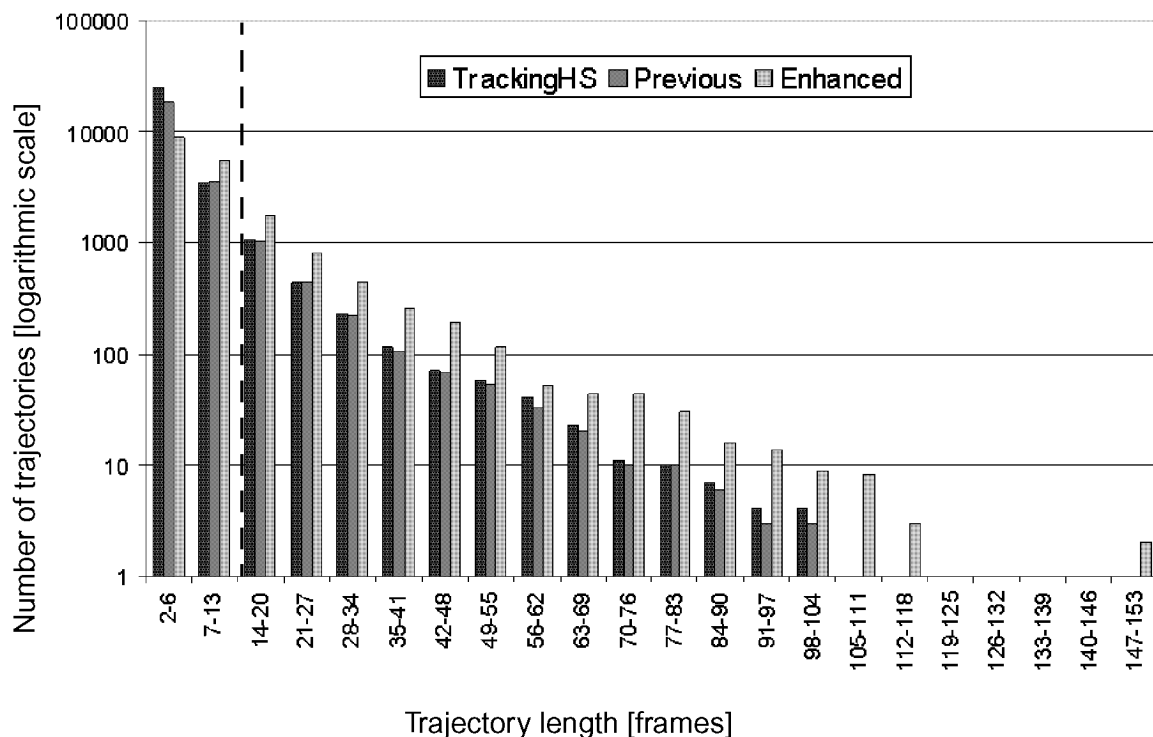


Fig. 45: Histogram of the trajectory lengths obtained with the different PTV approaches applied to the data set '1.0', the dashed line marks the minimum trajectory length for Lagrangian analysis determined to 14 frames from the dissipation of the measured flow field

7.3.3.8. Experiment ‘2.5’

Again 500 time steps of this experiment were processed and analysed. The flow field is shown in Fig. 46 displaying only the trajectories, which could be tracked more the 85 frames.

Again this data set was also processed with the approach ‘TrackingHS’, which yielded a slightly higher number of links than applying the method ‘Previous’. With the enhanced method the number of links could be increased by 35 % compared to the ‘TrackingHS’, respectively by 41 % compared to the previous approach. Comparing the tracking algorithms the tracking efficiency was only slightly improved by applying the enhanced method. The average length avl_{traj} of the reconstructed trajectories was increased by factor ~ 2 . The longest trajectory obtained with the ‘TrackingHS’ method was 171 frames (155 with previous) while the enhanced approach could track a particle over 236 time steps. For a better visualization, the histogram of the trajectory lengths (Fig. 48) does not include all trajectory length classes (sequence length 500 frames), as only three particles could be tracked longer than 160 time steps.

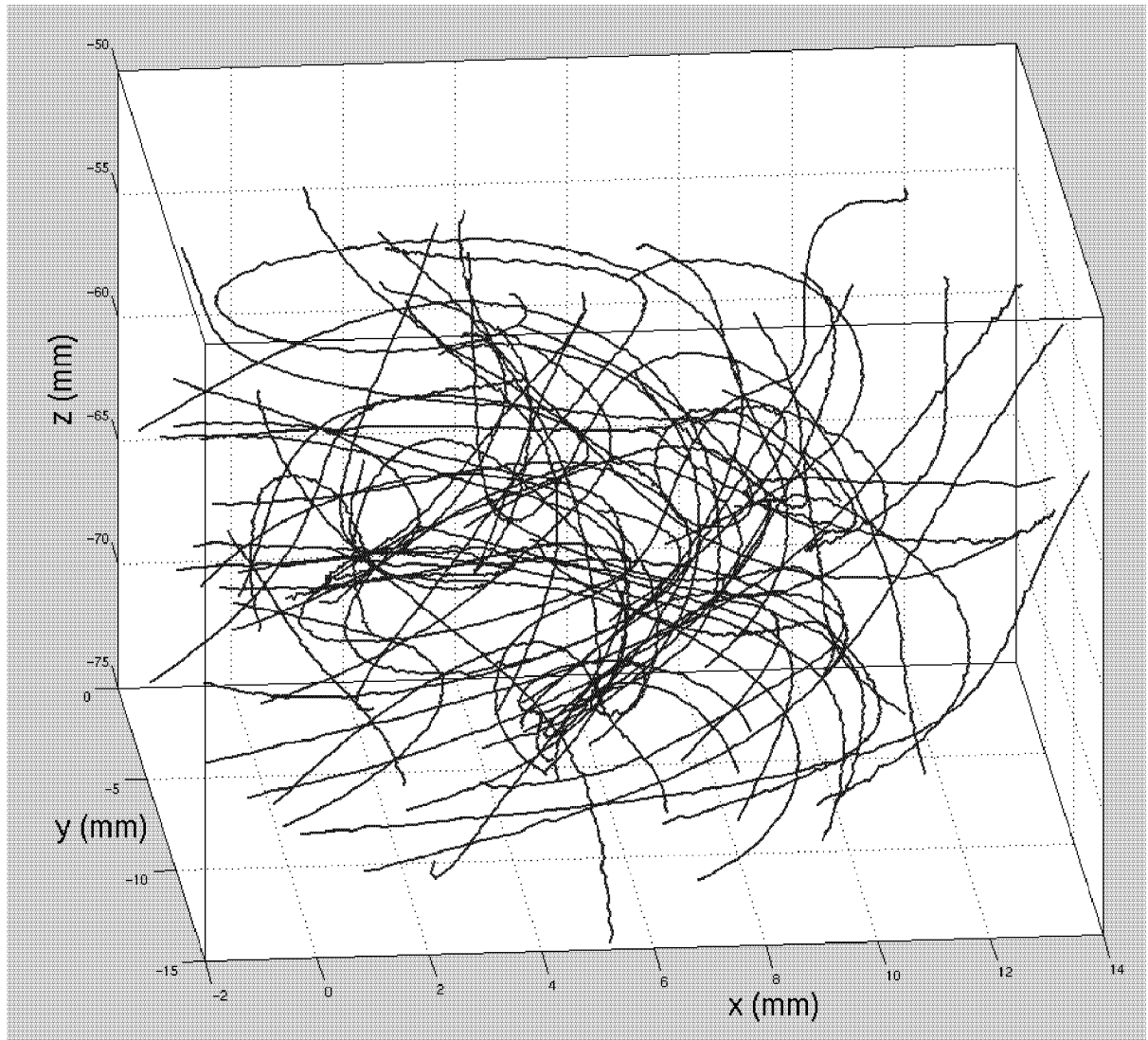


Fig. 46: Velocity field of data set ‘2.5’, showing the particles, which could be tracked longer than 85 frames

7.3. Tests using real data

As for this data set the Kolmogorov scales were not determined from the measured velocity field only an estimation of 8 frames is given for τ_η . Probably this estimation for the minimum length is too short, but as particle motion due to the higher DC current is faster than in experiment ‘1.0’, the Kolmogorov time τ_η for sure is less than 14 frames. Compared to the previous tracking method again the enhanced approach is superior in all length classes, which contribute to the Lagrangian analysis (trajectory length distribution shown in Fig. 48).

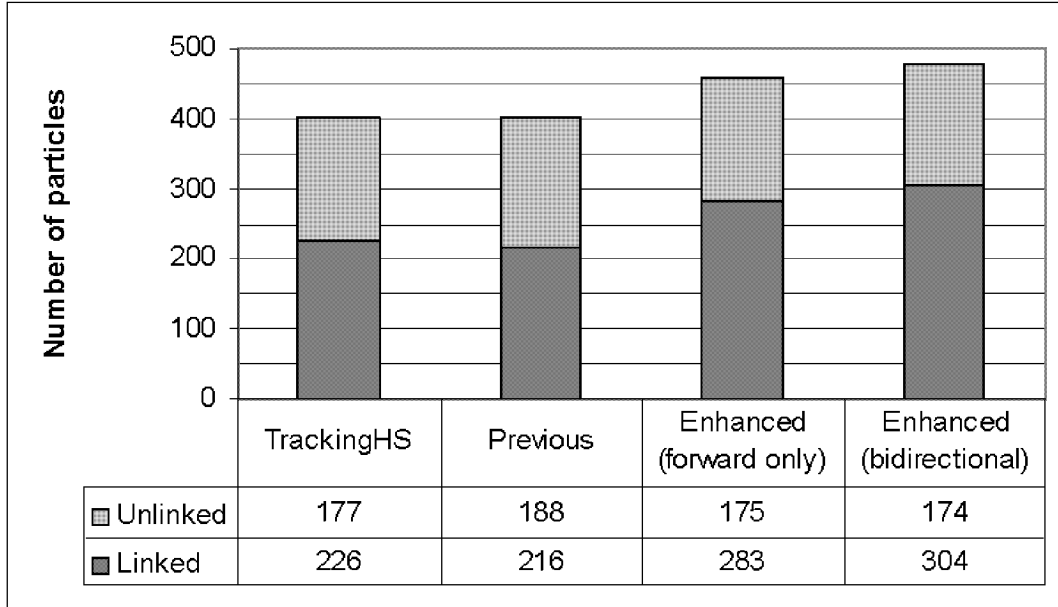


Fig. 47: Average number of particles and links over 500 time steps determined with the previous and enhanced PTV approach applied to the data set ‘2.5’

Table 8: Performance characteristics N_{traj} , avl_{traj} and L_{traj} of the data set ‘2.5’

Tracking method	Number of trajectories N_{traj}	Average trajectory length avl_{traj}	Total number of all established links L_{traj}
TrackingHS	23’749	5.8	136’653
Previous	19’098	6.6	126’524
Enhanced (forward only)	14’737	10.5	154’628
Enhanced (bidirectional)	14’389	11.6	166’269

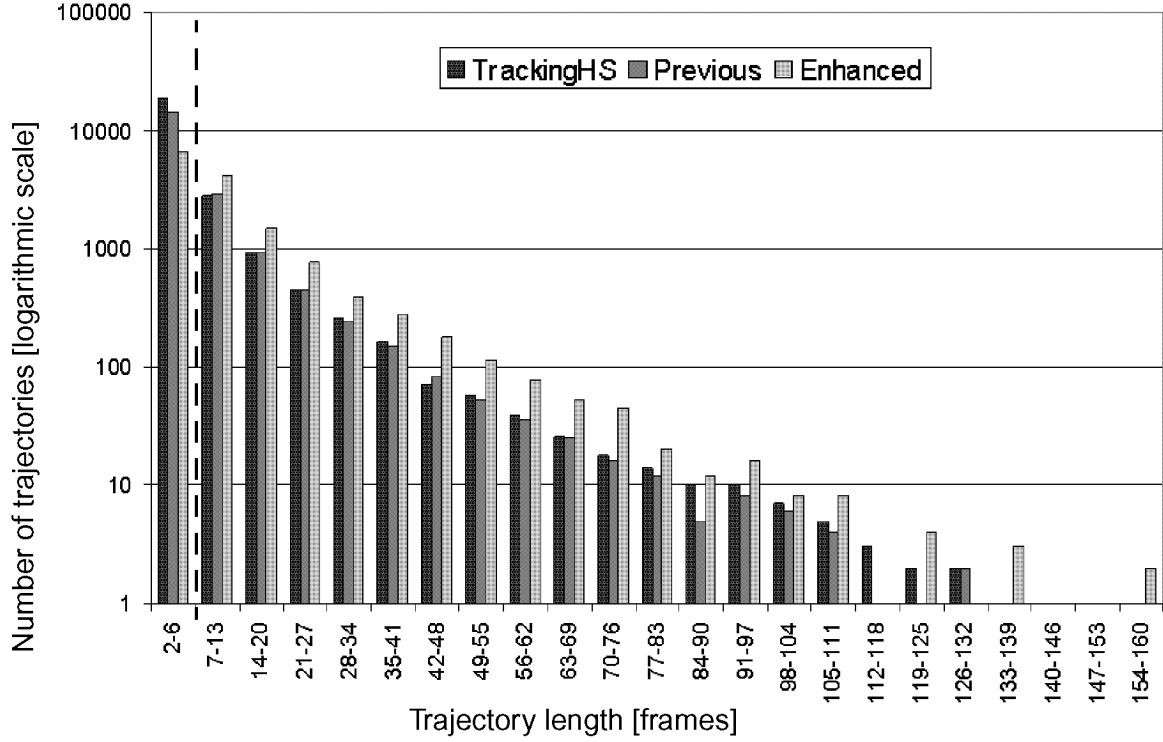


Fig. 48: Histogram of the trajectory lengths obtained with the different PTV approaches applied to the data set '2.5', the dashed line marks the minimum trajectory for Lagrangian analysis, which is estimated to 8 frames

7.3.3.9. Statistical basis for Lagrangian analysis

Given that a particle is tracked at least over one Kolmogorov time τ_η its trajectory can contribute to a Lagrangian analysis. The number of all valuable simultaneous trajectories should be large enough to form a sufficient basis for a statistical analysis. If τ_η is known the mere amount of available data yielded with the different tracking approaches can be used to draw conclusions about their performance.

As τ_η is only known for the three flow fields from the experiments 'copper sulphate', '1.0' and '2.5' the comparison of the available data amount is made just for those data sets. Table 9 shows that the available data amount was increased up to more 89 % providing an enlarged basis for a statistical analysis.

Table 9: Number of available trajectories tracked longer than Kolmogorov time τ_η , respective contributing to the Lagrangian analysis

Tracking method	'copper sulphate' $\tau_\eta > 10$ frames	'1.0' $\tau_\eta > 14$ frames	'2.5' $\tau_\eta > 8$ frames
TrackingHS	not evaluated	2086	4153
Previous	1729	2016	4183
Enhanced (bidirectional)	2699	3824	6817
Gain compared to TrackingHS, respective (Previous)	56 %	83 % (89 %)	64 % (63 %)

7.4. Application of 3D PTV in space 'MASER 8 Project'

In a cooperation between the Swedish Space Corporation, the Microgravity Research Center of the Université Libre de Bruxelles and the Institute of Geodesy and Photogrammetry a system for the measurement of three-dimensional particle motion field in an experimental vessel under micro-gravity conditions has been designed and constructed. The imaging system consists of four SONY 8500 B/W CCD cameras and a mirror system allowing a good photogrammetric network quality in combination with an extremely compact design. The cameras are equipped with a 1/2" Hyper HAD chip, the output images had a resolution of 768×576 pixels. The experiment unit was designed for the MASER 8 sounding rocket JET experiment with the aim of a first direct observation of the so-called chemojet motion of free flying small growing crystals. The experiment was conducted in a reactor chamber with a dimension of $10 \times 11 \times 14 \text{ mm}^3$ into which particles are injected from a particle bin during the flight. The particle bin has a grid width 32×32 conical holes covering an area of 60 mm^2 . The particles are placed in each of the holes. Four synchronized CCD cameras image the particles. The chamber is illuminated from the backside via a milk-glass window. The front wall of the chamber is an observation window used for imaging the particles. According to the reliability requirements of 3D PTV, the reactor chamber has to be imaged from at least three different directions. A fourth camera was added to enable the discrimination of two different particle substances via a special illumination in combination with a filter. The suitability of the technique for measurements under micro-gravity conditions has been discussed in (Maas et al., 1997) and (Willneff/Maas, 2000). Based on these results, 3D PTV was chosen as measurement technique for the examination of chemo-jet phenomena on the MASER 8 sounding rocket experiment. A detailed description of the chemo-jet phenomena can be found in (Melikhov/Verdernikov, 1995) and (Vedernikov/Melikhov, 1994).

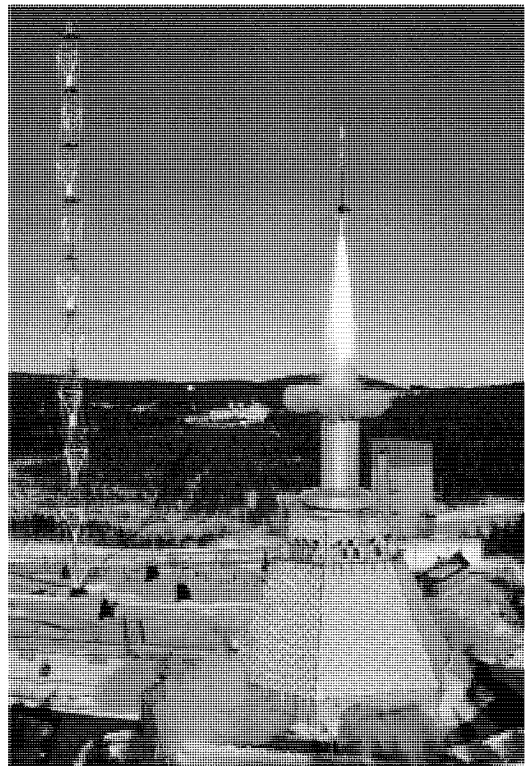


Fig. 49: Launch of sounding rocket, taken from (Swedish Space Corporation, 1998)

Launched to a height of 260 km, this rocket offered 6 minutes and 18 seconds of micro-gravity conditions (Fig. 49). During this time, 500 liquid crystal particles were released into the observation chamber of $10 \times 11 \times 14 \text{ mm}^3$. Due to the chemo-jet effect, the motion of these particles is supposed to deviate from random motion. As a proof, another 500 neutral particles are added. To enable optical differentiation between active and neutral particles, the latter ones were chosen as gold plated hollow glass spheres. The particle trajectories are determined with an adapted 3D PTV system, with a filter to discriminate the two particle substances in the optical path of one of the cameras. Further information about the JET growth motion in aerosol experiment module can be found in (Dupont et al., 1999), (Lockowandt et al., 1999a), (Lockowandt et al., 1999b) and (Willneff, 1999b). The hardware setup of the image acquisition system with its inhomogeneous illumination conditions in combination with the long focal length led to a deterioration of the potential. Regarding the seeding density of the velocity field the number of particles that are injected into the object volume is rather small (less than 500 particles) and did not exhaust the capability of PTV.

7.4.1. Description of the four headed camera system

The available space to accommodate the reactor chamber as well as the illumination and imaging modules is limited to the diameter of the sounding rocket, which is 0.4 m. For this reason the experiment unit had to be designed as compact as possible. The image acquisition system is based on one single almost distortionfree objective that collects light coming from different viewing directions via four mirrors and transfers it to the four CCD cameras via another four mirrors. Image quadruplets from these cameras are grabbed simultaneously, intermediately stored and then written to a compact analogue storage device via a multiplexer. An image of the complete JET module including imaging system, particle injection unit, illumination facility, temperature and pressure control is shown in Fig. 50. The video signal is also transferred to ground via a video module in the payload. On the ground the signal is recorded. Compactness of the system is furthermore achieved by a 90-degree angle in the optical path. To be able to apply the standard photogrammetric model of 3D PTV based on the collinearity condition, multimedia geometry and additional camera calibration parameters, the optical paths for the four cameras were 'unfolded' for further processing, leading to a configuration with four virtual projection centers and virtual camera positions with a convergent arrangement. The mechanical design of the imaging head including the optical paths is shown in Fig. 51.

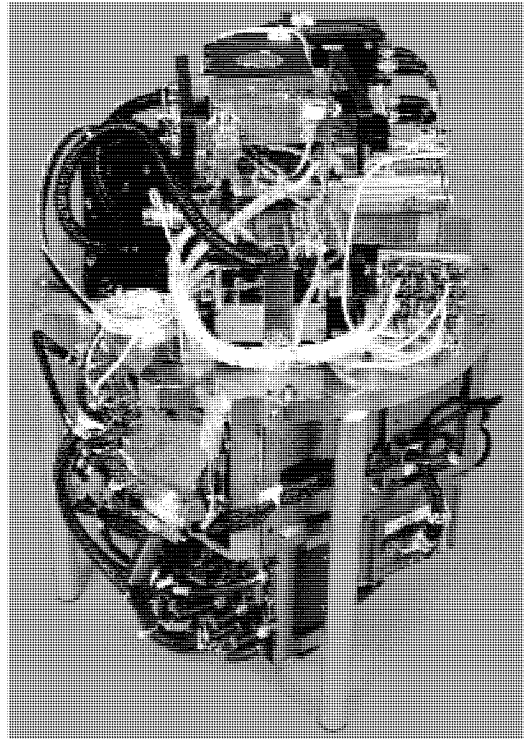


Fig. 50: JET Module, taken from (Lockowandt et al., 1999b)

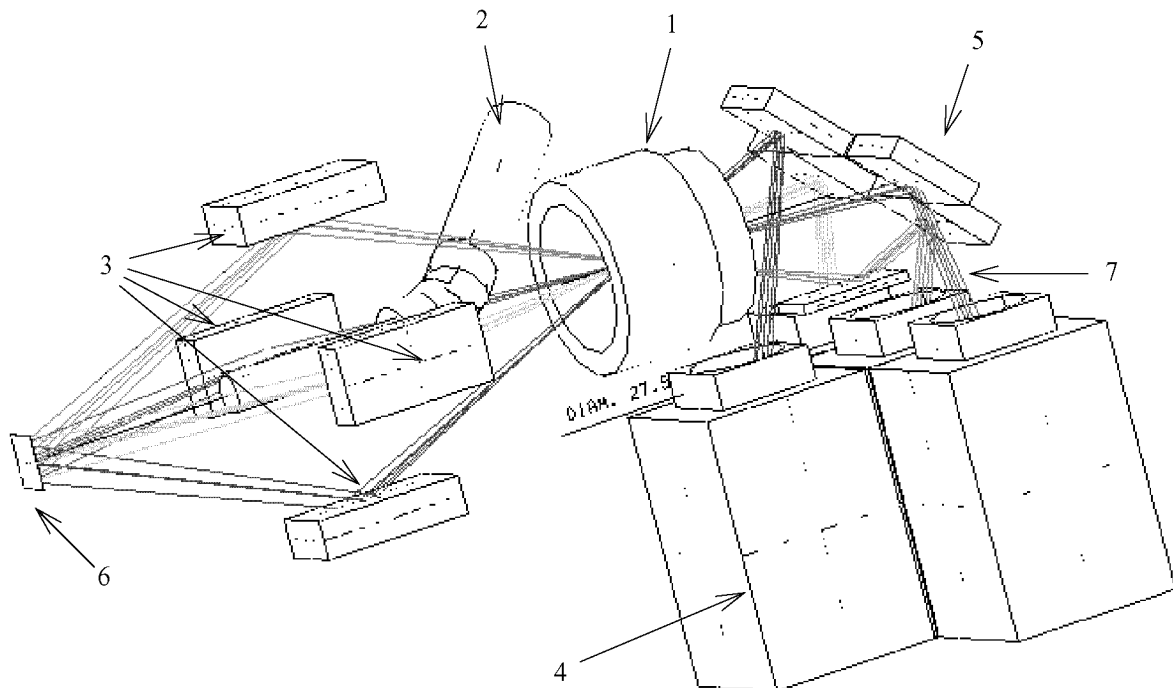


Fig. 51: Mechanical design of the imaging head: 1, objective; 2, front illumination; 3, mirrors; 4, CCDs; 5, mirrors; 6, reactor chamber; 7, additional mirror

7.4.2. Calibration of the image acquisition system

To be able to establish correspondences between particle images and to compute 3D particle coordinates, the (virtual) orientation and calibration parameters of the system have to be determined in a calibration procedure. The calibration is being performed using images of a 3D-reference body with discrete targets, which is inserted into the reaction chamber before and after the experiment. Using the mathematical model of spatial resection, the orientation and calibration parameters of a camera can be determined from one single image of the calibration reference body under suitable illumination, if the 3D coordinates of the targets are known. Based on this calibration facility, particle tracking with micron-accuracy becomes possible.

For the determination of the orientation parameters the fact that the optical paths (those of three cameras are folded twice, the fourth one thrice) of the image acquisition system are folded has to be taken in account. The calibration reference body was fabricated by spark erosion techniques in aluminium with 40 mechanically generated reference points in an anodized surface with a precision in the order of one micron.

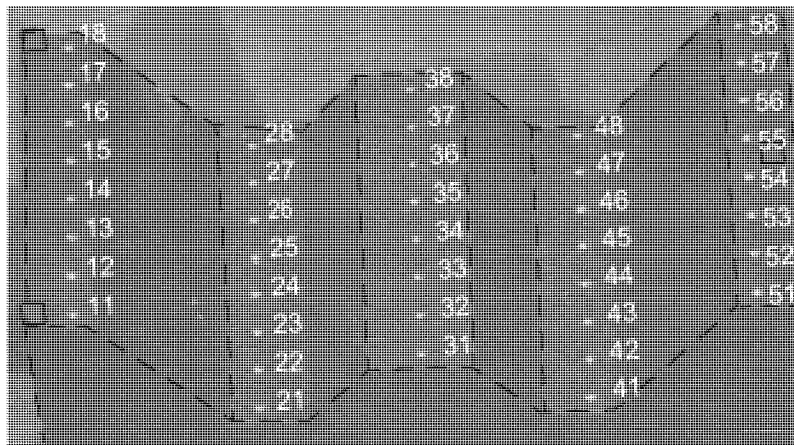


Fig. 52: 3D calibration reference body

The reference body used for the calibration is shown in Fig. 52. To calibrate the system in its actual configuration the calibration body should be put into the experiment cell immediately before launch. The reference body is used to define the coordinate system. The X-Y-plane is chosen identical with the inner side of the front glass plate. The Z-axis is perpendicular to the front glass plate and has its positive direction away from the observation volume. The origin and the directions of the X- and Y-axis is depending on the placement of the calibration body. Due to the fact that there is no fixation for the calibration body the orientation of the X- and Y-axis and the origin of the coordinate system depends on the actual position of the calibration body during the acquisition of the calibration images. This is irrelevant due to the relative character of the particle motion. For the experiment it was assumed that the arrangement is stable throughout the flight.

7.4.2.1. Image quadruplet used for the calibration

The time delay between the acquisition of the images used for the calibration and the actual experiment should be kept to a minimum to reduce the influence of temporal changes of the configuration. Due to the convergent setup and the depth of the observation chamber, the common viewing volume of all four cameras is relatively small. The image quadruplet used for the calibration with the detected image positions of the points of the reference body is shown in Fig. 53.

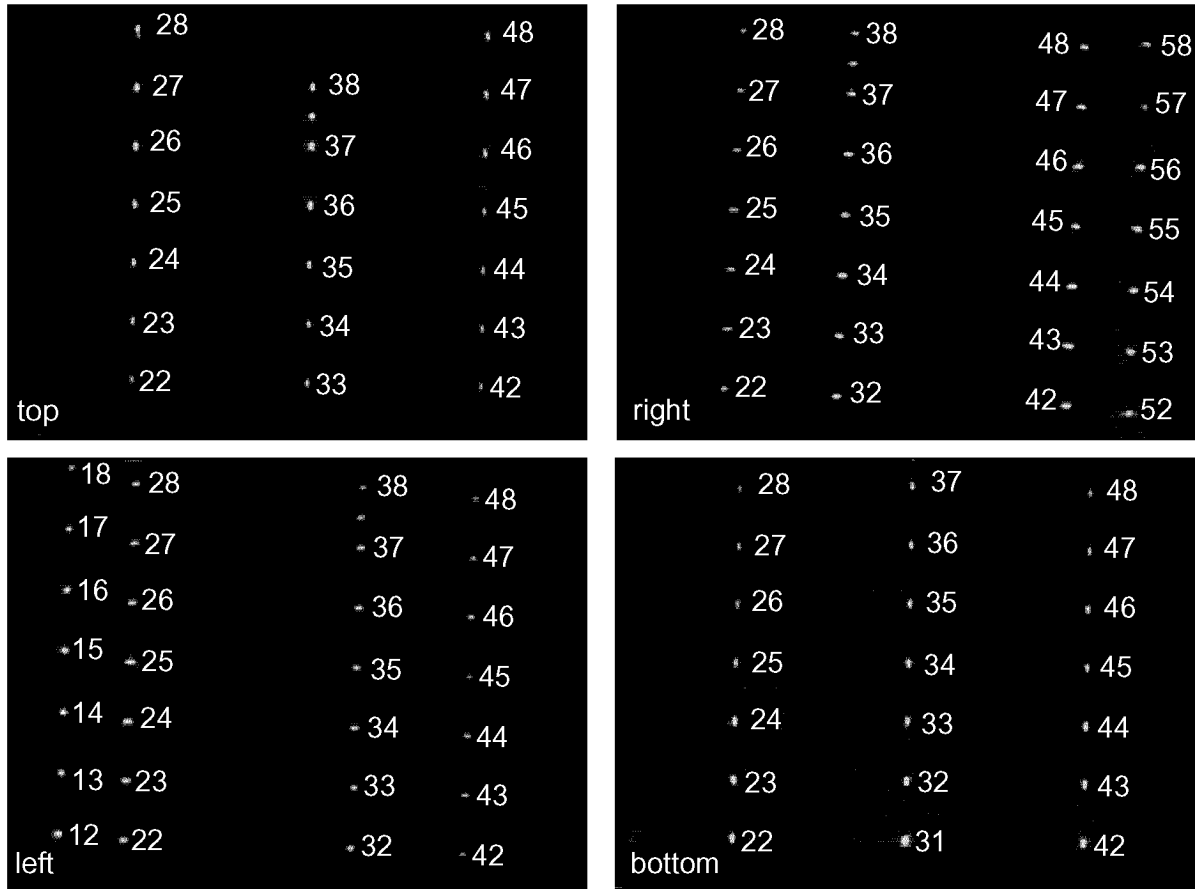


Fig. 53: Views of the calibration body by the four camera system

7.4.2.2. Results of the calibration

The four camera system was calibrated by spatial resection. From each calibration image more than 20 points of the reference body were detected and used for the determination of the photogrammetric parameters. Only the central part of the reference body is in the field of view of the cameras. Those points that were detected were nearly visible in all four calibration images. As a conclusion the observable object volume is rather small, but the field of view of the four cameras is almost identical. As the mathematical model does not contain mirrors, the optical paths were 'unfolded' for further processing, leading to a configuration with four virtual projection centres and four virtual camera positions with a convergent camera arrangement and principal point coordinates deviating strongly from the centre of the image. The calibration yielded the following results:

- The standard deviation of unit weight was between 2.39 - 4.94 μm for the four images. This is certainly suboptimal, but has to be contributed to the micro-structure of the targets plus illumination effects.
- The camera constant could not be determined. This is due to the extremely narrow opening angle (planned setup design value is 22.5 degrees), which leads to high correlations between parameters of exterior and interior orientation. From the results of the calibration the angles between the optical axes of the cameras and the glass front of the experiment chamber were derived (values between 19.9 and 24.4 degrees). The mathematical model depicts an overparameterization to the chosen configuration. Therefore the camera constant can be

introduced as a fixed parameter with a value of 108.83 mm computed from the parameters of the optical system, and the effects of deviations from this value are covered by parameters of the exterior orientation.

- The principal point is turned outward between 25 mm and 42 mm for the four cameras and is thus lying far outside the actual sensor format.
- No other significant parameters could be determined.

Further details about the results of the calibration can be found in (Willneff/Maas, 2000). The arrangement of the four cameras is shown in Fig. 54.

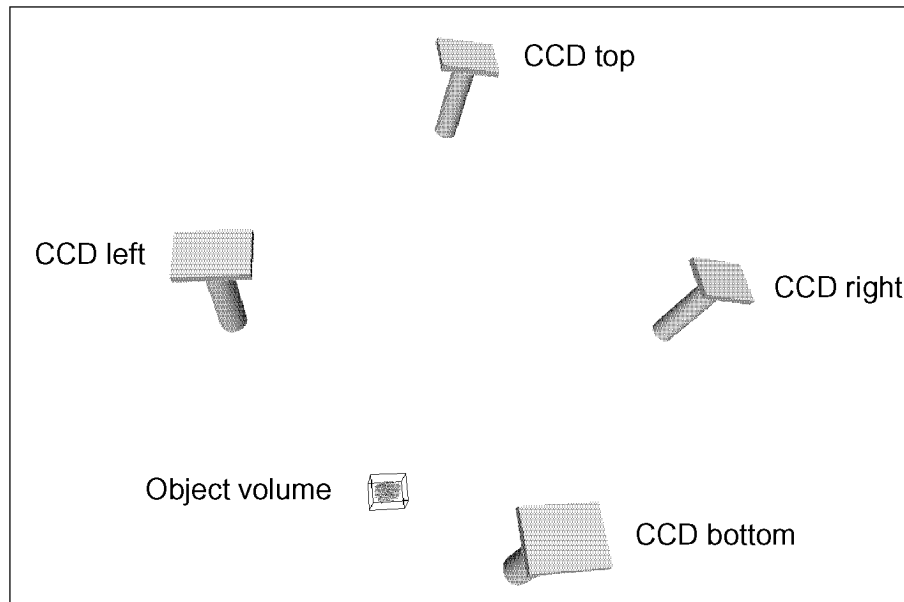


Fig. 54: Front view of the camera arrangement

7.4.3. Image preprocessing

In the framework of this project two image acquisition campaigns were performed. The purpose of the first campaign (parabolic flights, described in section 7.4.4.) was to test the JET module under similar conditions as to be expected during the second one, the actual experiment of the MASER 8 flight (see in section 7.4.5.). Before the image sequences could be processed with PTV a certain effort of image preprocessing was necessary to get suitable input data. The steps of preparation are described in this section.

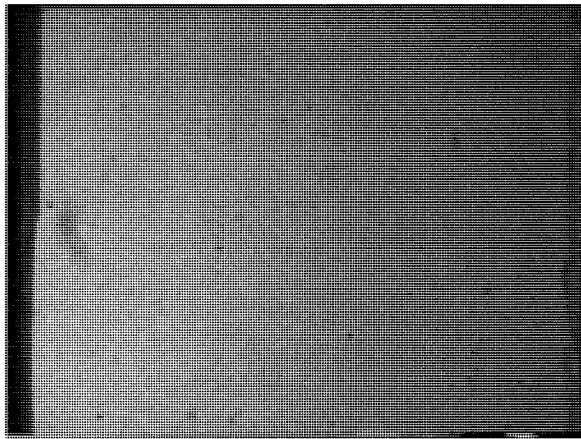
While the data of the parabolic flight campaign was quite satisfying, the quality of the MASER 8 flight images was significantly lower. The data was recorded in two ways during the MASER 8 flight. But not only the ground tape data has a high noise level, also the flight tape data shows less quality than the test images acquired during the parabolic flights carried out in 1998 (Swedish Space Corporation, 1998). This preprocessing contained the following steps and was applied to the data sets of both campaigns:

- Creation of a suitable background image for each of the four cameras to remove non-uniformities of the back ground intensity level due to reflections and the intensity profile of the illumination. The first images are recorded before the particle injection and contain no particle images. For each view an images with no particles served as background image. To reduce the effect of adding high frequency noise from the background image to the sequence

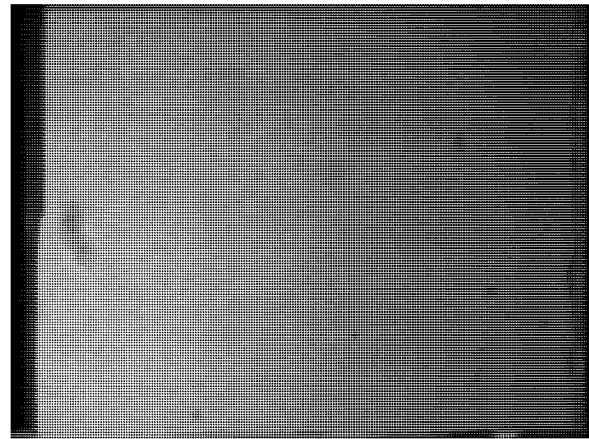
image these four images were filtered with a low pass filter. The background images then were subtracted from each sequence image.

- In the resulting images the particles appear as bright stains on a dark background. Each image was added to itself to increase contrast.
- To get rid of the defocussed regions on the edges of the sequence images a mask (one per each camera) was used to cut out the regions of interest.
- The images recorded by the left CCD had a higher noise level than the other cameras. To handle this the contrast in this images was reduced to decrease the number of false particle detections, which otherwise would disturb the establishment of particle correspondences.

After the image preprocessing the particles appear as bright spots on a more or less dark background as generally required for 3D PTV. An example of the image preprocessing is shown in Fig. 55. Another advantage is that for all four cameras the same parameters for the particle detection can be used because the differences in the illumination are homogenized to a common level. The difference between the grey values of the imaged particles and the background is 10 up to 100. After this preprocessing the image sequence data could be used for PTV evaluation.



Original sequence image



Background image
(for subtraction from original)



Image mask
(cut out defocussed edges)



Sequence image after preprocessing

Fig. 55: Image preprocessing of sequence images

7.4.4. Parabolic flight campaign

To prove the applicability of the system the JET module was tested during the 29th ESA parabolic flight campaign (Swedish Space Corporation, 1998). To achieve similar conditions as during the MASER 8 campaign the test experiments were conducted under micro-gravity condition achieved by parabolic flight path. During three parabolic flights with an Airbus A300 in total 10 image sequences were acquired. The image sequences were processed with PTV to derive trajectories of the moving particles. As described in (Willneff, 1999a) all of the acquired sequences were processed successfully. In some of the experiments only a rather low number of particles were released into the observation volume by the particle injection unit. In this section only the processing and the results of one representative data set is discussed.

7.4.4.1. Processing of parabolic flight data

As an example of the parabolic flight data sets the image sequence ‘pb08’ over 70 time steps (equivalent to 14 s) is analysed. Due to a low number of particles moving with moderate velocities the tracking of the particles should be possible without exhausting the potential of the PTV method. The reconstructed velocity field of the ‘pb08’ data sets is shown in Fig. 56.

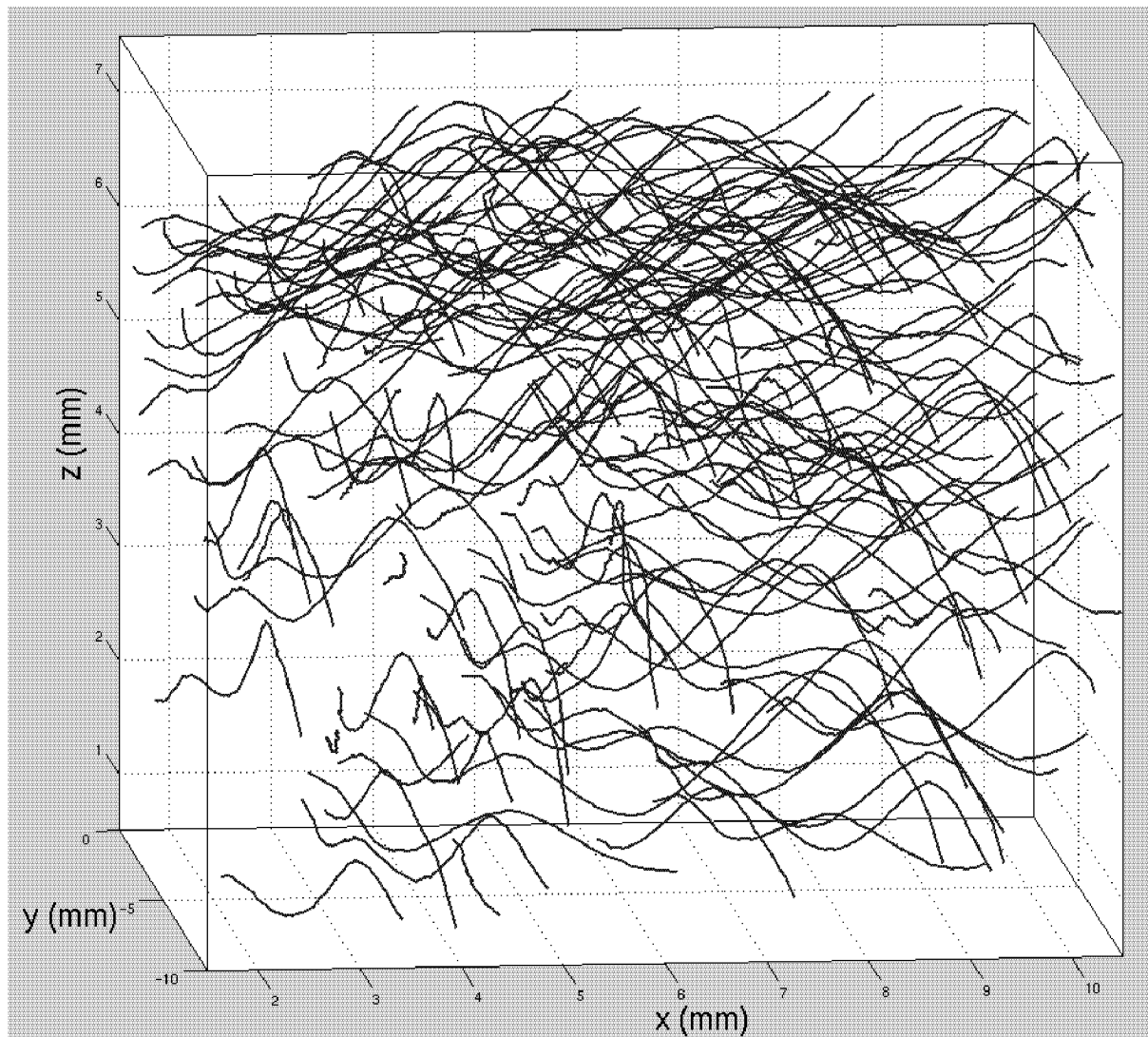


Fig. 56: Velocity field of parabolic flight sequence ‘pb08’, showing only the trajectories which could be tracked longer than 30 frames

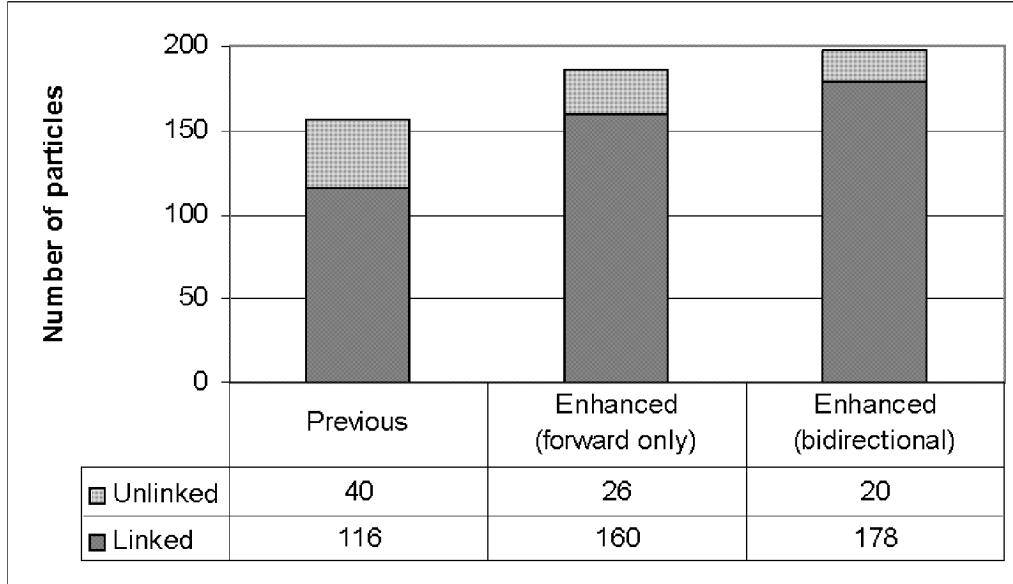


Fig. 57: Average number of particles and links over 70 time steps determined with the previous and enhanced PTV approach applied to the data set 'pb08'

Fig. 57 shows the average number of particles and links by applying the previous and the enhanced tracking method. Also in the case of this data sets the enhanced method yielded a significantly higher number of particle links than the previous approach. The average length avl_{traj} of the trajectories was increased by almost factor ~ 3 . The longest trajectory obtained by the previous method has a length of 60 frames. Namely this could only be elongated to a length of 66 frames with the enhanced method, but at the same time the trajectories longer than 60 frames was increased to a number of 34. Fig. 58 shows the distribution of the trajectory lengths, which again shows good coherence to the expected effects described in 6.5.

The yielded results of the parabolic flights are quite promising, proving the applicability of the technique for space applications like the planned MASER 8 campaign.

Table 10: Performance characteristics N_{traj} , avl_{traj} and L_{traj} of the data set 'ph08'

Tracking method	Number of trajectories N_{traj}	Average trajectory length avl_{traj}	Total number of all established links L_{traj}
Previous	1'206	7.4	8'924
Enhanced (forward only)	627	18.1	11'331
Enhanced (bidirectional)	562	21.9	12'345

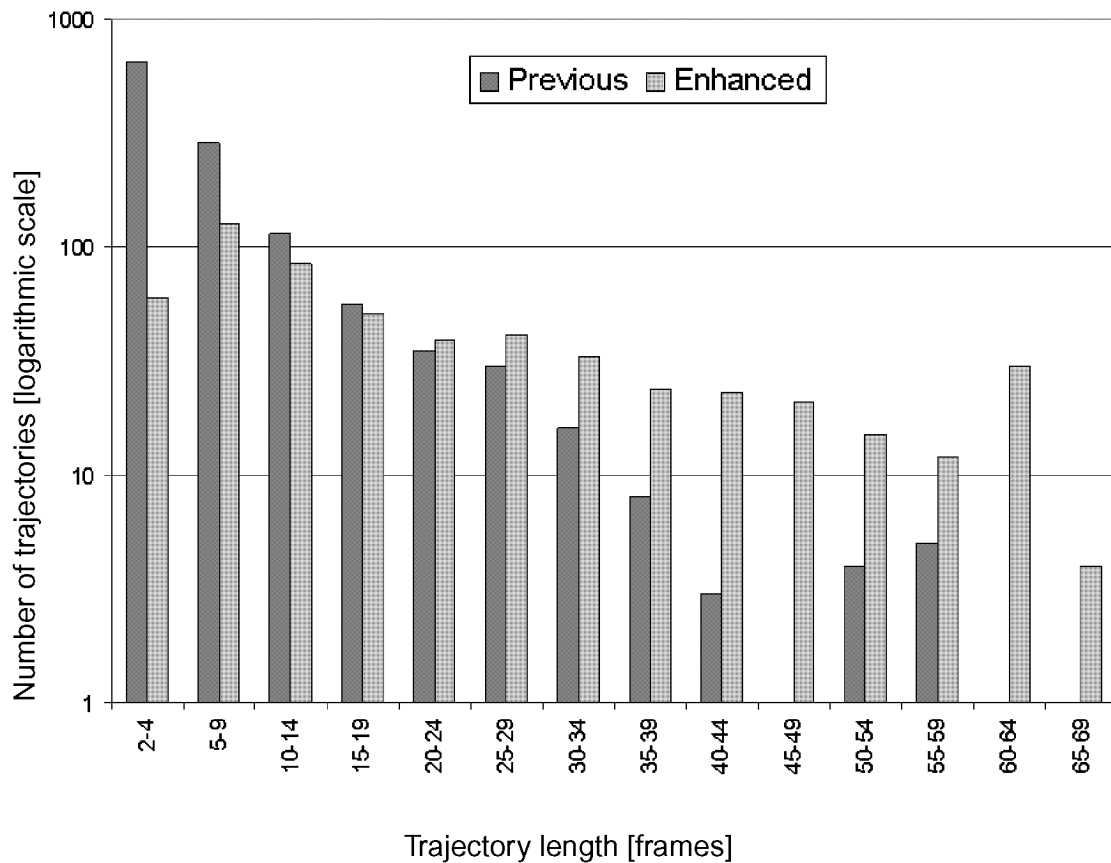


Fig. 58: Histogram of the trajectory lengths obtained with the previous and enhanced PTV approach applied to the data set ‘pb08’

7.4.5. MASER 8 campaign

The experiment was performed successfully and the JET module worked nominal during the flight. During the flight of MASER 8 an image sequence of around 7 minutes was recorded and the movement of the particles could be observed (Swedish Space Corporation, 1999). In total ca. 1500 time steps were analysed. This refers to the first five minutes; the last two minutes were not evaluated because no particle movement could be detected.

7.4.5.1. Processing of MASER 8 data

After the preprocessing the image sequence data is suitable for the processing with PTV. The system orientation and calibration parameters as determined in chapter 7.4.2. were used for the processing of the data. After around 70 time steps the particles start to appear on the sequence images. Per each image around 50 and more image positions are determined. This number also contains the false detections, which will be removed while searching for corresponding candidates in the images of the other cameras. The high number of false detection is caused by the low image quality. Inspections of the particle injection unit of the system showed that only a tenth of the particles (approximately 100 out of 1000) were injected into the observation volume, resulting to a low number of particles to be reconstructed in object space.

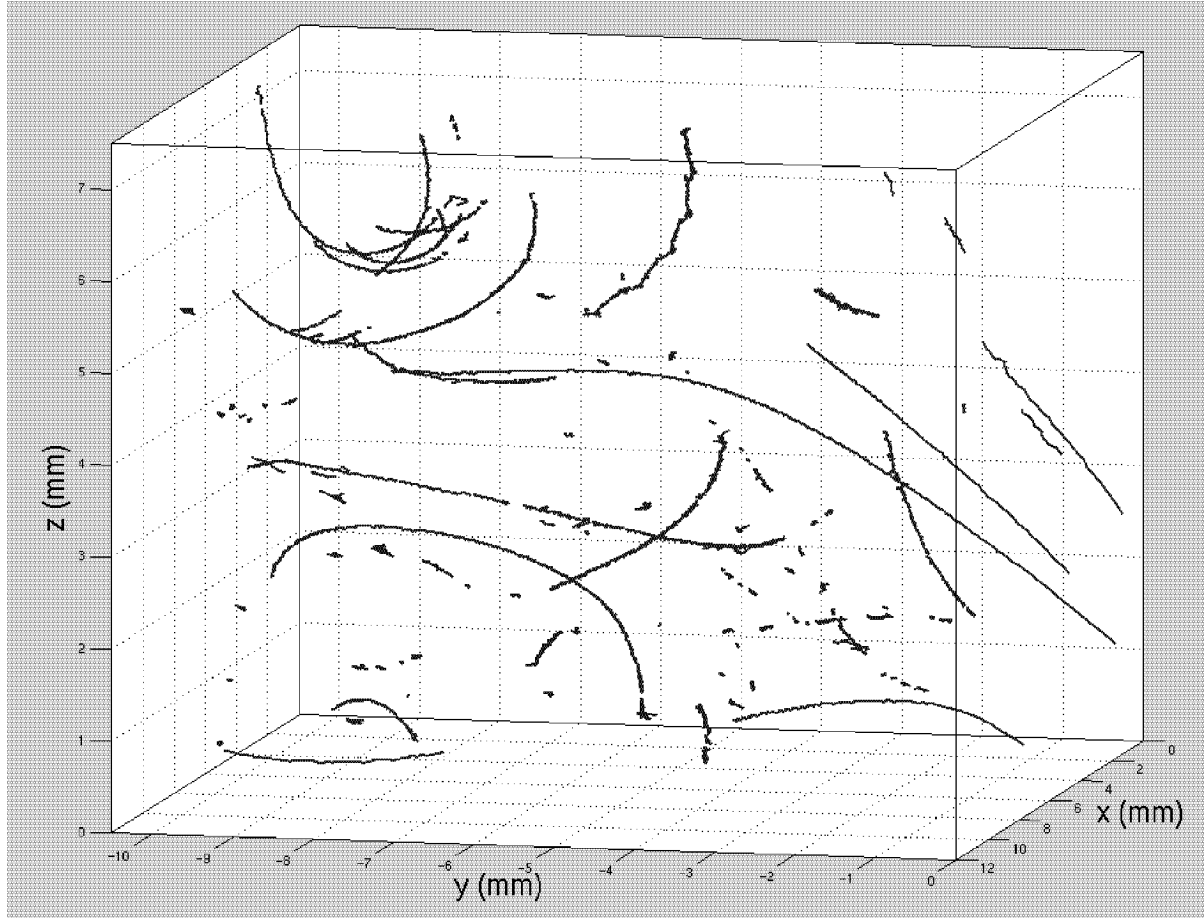


Fig. 59: Velocity field of MASER 8 flight, showing all trajectories tracked longer than 5 frames

As the length of the relevant part of the epipolar line can be restricted by the knowledge of the depth range in object space it was limited by the front glass and the back of the reaction chamber. After the instant of the particle injection between 15 up to 25 particle correspondences were found.

All four cameras were used for the determination of the 3D particle coordinates. The standard deviations of unit weight was between 7 - 12 μm , the standard deviation of the 3D coordinate determination by spatial intersection was around 0.01/0.01/0.03 mm in X/Y/Z. These standard deviations are also influenced by the precision and stability of the orientation parameters, as well as by the irregular shape of particles and sub-optimality in illumination. As these effects will show a high correlation on successive positions of the particle trajectory, the precision of the velocity vector components can be assumed to be significantly better.

As the seeding density of the observed object volume can be considered as very low in combination of small particle movements the establishment of temporal correspondences in the tracking procedure should be clear without ambiguities. A visualization of the results is shown in Fig. 59.

The fourth camera should enable the discrimination of two different particle substances via a special illumination in combination with a filter. The planned classification of the particles in two groups (reference and crystals) was performed as a simple binary decision. If a particle is detected on the images of the decisive camera then it is classified as a reference particle. Due to

the reason that the crystal particles were also visible and detectable on the images of the decisive camera acquired during the flight no reliable classification is possible with a binary decision. Probably this problem could be solved with an alternative classification procedure but is not a shortcoming of the PTV method itself. Another problem occurred due to an insufficient signal-to-noise ratio of the image sequence data of the rocket flight. The particles sometimes appear only in each second or third time step, thus can not be detected in image space making it impossible to build up the particle trajectories. This led to missing links in the 3D data sets and to series of very short tracks, which obviously belong to the same particle.

7.4.5.2. Tracking results from data set ‘MASER 8’

Regarding the low number of particles and the high noise level in this data set, statistical conclusions might be not reliable and probably questionable. Nevertheless the ascertained tendencies observed in the other processed data sets could be confirmed. Applying the enhanced method could increase the number of links and the efficiency (Fig. 60). The average length avl_{traj} of the trajectories could be increased by more than factor ~ 2 . Trajectory fragments were connected to longer trajectories thus reducing their total number (Table 11).

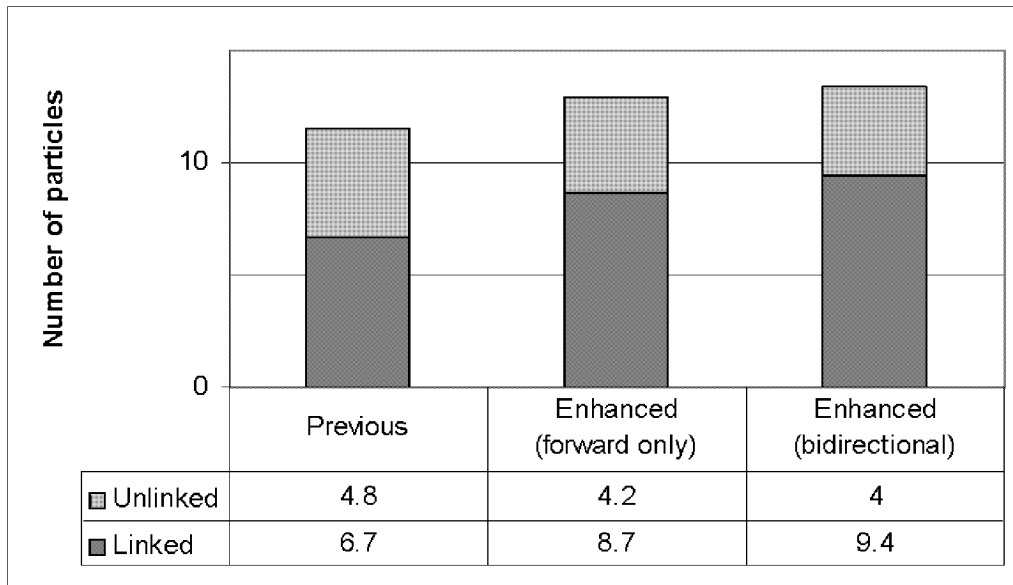


Fig. 60: Average number of particles and links over 70 time steps determined with the previous and enhanced PTV approach applied to the data set ‘MASER 8’

Table 11: Performance characteristics N_{traj} , avl_{traj} and L_{traj} of the MASER 8 data set

Tracking method	Number of trajectories N_{traj}	Average trajectory length avl_{traj}	Total number of all established links L_{traj}
Previous	1'143	9.2	10'459
Enhanced (forward only)	691	18.5	12'758
Enhanced (bidirectional)	637	21.4	13'646

Fig. 61 shows that starting from a trajectory length of 10 frames the enhanced tracking method is significantly superior compared to the previous approach. The number of trajectories longer than 20 time steps could be increased from 58 to 107.

But as mentioned the statistical basis for the performance evaluation of the tracking methods is questionable due to the low number of particles that could be reconstructed from the image sequence of this data set.

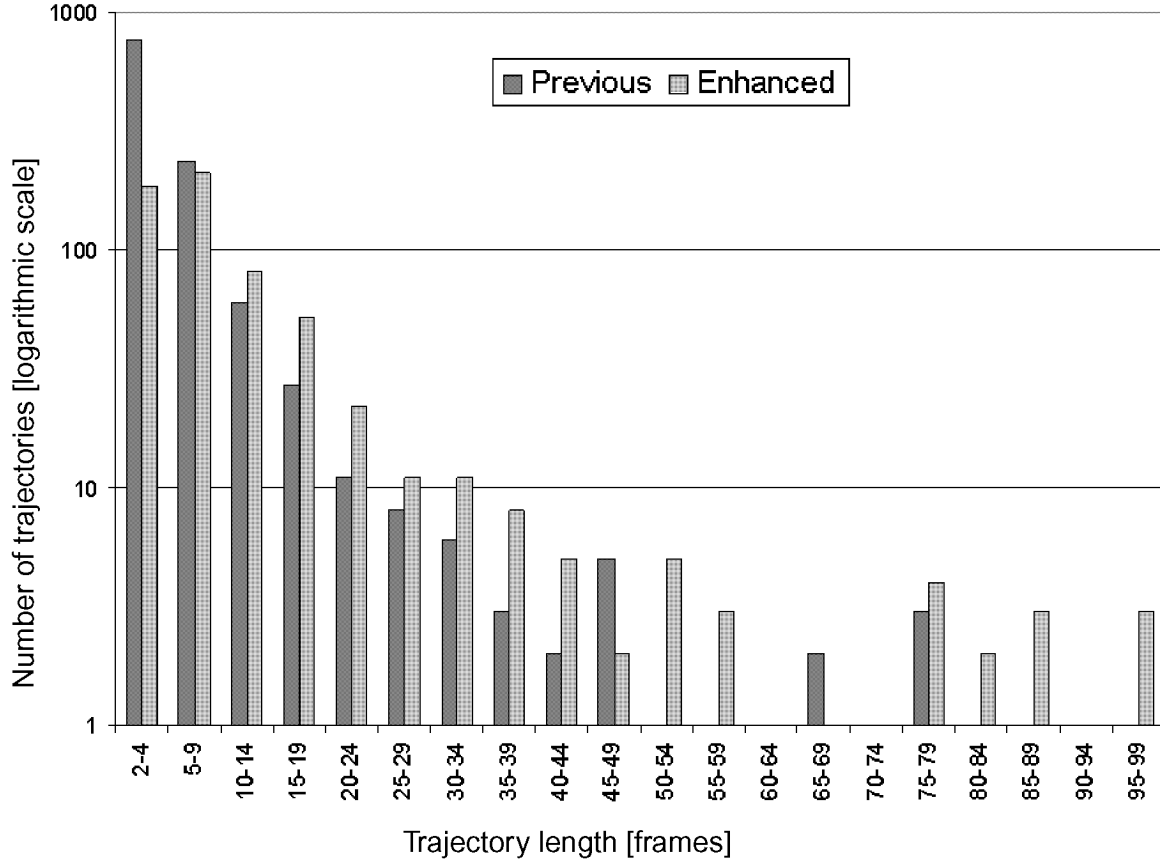


Fig. 61: Histogram of the trajectory lengths obtained with previous and enhanced PTV approach applied to the MASER 8 data set

7.5. Results

In the following section the yielded improvements of the enhanced spatio-temporal matching algorithm for PTV will be demonstrated with some representative examples from simulated as well as from real experiment data. Furthermore an overview about the evaluated performance measures (as proposed in 7.1.) derived from all processed data sets is given.

7.5.1. Examples from the data set ‘simulated vortex’

As mentioned in 6.5. the enhanced method reconstructs the particle trajectories more completely and thus increase the length of the trajectories. The different possibilities to complete a trajectory are shown in Fig. 62. These examples could be derived from the data set of a simulated vortex flow, which is described in chapter 7.2.2. Other examples of reconstructed trajectories from real experiment data are shown in the next section.

The trajectories are represented in the following way, the calculated particle position is marked with a sphere, which is connected with the consecutive particle. The colour gives the information if a particle was already determined by applying epipolar line intersection or by the spatio-temporal matching during the tracking procedure. The size of the spheres is chosen considering visualization aspects and has nothing to do with real particle dimensions or shapes. The particles determined by epipolar line intersection correspondences are marked in dark grey, the added particle position are marked in light grey. With the previous implementation the trajectory of the particle could only be reconstructed incompletely and in parts of shorter trajectories, while the new spatio-temporal matching algorithm was able to track the particles without gap.

The examples in Fig. 62 show the bridging of gaps over one or several time steps. But also the continuation of a trajectory is shown in example lower-right. Starting from initial particle positions derived by epipolar line intersection this trajectory is continued with only additional particle positions. This might occur when a particle leaves the object volume observed by all cameras and therefore vanishes sequentially from the field of view of the cameras. The reduced image space information leads to ambiguities in the epipolar line intersection, which can not be solved without considering the particle motion. With a reliable prediction of the particle position - possible from former links - these ambiguities can be solved if image space information from at least two camera views is available (see 6.5.). Therefore the particle trajectories are also reconstructed throughout an increased object volume. Of course not every trajectory reconstruction will be improved in that impressive way, but even closing a gap of one or two time steps is a substantial enhancement for the hydrodynamic analysis.

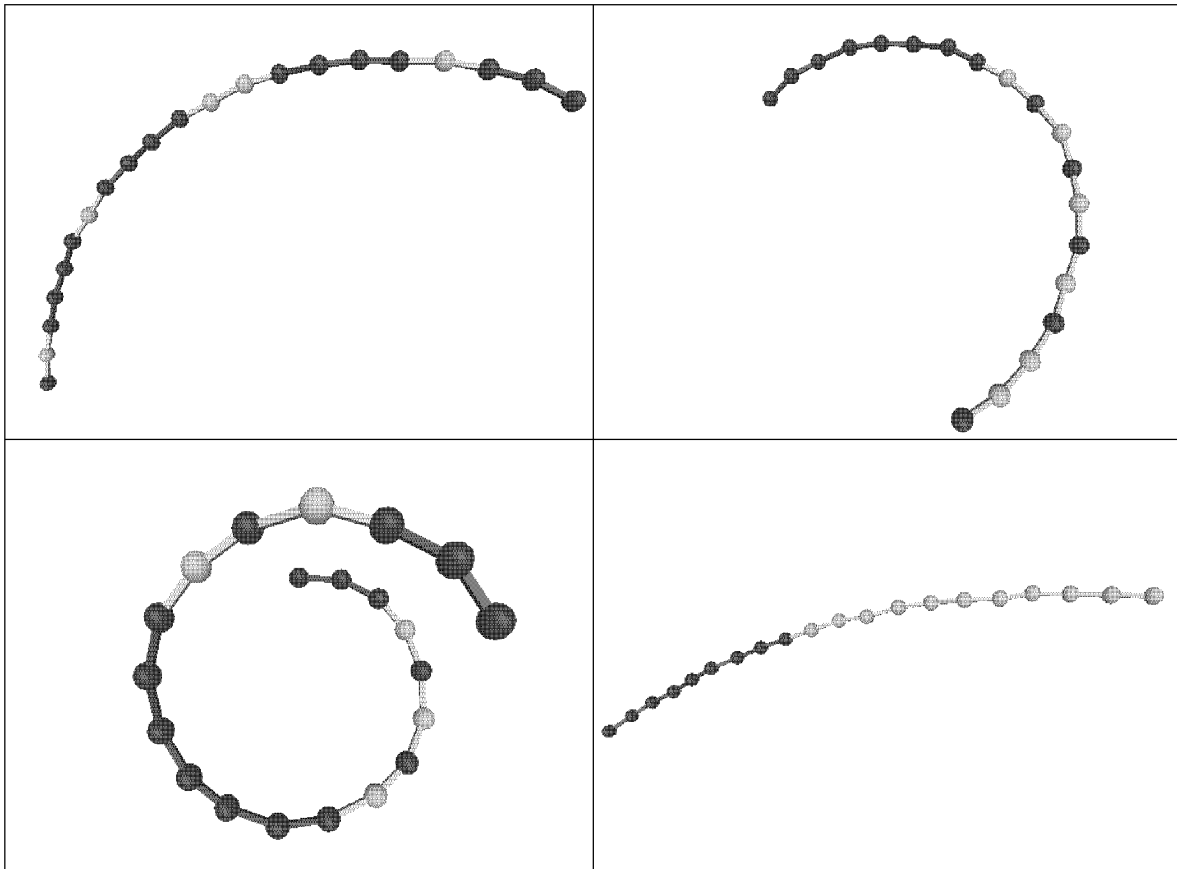


Fig. 62: Examples of reconstructed trajectories with additionally determined particles (light grey), particles determined by epipolar line intersection are marked in dark grey.

7.5.2. Examples from real experiment data

To demonstrate that the expected improvements also occur while processing data from real experiments some representative examples of reconstructed trajectories are shown in Fig. 63. These four trajectory examples were derived from different data sets and show the bridging of gaps over one or several time steps as well as the continuation of trajectories. Of course not all trajectories are improved like shown in Fig. 63 since many particle positions can already be determined with the epipolar line intersection. As these examples are derived from various data sets the general applicability of the method is demonstrated.

The examples of single trajectories are useful to show how the improvements are obtained, but not suitable to get an impression about the overall situation concerning the whole observed object volume.

An overview about the number of added particle positions to close gaps or to continue trajectories regarding the whole observation volume is given in Fig. 64. The trajectories are extracted from an image sequence over 200 time steps, but only 50 time steps and a selection of the trajectories are shown. In this visualization there are trajectories, which consist completely of newly added particles, which is possible because these trajectories start before the first or respectively end after the last of the 50 chosen time steps. Again this means that all trajectories might be longer than displayed in Fig. 64. Anyway it shows that a high percentage of the trajectories contain newly calculated particle positions.

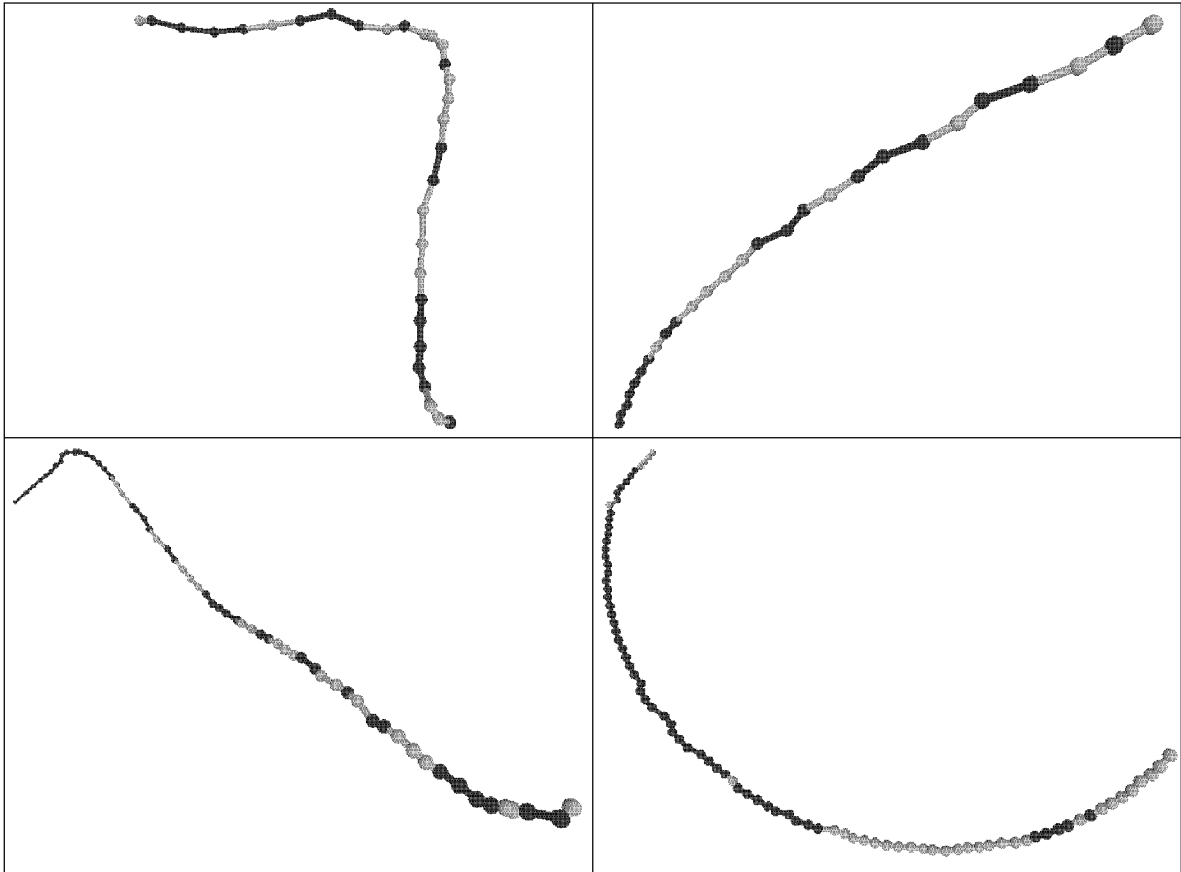


Fig. 63: Examples of reconstructed trajectories from the different data sets ‘Trinocular’, ‘copper sulphate’, ‘pb08’ and ‘2.5’, with additionally determined particles (light grey), particles determined by epipolar line intersection are marked in dark grey

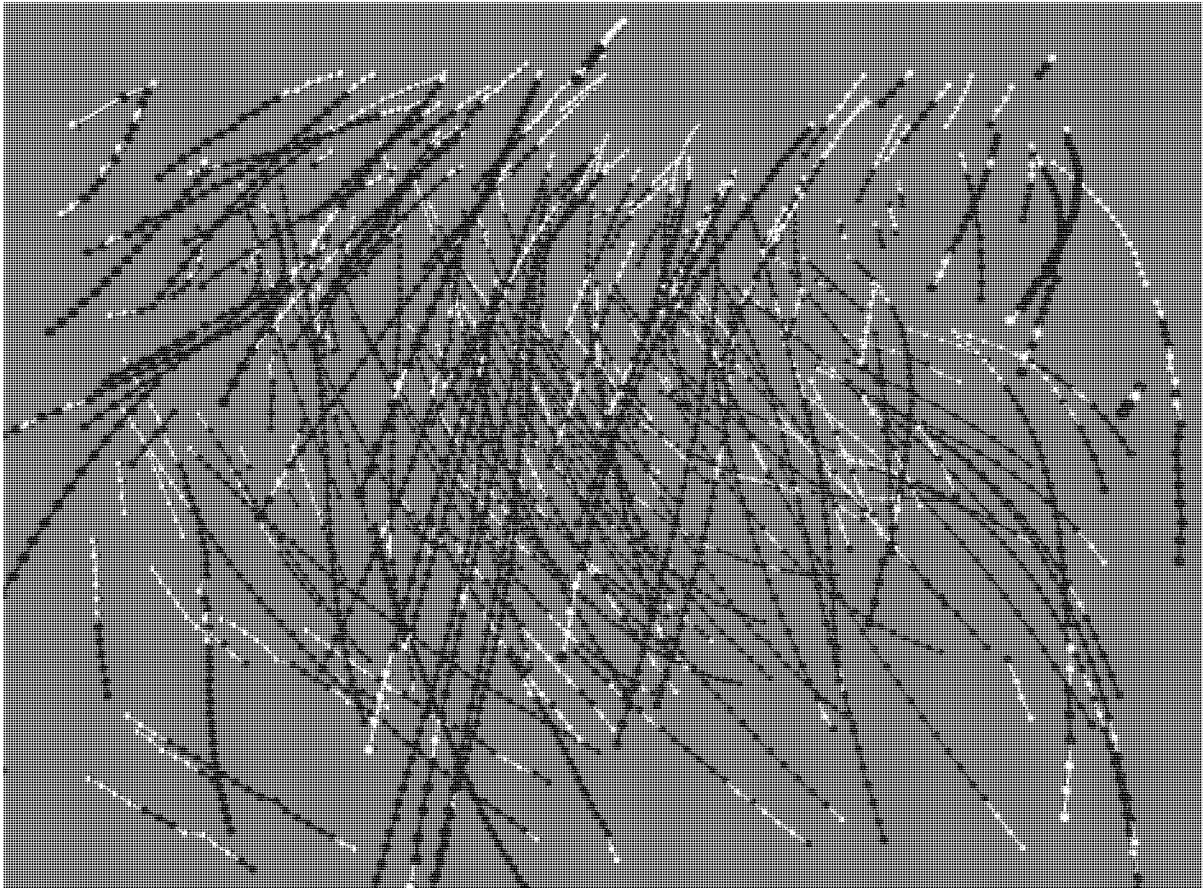


Fig. 64: Reconstructed trajectories from the data set 'copper sulphate' with additionally determined particles (light grey), particles already determined by epipolar line intersection are marked in dark grey, 50 of 200 time steps, only a selection of the trajectories is shown

7.5.3. Accuracy considerations and trajectory smoothness

The three-dimensional particle positions are determined by spatial intersection as described in 3.2., also providing accuracy information about the image coordinate measurement and the object coordinates. In both cases - for the correspondences established by the epipolar line intersection as well as for the particle positions added during the tracking procedure - the same approach is used. Accuracy and reliability are depending on the image coordinate measurement and the number of observations used for the point positioning. In general the number of observations can be expected to be higher in the case of the particle positions determined by the epipolar line intersection (mostly quadruplets or triplets) than for the particle positions added during the tracking procedure (which are also calculated from pairs). The reduced number of observations leads to a decreased reliability.

Considering the quality of both types of particles a slightly decreased accuracy level is observed for the additionally determined particle positions. Most of the additionally calculated particle position are of the same order of accuracy as those determined by the epipolar intersection, but there are cases, where the 3D position is not reliably determinable. The RMS values increase up to factor 3, in particular cases even worse. The distribution of the RMS values is less homogeneous, which can be explained by the lower number of observations leading to a

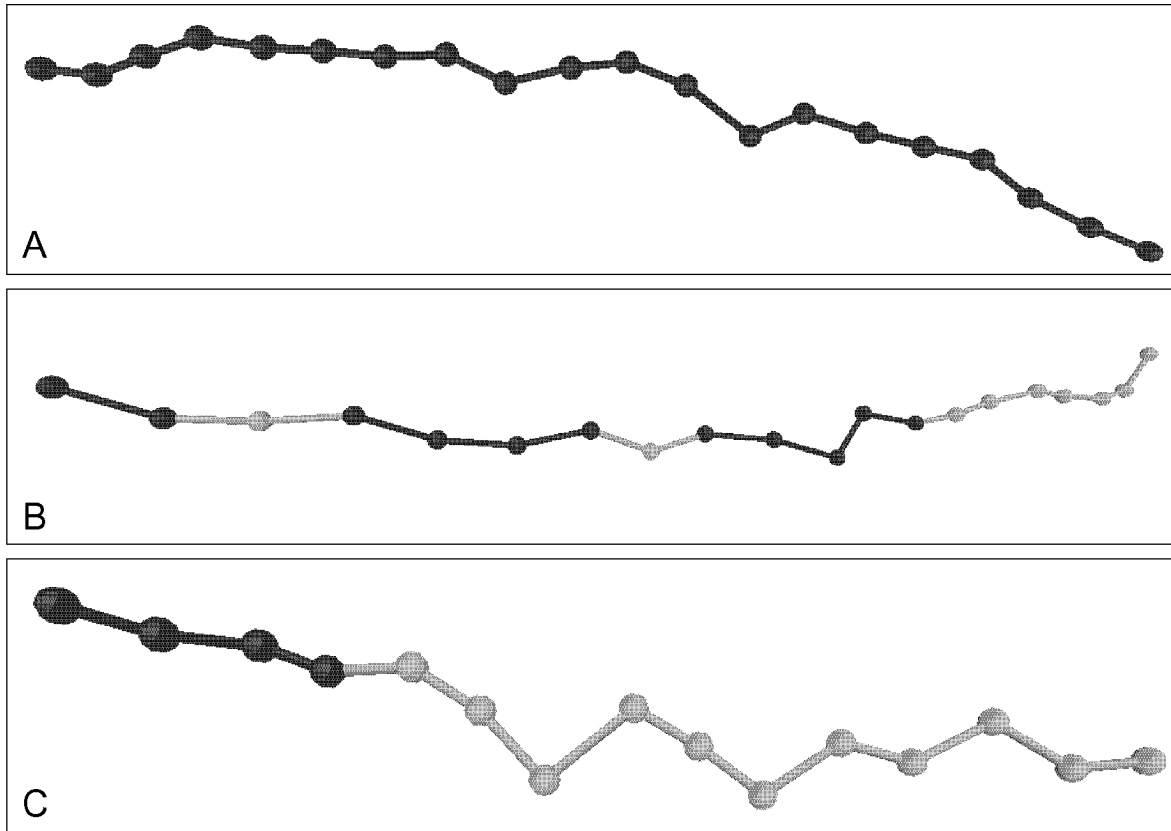


Fig. 65: Examples of unsmooth particle trajectories, A) trajectory completely reconstructed with particle positions from epipolar line intersection (dark grey), B) trajectory with particle positions from epipolar line intersection (dark grey) and particles positions added during the tracking procedure (light grey), C) trajectory initialized with particle positions from epipolar line intersection (dark grey) continued with additionally calculated particle positions

lower reliability. Often only two image coordinate pairs are available for the determination of the added particle position. If those less observations are deteriorated (e.g. due to overlapping particle images, which can not be separated), the influence on the particle position and on the accuracy measures can be high. On the other hand inconsistencies might be lower if less observations - which have to 'fit' - are concerned, thus also leading to the small residuals.

Investigations on the tracking results have shown that the accuracy measures of the spatial intersection only provide limited information about the smoothness of a reconstructed particle trajectory. Additionally calculated particle positions with rather low accuracy fitted quite smoothly in a trajectory, where in other cases particle positions with low RMS values led to zigzagged trajectory segments. For the tracking procedure maximum values for acceleration and divergence angle are set. The smoothness of the trajectories can directly be controlled by those parameters. This is valid for all reconstructed trajectory segments independent from the way the according particle positions were determined. The trajectories show less smoothness in viewing direction of the cameras due to the geometrical configuration, which again is valid for both types of particles. Fig. 65 shows some examples of unsmooth trajectories. Especially trajectory C contains particle positions, which could not be determined reliably.

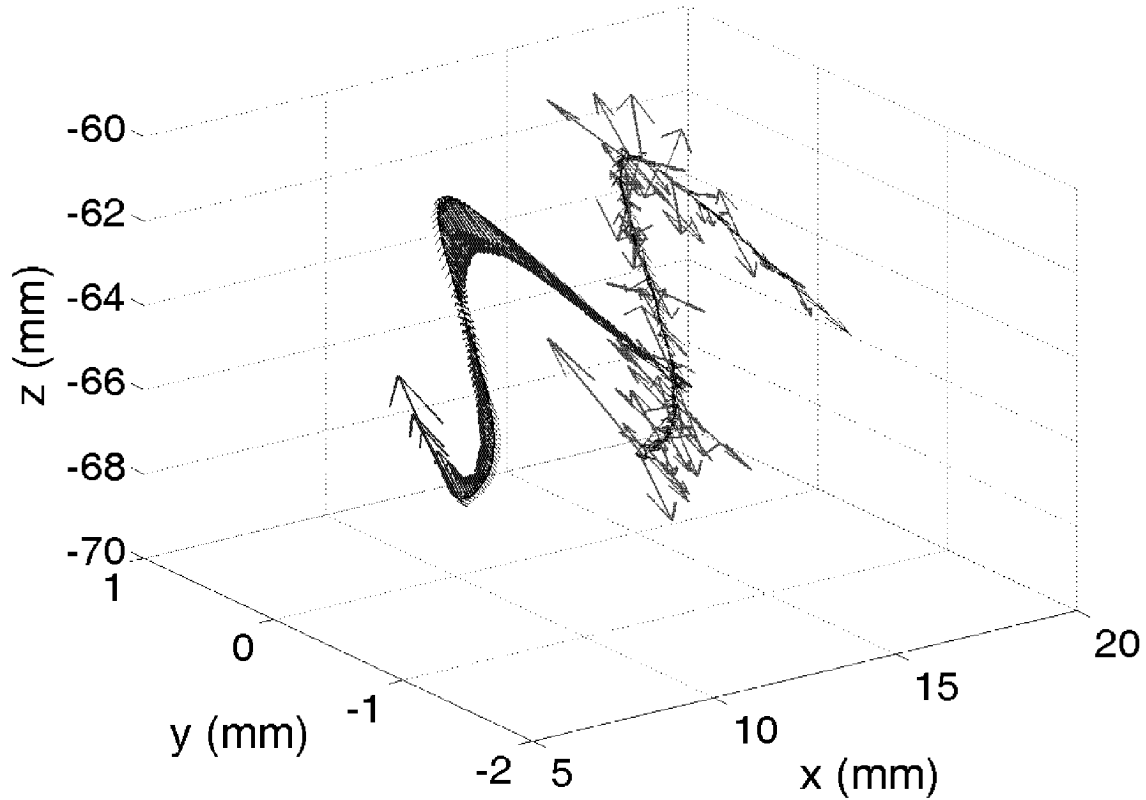


Fig. 66: The effect of the 'moving-spline' procedure is demonstrated on a qualitative level. Two renderings of an arbitrarily selected trajectory from the experiment '2.5' are shown. For this trajectory a particle is tracked through 80 time steps. The arrows represent Lagrangian acceleration. The trajectory on the left has been processed with the 'moving-spline' procedure while the Lagrangian acceleration of the trajectory on the right is obtained using a central approximation only, taken from (Lüthi, 2002)

In general the trajectories can be reconstructed with less noisy particle positions (see Fig. 63). As mentioned above it is possible to adjust the tracking parameters to exclude unsmooth particle links, which leads to smoother but on the other hand less complete trajectories.

A suitable procedure to handle unsmooth particle trajectories was proposed by Lüthi, who performed a post-processing to the tracking results yielded with the PTV approach. Lüthi applied a polynomial fitting to the discrete particle trajectory information measured with PTV for his analyses (Lüthi, 2002). The polynomial fitting reduces the influence of single, 'unsmooth' particle positions. Fig. 66 shows a trajectory before and after the polynomial fitting procedure.

7.5.4. Performance characteristics applied to the PTV data sets

According to 7.1. the performance characteristics are determined for each data set and give documentation about the increase of the potential of the PTV method. The values of the performance characteristics applied to the data sets are listed in Table 12.

Applying the enhanced PTV method delivers a higher tracking efficiency eff_{3d} throughout all investigated data sets. Concerning the values of the relative efficiency in four of the eight data sets an $eff_{3d}(rel)$ of more than 100 % could be achieved. This means that the enhanced method

could establish more links than the number of particles determined by the previous method. This becomes possible by the improved exploitation of image and object space based information allowing the determination of additional particle positions.

Compared to the previous method the gain of reconstructed links is between 25 up to 54 % when the enhanced tracking algorithm is applied to the presented data sets. Despite the variety of the presented data sets the gain might be lower in other cases. Especially if due to an accurate calibration and good image quality only little ambiguities occur, the already high tracking efficiency might not be increased any further with the enhanced method.

From the hydrodynamic point of view the important improvement of the method is not only a higher number of links from one time step to the next, but also the reconstruction of longer trajectories. The alternative performance characteristics as the average trajectory length avl_{traj} and the total length L_{traj} of all trajectories were already discussed in the sections where the processing of the according data set is described.

The quality of the yielded results derived from the various data sets proved the general applicability of the developed PTV method for manifold flow measurement tasks.

Table 12: Overview over performance characteristics for each processed data sets

Data set	Previous method	Enhanced method		
	Efficiency eff_{3d} in [%]	Efficiency eff_{3d} in [%]	relative Efficiency $eff_{3d}(rel)$ in [%]	Gain g_{3d} in [%]
Simulated vortex	88.7	96.4	112.2	25.0
Trinocular	80.6	91.4	116.0	43.9
Forward facing step	65.5	69.0	82.0	25.2
Copper sulphate	74.8	87.9	115.3	54.1
1.0 (to TrackingHS)	53.1	61.4	73.9	39.2
2.5 (to TrackingHS)	56.1	63.6	75.4	34.5
pb08	74.4	89.9	114.1	53.4
Maser8	58.3	70.1	81.7	40.3

8. Conclusions and perspectives

In this final chapter some concluding remarks about the new spatio-temporal matching algorithm for 3D PTV are given. Furthermore some perspectives for future work are proposed.

8.1. Conclusions

The PTV technique developed at the Institute of Geodesy and Photogrammetry is an operational and reliable tool, which was already applied in various measurement tasks. The former implementation worked with an object space based tracking procedure. An important processing step is the establishment of multi-image correspondences. Due to the large number of particles not all ambiguities in the epipolar line intersection can be solved even when the flow is observed with a four camera arrangement. The establishment of spatial and temporal correspondences between particles images is strictly separated in this implementation. An increase of the method's potential was expected by a more efficient way of using the redundant information, which is available for the spatio-temporal assignment.

The number of unsolved ambiguities resulting from the epipolar line intersection technique can be decreased if the motion of a particle from previous time steps is considered. Based on the existing system a new implementation for PTV was developed, implemented and tested. The main goal was to increase the tracking rate, which was achieved by a more efficient exploitation of the information available from image and object space. Formerly unused particle detections, which could not be matched due to ambiguities in the epipolar line intersection can now contribute to a more complete trajectory reconstruction. In the context of the particle motion it is possible to determine additional particle positions to close gaps over one or more time steps, even the continuation of trajectories is feasible. To quantify the improvement of the enhanced method it was tested on several data sets. In all cases the number of particles as well as the tracking efficiency is higher when the data set is processed with the enhanced PTV method. The gain of the enhanced method with respect to the previous approach is in the order of 25 % in the case of the synthetically generated data set and between 25 % up to 54 % for the processed data sets from real experiments.

The increased number of established links is not the only gain of the enhanced approach. From the hydrodynamic point of view the important improvement of the method is also the reconstruction of longer trajectories. A major advantage of the enhanced method is a significantly increased number of long trajectories forming a more reliable statistical basis for Lagrangian analysis. For some purposes of hydrodynamic postprocessing like spline interpolation, which is only possible with particle trajectories of a certain length, more usable information about the velocity field is obtained.

In the case of the data sets acquired for the investigation of velocity derivatives in turbulent flows the Kolmogorov time τ_η was determined from the flow field measurements or at least a good estimation could be made. With this knowledge the minimum length of a trajectory, which can contribute to a Lagrangian analysis can be specified. This allows a consolidated

quantification of the results obtained with the different tracking approaches. In the case of the data sets, where the Kolmogorov time τ_η was determined it has been shown that the number of trajectories forming the basis for such analyses could be increased by 56 % up to 83 %.

The developed tracking method based on object- and image space based information was not only tested on various data sets by the author himself, but was already successfully applied by Lüthi for the investigation of velocity derivatives in turbulent flows described in his thesis '*Some Aspects of Strain, Vorticity and Material Element Dynamics as Measured with 3D Particle Tracking Velocimetry in a Turbulent Flow*' (Lüthi, 2002). As Lüthi concludes that the enhanced method could contribute to new insights in some aspects of strain and enstrophy dynamics and to the understanding of differences between stretching of vortex lines and material lines and the behaviour of material surfaces and volumes. Further experiments applying the enhanced PTV will be conducted soon at the Institute of Hydromechanics and Water Resources Management.

In this thesis the high potential of the new 3D PTV solution and its applicability was demonstrated. The method can be considered as a powerful tool in various applications for three-dimensional flow field measurement.

8.2. Future work

As the PTV software is thought to be used for the measurement of flow fields it should be applicable by users with a hydrodynamic (thus in most cases a non-photogrammetric) background. Therefore it is requested that the implementation provides a high degree of ease regarding the handling of the system. A possible improvement could be achieved through the simplification of the calibration procedure as proposed in section 8.2.1.

A further topic of investigation arose by the analysis of the flow field data acquired for the research work of Lüthi (described in great detail in (Lüthi, 2002)) and is briefly discussed in section 8.2.2.

In section 8.2.3. further developments of hard- and software solutions for PTV are discussed.

8.2.1. Simplification of the calibration procedure by DLT

To be able to establish the correspondences in the multi images, the interior and exterior orientation parameters have to be determined. A bundle adjustment is performed to determine the values of those parameters. Due to the non-linearity of the problem, the user has to provide suitable approximations. The preparing steps to find suitable approximations for these parameters is time-consuming and requires experience. If they are not set sufficiently accurate the adjustment might fail (diverge). Using direct linear transformation (DLT) to derive these values without the need to set approximations would make the existing PTV software solution user-friendlier.

A similar approach, where DLT is used for the camera calibration, is described in (Engelmann, 1998). As far as the multimedia geometry is concerned, the procedure presented there yields better results without multimedia correction. This is in contradiction to the results of the analyses discussed in (Maas, 1992b). Therefore the following procedure is proposed:

- DLT is performed without multimedia correction to yield a set of initial values
- the initial values derived with DLT are used for a bundle adjustment considering the multimedia corrections

In the current implementation the user has to measure manually the approximate image coordinates of four well-distributed control points in each calibration image. A small shortcoming of

the DLT method is the requirement that at least six control points are needed to calculate an orientation solution. But as the calibration procedure is performed only once for each experiment this slight increase of manual measurements should be acceptable considering that the finding of suitable approximations will be better automated.

8.2.2. Investigation of the traceability of particles

In some experiments the observed volume is only a rather small part of the whole flow field. Depending on the particle motion it can be assumed that particles enter and leave the observed volume. A particle moving fast might not be tracked for a longer time due to the fact that it remains in the object volume only for a short period. But considering simply the tracking results one could conclude the faster a particle moves the shorter it can be tracked, which might not be the case.

Therefore it could be helpful to investigate the traceability during the time a particle is inside the observation volume. Full traceability would mean that either a particle could be tracked throughout the whole sequence or throughout all time steps between entry and exit of the observation volume. In general full traceability will hardly be reached.

For the analysis of the PTV results, a simple check if the start and end of a particle trajectory is inside or outside the observation volume can be performed to label a trajectory as complete or fragmented. The knowledge of the relation between complete and fragmented trajectories gives a measure of the traceability and could further contribute to a performance evaluation. Also for the conclusions of the hydrodynamic analysis ('fast particle problem' mentioned above) the traceability might be important.

From a technical point of view the main problem would be the determination of the dimensions of the observation volume. But in a first approximation a rectangular box enclosing a certain percentage of the determined particle positions is thought to be sufficient, at least to get the order of the particle traceability. This knowledge would give information about the completeness of the particle trajectory reconstruction and might help to confirm the conclusions drawn from the measurement results. It would help to quantify the overall performance of the method.

8.2.3. Further developments of 3D PTV systems

From the algorithmic point of view the current 3D PTV tracking method could be modified such that the neighbouring motion correlations are considered. Depending on the investigated flow this might yield higher trackings rates. To keep the system's flexibility the consideration of the neighbouring correlation should be implemented in a way that they can be used optionally. For the implementation of the neighbouring motion correlation the same approach as proposed in (Papantoniou/Maas, 1990) could be used. According to models of hydrodynamic theories the rather simple kinematic model used in the existing implementation could be replaced by a more sophisticated one. The existing knowledge about velocity fields in flows might help to yield better results.

One limitation of the system is the requirement that the flow field has to be observed by a sufficient number of cameras. To increase the size of object volume, thus enabling to observe more extended flow phenomena, the system could be extended to more than four cameras. With more than four cameras an increased volume could be observed with an equal spatial and temporal resolution. The cameras might be arranged in a way that every part of the object volume is observed by a sufficient number of cameras, but their field of view cover a larger area (following the photogrammetric strip or block concept). The fusion of the information captured by all cameras must be managed in a reasonable manner. With such a system it would

be possible to observe e.g. the particle motion along a channel flow, without moving the cameras.

A major shortcoming of the 3D PTV method is the rather low temporal resolution. In many flow measurement tasks where velocities are rather high, the current system cannot be applied. The frame rate of the used sensors is the limiting factor. High speed cameras are available on the market, but the storage of longer image sequence is problematic or even impossible. In consideration of the developments of digital storage devices the acquisition and storage of longer image sequences at high frame rates may become feasible. An alternative is the use of sensors with a different architecture than the conventional CCD chips. The CMOS technology with the ability of online image processing may offer suitable solutions in the future. The principle of the 3D PTV would remain the same, but with higher frame rates the temporal resolution could be increased in a way that the method's applicability is extended to observe flow phenomena with higher velocities.

9. Acknowledgements

I would like to thank all who supported me during the preparation of my thesis.

I thank Prof. Dr. Armin Grün for giving me the opportunity to work in his group, for providing an excellent research environment and for being my examiner.

I also want to thank Prof. Dr. Hans-Gerd Maas for being my co-examiner. I am very grateful for his valuable contribution to this work and for the review of the written report.

Thanks to the members of the group of Prof. Kinzelbach (IHW), especially Beat Lüthi, for providing me with the various data sets and for the fruitful discussions of hydrodynamical aspects.

This research work on the development of the spatio-temporal matching algorithm was supported by a grant of the Swiss National Science Foundation (Grant No 2100-049039.96/1). The research work on the Jet Growth Motion in Aerosols Experiments Module was funded by the European Space Research and Technology Centre (ESTEC) under Contract-No. SUM85-P-13.

I appreciate all my colleagues at the Institute of Geodesy and Photogrammetry, who created a lively and multicultural atmosphere. Especially Jana Niederöst, Fabio Remondino, Daniela Poli, Andreas Roditakis, Gabriela Seiz, Chunsun Zhang and Martin Sauerbier, with whom I enjoyed work at ETH as well as private activities. Thanks also to Karsten Lambers and Kirsten Wolff for their enduring support in editorial aspects, without which this written report would be like a leafless tree. I would also like to mention Beat Rüedin who always kept the machines running properly.

Not to forget the former staff members of the Institute of Geodesy and Photogrammetry Nicola D'Apuzzo, Thomas Bühner, Markus Niederöst and Marc Honikel. I salute you!

Having been involved also in teaching issues, I want to thank the students of geomatic engineering for bringing some change in everyday research work.

I also want to thank Maria Bühler for keeping me in contact with my home town.

Throughout the years of my doctorate I had the luck to live in Wallisellen. I really enjoyed my stay together with the housemates of the Röslistrasse 12, especially Else Bünemann and Julian Ihssen as well as with landlord Andreas Forrer.

Last but not least, I wish to express my gratitude to my parents and my brother.

Appendix

A.1 Handling of the 3D PTV software

Techniques of digital photogrammetry are suitable for static applications as well as for 3D measurement tasks in dynamic processes (El-Hakim, 1986). 3D PTV can be considered a typical application field of digital photogrammetric techniques (Grün, 1994). The method requires the acquisition and processing of stereoscopic, synchronized image sequences of the moving particles.

In the following sections a step by step advice for running PTV, some information on the input/output files is given.

A.2 Running the 3D PTV software under different operation systems

The source code of the PTV software is written in C, Tcl/Tk is required for the graphical user interface (GUI). The software can be compiled on any operation system where C and Tcl/Tk is available. The current PTV implementation runs under UNIX as well as Windows operating systems. For the image sequence data acquisition PCs with Windows operation system are used. The GUI is implemented with Tcl/Tk (current version is 8.4.2, released in march 2003, (Tcl, 2003)), which is freely available for Windows and UNIX platforms. Considering that most potential PTV users might only work with one of the mentioned operating system, the portability also could contribute to an easy distribution of the developed PTV method.

A.3 Parameter files for 3D PTV

Before running PTV, several parameter files (in ASCII) have to be created in a subdirectory of the project directory, it has to be called *parameter* and must contain the following files:

ptv.par	main parameter file
criteria.par	object volume and correspondences parameters
sequence.par	sequence parameters
targ_rec.par	parameters for particle detection
cal_ori.par	calibration plate, images, orientation files
detect_plate.par	parameters for control point detection
man_ori.par	point number for manual pre-orientation
orient.par	flags for camera parameter usage
track.par	tracking parameters
sortgrid.par	sortgrid parameter
pft_version	flag for peak fitting version

For storing of the results a directory named *res* should exist. Working with PTV the Tcl/Tk-GUI allows editing parameter files, to process a single time step or whole sequences. As a preparing steps a calibration of the image acquisition system is required. The main window is shown in Fig. 67. Each processing step can be started from the task bar, the processing status and the actual mouse button functions are displayed in the information window below. With

Start the project parameters are loaded from the input files and additional windows for the display of the images for each camera are opened.

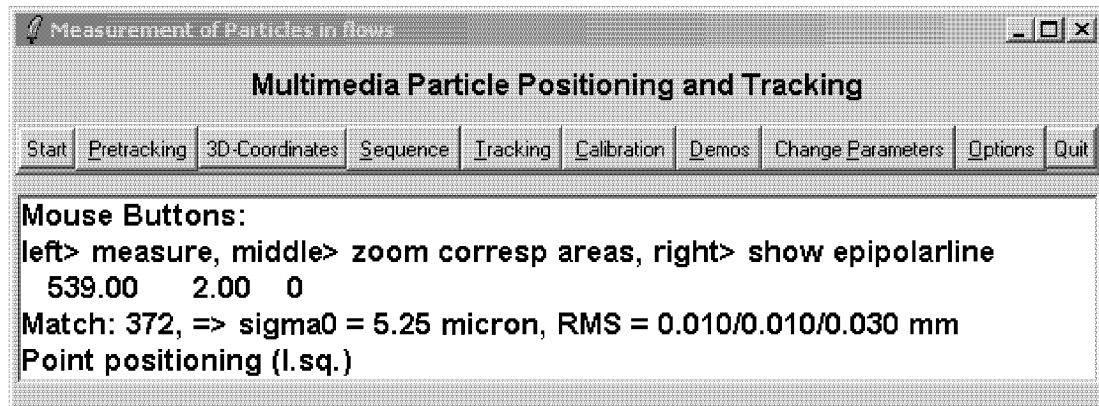


Fig. 67: Main window of PTV software

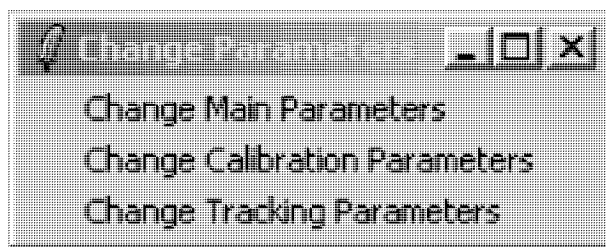


Fig. 68: Submenu Change Parameters

The settings for the PTV processing can be edited through three different parameter windows (to be opened under the submenu **Change Parameters**, shown in Fig. 68). The windows for the editing of the parameters can be found under **Change Main Parameters** (shown in Fig. 69), **Change Calibration Parameters** (Fig. 70) and **Change Tracking Parameters** (Fig. 75).

Main Parameters

Number of cameras: 4

Name of 1. image:	img/melMai25Cam1.111	Calibration data for 1. camera:	Cam1
Name of 2. image:	img/melMai25Cam2.111	Calibration data for 2. camera:	Cam2
Name of 3. image:	img/melMai25Cam3.111	Calibration data for 3. camera:	Cam3
Name of 4. image:	img/melMai25Cam4.111	Calibration data for 4. camera:	Cam4

☒ Highpass-Filter ☒ TIFF Header ☒ Frame ☐ Field odd ☐ Field even

Refractive indices:

air: 1.000 glass: 1.46 water: 1.38 thickness of glass (mm): 6.18

Parameters for particle recognition

Greyvalue threshold: 1. img: 8 2. img: 22 3. img: 8 4. img: 15

min npix:	4	min npix in x:	2	min npix in y:	2
max npix:	1000	max npix in x:	30	max npix in y:	30
Sum of greyvalue:	100	Tolerable discontinuity:	30	Size of crosses:	2

Parameters for sequence processing

Sequence images: First: 100 Last: 119

Basename for 1. sequence:	img/melMai25Cam1.
Basename for 2. sequence:	img/melMai25Cam2.
Basename for 3. sequence:	img/melMai25Cam3.
Basename for 4. sequence:	img/melMai25Cam4.

Illuminated layer data

Xmin:	-5.0	Zmin:	-80	Zmax:	-50.0
Xmax:	25.0	Zmin:	-80	Zmax:	-50.0

Criteria for correspondences

min. con. for ratio nx:	0.02	min. con. for ratio ny:	0.02
min. con. for ratio npix:	0.02	sum of gr:	0.02
min. for weighted correlation:	10	Tolerance to epipolar band (mm):	0.02

OK

Fig. 69: Main parameter window

A.4 Data Input

The processing of image data with PTV requires for each camera a valid video sequence stored in TIFF- (8 Bits/Sample, single image plane) or as raw data files. The respective flag for TIFF or raw file must be set. The filename for the sequence image is a combination of a basename indicating the camera and a current number. For each camera an orientation data file (*name.ori*) and an additional parameters file (*name.addpar*) must exist and has to be accessible for PTV.

Calibration Parameters

Camera 1, Calibration image: Cam1 Orientation data: Cam1.ori
 Camera 2, Calibration image: Cam2 Orientation data: Cam2.ori
 Camera 3, Calibration image: Cam3 Orientation data: Cam3.ori
 Camera 4, Calibration image: Cam4 Orientation data: Cam4.ori

File of Coordinates on Plate: caFieldApril.txt

☒ TIFF-Header ☒ Frame ☐ Field odd ☐ Field even

Imagesize, horizontal: 640 vertical: 480
 Pixelsize, horizontal: 0.01 vertical: 0.01

Target recognition on plate

Greyvalue threshold, 1.: 60 2.: 50 3.: 60 4.: 60
 min npix: 40 min npix in x: 7 min npix in y: 7
 max npix: 1000 max npix in x: 50 max npix in y: 50
 Sum of greyvalue: 500 Tolerable discontinuity: 100 Size of crosses: 3

Point number for manual pre-orientation

Image 1	P1: 1	P2: 5	P3: 21	P4: 25
Image 2	P1: 1	P2: 5	P3: 21	P4: 25
Image 3	P1: 1	P2: 5	P3: 21	P4: 25
Image 4	P1: 1	P2: 5	P3: 21	P4: 25

Orientation parameters

Point number for orientation: 0
☐ Principle distance ☐ xp ☐ yp
 Lens distortion (Brown): ☐ k1 ☐ k2 ☐ k3 ☐ p1 ☐ p2
 Affin transformation: ☒ sck ☒ she
 OK

Fig. 70: Calibration parameter window

Examples for the parameterfiles:

ptv.par:

4
 cam3.100
 kal1
 cam0.100
 kal3
 cam1.100
 kal4

main parameter file

number of cameras
 image of first camera
 calibration data of first camera
 image of second camera
 calibration data of second camera
 image of third camera
 calibration data of third camera

cam2.100	image of fourth camera
kal5	calibration data of fourth camera
1	flag for highpass filtering, use (1) or not use (0)
1	flag for TIFF header (1) or raw data (0)
720	image width in pixel
576	image height in pixel
0.009	pixel size horizontal [mm]
0.0084	pixel size vertical [mm]
0	flag for frame, odd or even fields
1.0	refractive index air [no unit]
1.5	refractive index glass [no unit]
1.0	refractive index water [no unit]
9.4	thickness of glass [mm]

criteria.par: object volume and correspondence parameters

0.0	illuminated layer data, xmin [mm]
-10.0	illuminated layer data, zmin [mm]
0.0	illuminated layer data, zmax [mm]
10.0	illuminated layer data, xmax [mm]
-10.0	illuminated layer data, zmin [mm]
0.0	illuminated layer data, zmax [mm]
0.02	min corr for ratio nx
0.02	min corr for ratio ny
0.02	min corr for ratio npix
0.02	sum of gv
33	min for weighted correlation
0.02	tolerance to epipolar line [mm]

sequence.par: sequence parameters

cam0.	basename for 1. sequence
cam1.	basename for 2. sequence
cam2.	basename for 3. sequence
cam3.	basename for 4. sequence
100	first image of sequence
119	last image of sequence

targ_rec.par: parameters for particle detection

12	grey value threshold 1. image
12	grey value threshold 2. image
12	grey value threshold 3. image
12	grey value threshold 4. image
50	tolerable discontinuity in grey values
25	min npix, area covered by particle
400	max npix, area covered by particle
5	min npix in x, dimension in pixel
20	max npix in x, dimension in pixel
5	min npix in y, dimension in pixel
20	max npix in y, dimension in pixel
100	sum of grey value
1	size of crosses

<u>cal_ori.par:</u>	calibration plate, images, orientation files
ptv/ssc_cal.c3d	control point file (point number, X, Y, Z in [mm], ASCII
kal1	calibration image camera 1
kal1.ori	orientation data camera 1
kal3	calibration image camera 2
kal3.ori	orientation data camera 2
kal4	calibration image camera 3
kal4.ori	orientation data camera 3
kal5	calibration image camera 4
kal5.ori	orientation data camera 4
1	flag for TIFF header (1) or raw data (0)
0	flag for frame (0), odd (1) or even fields (2)

<u>detect_plate.par:</u>	parameters for control point detection
30	grey value threshold 1. calibration image
30	grey value threshold 2. calibration image
30	grey value threshold 3. calibration image
30	grey value threshold 4. calibration image
40	tolerable discontinuity in grey values
25	min npix, area covered by particle
400	max npix, area covered by particle
5	min npix in x, dimension in pixel
20	max npix in x, dimension in pixel
5	min npix in y, dimension in pixel
20	max npix in y, dimension in pixel
100	sum of grey value
3	size of crosses

<u>man_ori.par:</u>	point number for manual pre-orientation
28	image 1 p1 on target plate (reference body)
48	image 1 p2
42	image 1 p3
22	image 1 p4
28	image 2 p1
48	image 2 p2
42	image 2 p3
23	image 2 p4
28	image 3 p1
48	image 3 p2
42	image 3 p3
22	image 3 p4
28	image 4 p1
48	image 4 p2
42	image 4 p3
22	image 4 p4

<u>orient.par:</u>	flags for camera parameter usage 1=use, 0=unused
2	point number for orientation, in this case every second point on the reference body is used, 0 for using all points
1	principle distance
1	xp
1	yp
1	k1
1	k2
1	k3
0	p1
0	p2
1	scx
1	she

<u>track.par:</u>	tracking parameters
-0.8	dvxmin
0.8	dvxmax
-0.8	dvymin
0.8	dvymin
-0.8	dvzmin
0.8	dvzmax
120	dangle
0.4	dacc
1	add, flag for additional particles use (1)

<u>sortgrid.par:</u>	changes must be done with an editor
5.0	distance between detected image coordinate and reprojected control point in pixel

<u>pft version:</u>	flag for peak fitting version (newest)
3	

Those parameter files can be edited under **Changing Parameters** in the appropriate submenu windows (**Main Parameters** shown in Fig. 69, **Calibration Parameters** shown in Fig. 70 , **Tracking Parameters** shown in Fig. 75).

A.5 Examples for the parameter files *name.ori* and *name.addpar*

<u>name.ori:</u>	camera orientation file
101.8263 -9.9019 65.1747	projective center X,Y,Z, [mm]
0.4151383 -0.0069793 1.5073263	omega, phi, kappa [rad]
0.0634259 -0.9979621 -0.0069792	rotation matrix (3x3)
0.9130395 0.0608491 -0.4033067	[no unit]
0.4029095 0.0192078 0.9150383	
-0.6139 -0.0622	xp, yp [mm]
8.7308	principle distance [mm]

name.addpar:

additional parameters

-0.00342 0.00007 -0.00002 -0.000545 0.000632 1.004600 0.002856

=====

k1 [no unit], k2 [no unit], k3 [no unit], p1 [no unit], p2 [no unit], scale
in x [no unit], shearing in [rad]

A.6 Calibration of the image acquisition system

Before an image sequence can be processed the calibration of the image acquisition system has to be performed. As a result of the calibration the three coordinates X_O , Y_O , Z_O of the projective center and three angles ω , φ , κ describing the direction of the optical axis are determined (exterior orientation). To meet the physical realities the following parameters and model extensions are introduced (interior orientation and additional parameter):

- The camera constant c (computational imaging width).
- The principle point coordinates x_H , y_H .
- The lens distortion is modelled with up to five parameters (k_1 , k_2 , k_3 , p_1 , p_2).

Different clock rates of camera and framegrabber cause a horizontal scale factor s_x , which deviates from one. A further parameter δ is used for the shearing effect.



Fig. 71: Submenu with the steps of calibration procedure

In total 16 parameters (exterior orientation, interior orientation, additional parameters) can be used to model each camera. In the submenu **Calibration Parameters** (Fig. 70) the according flag for each parameter can be set. If the parameter flag is set the according value is determined in the bundle adjustment. Otherwise it is introduced as a fixed parameter. The **Calibration** submenu (Fig. 71) contains the following steps:

A suitable set of calibration images must exist as TIFF (8 Bits/Sample, single image plane) or as raw data files. The respective flag for TIFF- or raw file must be set.

To load the images for the calibration press **Show Calib. Image**. For the acquisition of the calibration images use a reference body suitable for the object volume.

The determination of the image coordinates of the reference points is started with **Detection**. It is the application of the peakfitting routine after a high pass filtering. The relevant parameters for the detection have to be set in the **Change Calibration Parameters** window (Fig. 70).

With **Manual Orientation** four points of the reference body can be measured manually in each calibration image. A file named *man_ori.dat* with the measured image coordinates is created. The points that have to be measured are displayed in the information window of the main menu (Fig. 67). The measurements are required for each calibration image, once measured the image coordinate are stored in the *man_ori.dat* file.

If the file *man_ori.dat* already exists the measurement could be reused with **Orientation with file**.

The automated points detection might produce mismatches e.g. due to scratches and other disturbances on the reference body. Points that will lead to mismatching in the *Sortgrid* routine should be deleted in advance.

With *Sortgrid* all points of the reference body are reprojected in image space using the approximate camera orientation data. The search radius for the detected points is defined in *parameters/sortgrid.par*. The value of the search radius in pixels has to be changed in the file itself, as it cannot be set over the GUI of the PTV software

Orientation calculates the parameters of the cameras in a bundle adjustment. As the approximation values for the orientation parameters might be unsuitable their determination probably have to be performed stepwise. The user should also avoid overparametrization as not all unknowns might be determined reliably.

Checkpoints shows residual in the control points. The display of the residuals can be used for a visual control of the orientation results.

Ap figures shows the effect of the additional parameters. The effect of the additional parameters is enlarged by a certain factor for visualization purpose.

A.7 Processing of a single time step

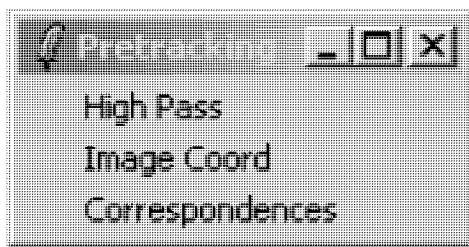


Fig. 72: Submenu Pretracking

Under *Pretracking* (Fig. 72) the processing of a single time step regularly starts with the application of a highpass filtering (*Highpass*).

After that the particles are detected (*Image Coord*) and the position of each particle is determined with a weighted grey value operator.

The next step is to establish correspondences between the detected particles from one camera to all other cameras (*Correspondences*).

With pressing of *3D-Coordinate* on the task bar of the main window the determination of the three-dimensional positions of the particles in object space is performed. The 3D data is written to disc, if existing into the directory named *res*, otherwise into the current directory. The processing of a single time step is necessary to adjust parameters like grey value thresholds or tolerance to the epipolar line.

A.8 Display of image sequences

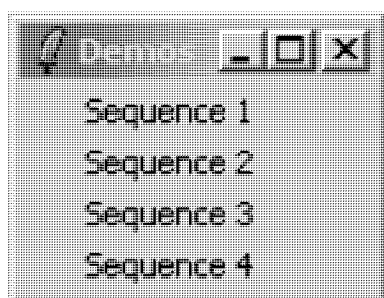


Fig. 73: Display of image sequences

Under the submenu *Demos* (Fig. 73) the display of the image sequence recorded by each camera can be started. After the choice of the camera number the sequence is displayed in the according image display window.

A.9 Processing of image sequences

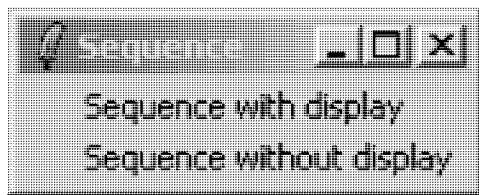


Fig. 74: Sequence processing

After having optimized the parameters for a single time step the processing of the whole image sequence can be performed under **Sequence** (Fig. 74) with or without display of the currently processed image data. It is not advisable to use the display option when long image sequences are processed. The display of detected particle positions and the established links can be very time consuming.

For each time step the detected image coordinates and the 3D coordinates are written to files, which are later used as input data for the **Tracking** procedure.

A.10 Tracking of particles

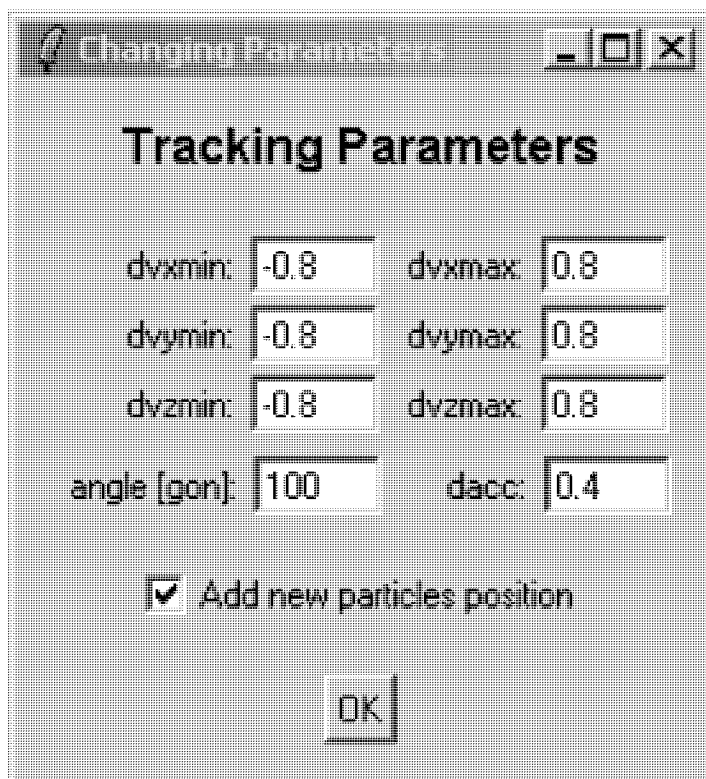


Fig. 75: Tracking parameter window

Before the tracking can be performed several parameters defining the velocity, acceleration and direction divergence of the particles have to be set in the submenu **Tracking Parameters** (Fig. 75). The flag 'Add new particles position' is essential to benefit from the capabilities of the enhanced method.

To derive a velocity field from the observed flow **Tracking with display**, **Tracking without display** and **Tracking backwards** under **Tracking** (Fig. 76) has to be performed. Again it is not advisable to use the display option if long sequences are processed. The tracking procedure allows bidirectional tracking.

Detected Particles displays the detected particles from the sequence processing.



Fig. 76: Submenu Tracking

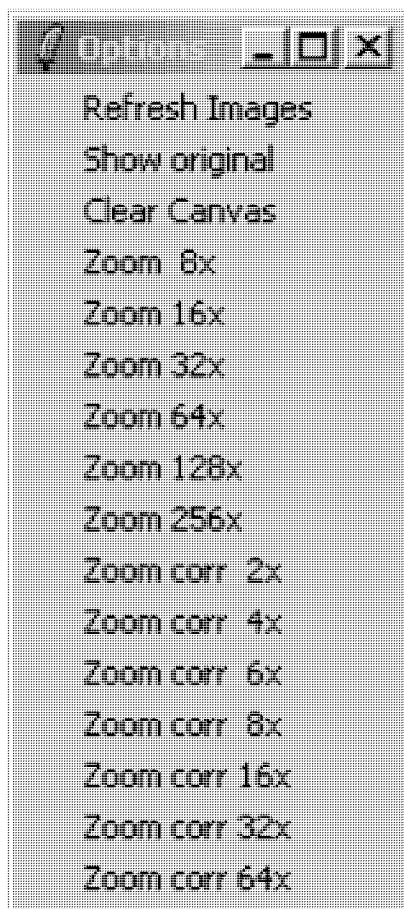


Fig. 77: Image display and zoom options

For a combined sequence processing and tracking in forward direction *Sequence/Tracking* can be started, *Tracking backwards* is not performed in this procedure.

Show Trajectories displays the reconstructed trajectories in all image display windows.

For the generation of VRML-files of the results from the sequence processing press *VRML Detection* to get an untracked point cloud, *VRML Tracks* to get exclusively the trajectories or *VRML Detection + Tracks* to get all 3D points and links. The VRML output is created in VRML version 1.0.

A.11 Options

Several Options for image display and zooming are accessible under *Options* (Fig. 77). Zooming is either performed for each image individually or in corresponding image regions.

A.12 Visualization of tracking results

For a visual analysis of the results three different visualization tools were used. VRML-output can be viewed in a common VRML-Browser, the output can be directly generated by the PTV implementation allows a 3D display of the trajectories in a static way.

A VRML-representation was also used for the visualization of single trajectories or velocity field where the particle types (epipolar intersection method, added particles) should be distinguished.

An alternative visualization, which also allows showing the motion of the particles was realized in MATLAB. The input data for this purpose cannot directly be generated by the PTV implementation, but by a small format conversion program. The MATLAB visualization tool was used to show the complete velocity field or selected trajectories of the regarding data set.

The most suitable velocity field visualization is possible by a software tool developed by Nicola D'Apuzzo (D'Apuzzo, to appear). With a GTK-GUI is can show the velocity field in static and dynamic way in different modes. During the display of the particle motion the view-point can be changed interactively. Single trajectories or region of the velocity field can be selected and visually analysed in detail. This tool is very helpful for a qualitative assessment of the results of the PTV processing. Remarkable is its performance considering the visualization of large data sets. Fig. 78 shows the GUI of the software tool to visualize the tracking results.

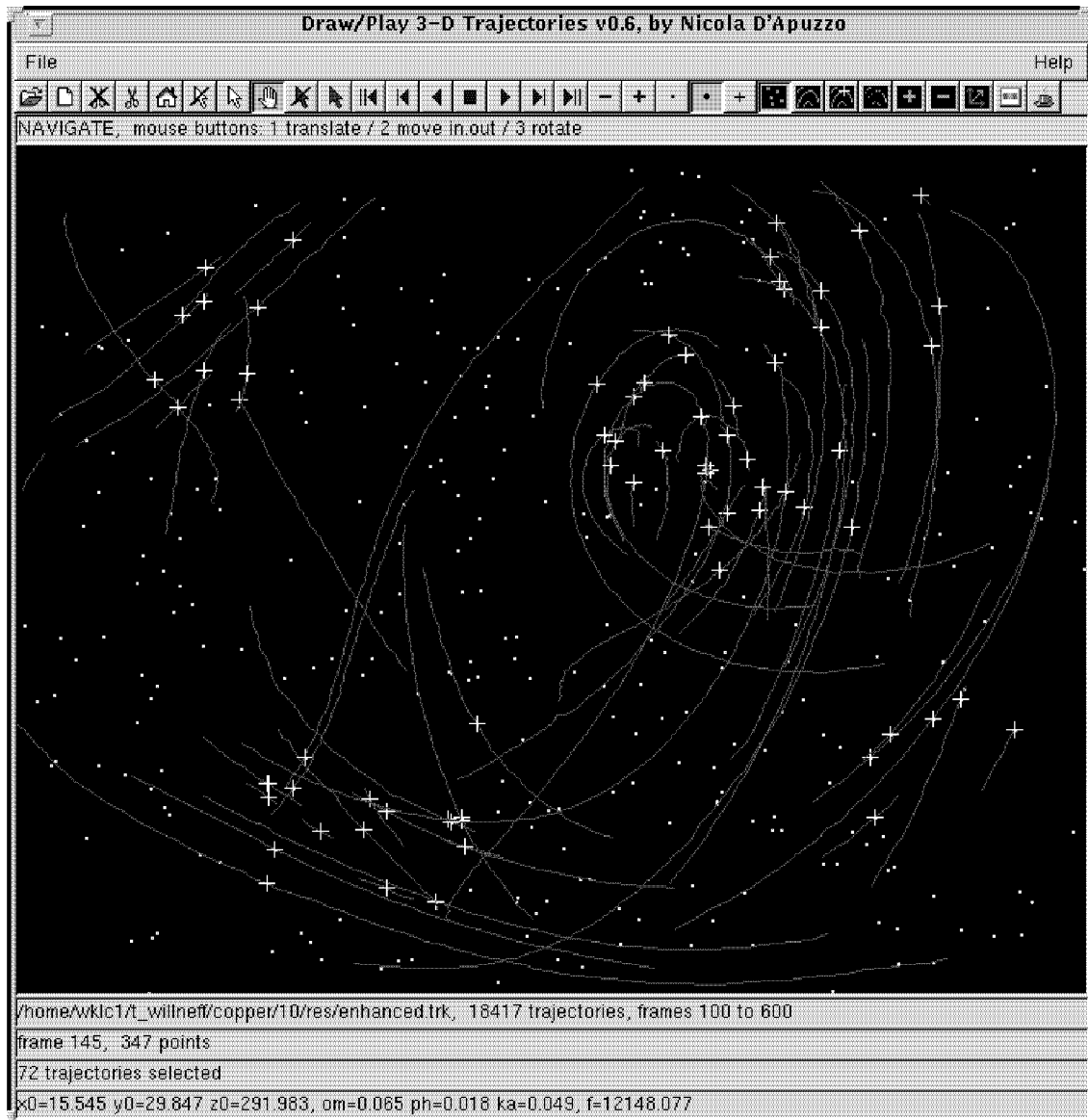


Fig. 78: Software tool for the visualization of tracking results, developed by D'Apuzzo

References

- AIAA, 2003: American Institute of Aeronautics and Astronautics (AIAA), *Planar Laser-Induced Fluorescence*, Web-site: www.aiaa.org/tc/amt/techniques/plif.html, 2003
- Adrian, R., 1986: *Multi-Point Optical Measurements of Simultaneous Vectors in Insteady Flow - a Review*. *Int. J. of Heat and Fluid Flow*, Vol. 7, No. 2, pp. 127 - 145
- Adamczyk, A., Rimai, L., 1988a: *2-D Particle Tracking Velocimetry (PTV): Technique and Image Processing Algorithms*. *Experiments in Fluids*, Vol. 6, pp. 373-380
- Adamczyk, A., Rimai, L., 1988b: Reconstruction of a 3-Dimensional Flow Field from Orthogonal Views of Seed TRack Video Images. *Experiments in Fluids* 6, pp 380-386
- AudioVideoSupply, 2003, Product information about Sony SSC-DC50, Web-site: <http://www.avsupply.com/>
- Ayache, N., Lustman, F., 1987: Fast and reliable passive trinocular stereovision. First International Conference on Computer Vision, Computer Society Press, London, pp. 422-427
- Baker, H., Bolles, R., 1994: Realtime stereo and motion integration for navigation, *IAPRS*, Vol. 30, Part 3/1, pp 17-24
- Becker, J., Gatti, L., Maas, H.-G., Virant, M., 1995: *Three-Dimensional Photogrammetric Particle-Tracking Velocimetry*. *Preparing for the Future*, Vol. 5, No. 3
- Bertschler, M., 1985: *Untersuchung der Turbulenzstruktur im offenen Gerinne über glatter Sohle und mit Rauigkeitselementen*, Ph.D. thesis, ETH Zürich
- Bolinder, J., 1999: *On the accuracy of a digital particle image velocimetry system*, Technical Report, ISSN 0282-1990, ISRN LUTMDN/TMVK -- 3186 -- SE, Sweden
- Bolles, R., Woodfill, J., 1993: *Spatiotemporal consistency checking of passive range data*. In *International Symposium on Robotics Research*, Pittsburg, PA, USA
- Brown, D., 1971: *Close-Range Camera Calibration*. *Photogrammetric Engineering*, Vol. 37, No. 8
- Brown, D., 1976: *The bundle adjustment - progress and prospects*. *IAPRS* Vol. XXI, Part 3
- Dahm W. J. A., Dimotakis, P. E., 1990: Mixing at large Schmidt number in the self-similar far field of turbulent jets, *J. Fluid Mech.*, 217, pp 299-330
- Dahm W. J. A., Southerland, K., Buch, K., 1990: *Four-dimensional laser induced fluorescence measurements of conserved scalar mixing in turbulent flows*, 5th Int. Symp. on the Appl. of laser techniques to fluid meachanics, Lisbon
- Dahm, W. J. A., Southerland, K., Buch, K. A., 1991: *Direct, high resolution, four-dimensional measurements of the fine scale structure of $Sc \gg 1$ molecular mixing in turbulent flows*, *Phys. Fluid A3*, pp 1115-1127
- Dantec Dynamics A/S, 2003, Denmark, Web-site: www.dantecmt.com
- D'Apuzzo, N., 2002: *Surface measurement and tracking of human body parts from multi image video sequences*, *ISPRS Journal of Photogrammetry and Remote Sensing* 56, pp 360-375.
- D'Apuzzo, N., not published yet: *Surface Measurement and Tracking of Human Body Parts from Multi-Station Video Sequences*, ETH Zürich - Ph.D. thesis, to appear

- Dupont, O., Dubois, F., Vedernikov, A., Legros, J.-C., Willneff, J., Lockowandt, C., 1999: *Photogrammetric set-up for the analysis of particle motion in aerosol under microgravity conditions*. Measurement Science and Technology, Volume 10, Number 10, October 1999, Special Issue: Instrumentation and Diagnostics for Microgravity Experiments, pp 921-933
- Dold, J., Maas, H.-G., 1994: *An application of epipolar line intersection in a hybrid close range photogrammetric system*, ISPRS Com. V Symposium, Melbourne, Australia, March 1-4. IAPRS Vol. 30, Part V
- El-Hakim, S.F., 1986: *Real-Time Image Metrology with CCD Cameras*. Photogrammetric Engineering and Remote Sensing, Vol. 52, No. 11, pp. 1757 - 1766.
- Engelmann, D., Garbe, C., Stöhr, M., Geissler, P., Hering, F., Jähne, B., 1998: *Stereo Particle Tracking*, in Proceedings of the 8th International Symposium on Flow Visualisation, Sorrento, Italy, September 1-4, pages 240.1249.9, 1 Sept. 1998.
- Engelmann, D., 2000: *3D-Flow Measurement by Stereo Imaging*, Dissertation, Rupertus Carola University of Heidelberg, Germany.
- Förstner, W., Karpinsky, G., Krain, H., Röhle, I., Schodl, R., 2000: *3-Component-Doppler-Laser-Two-Focus Velocimetry applied to a transonic centrifugal compressor*, in Proceedings of 10th International Symp. on Application of Laser Techniques to Fluid Mechanics, Lisbon, Portugal, Paper 7-2, July 2000
- Fraser, C., Shao, J., 2001: *On the tracking of object points in a photogrammetric motion capture system*, Videometrics and Optical Methods for 3D Shape Measurement, Proceeding of SPIE, Volume 4309, pp 212-219, 22-23 January 2001, San Jose, California, USA
- Frisch, U., 1995: *Turbulence: The legacy of A. N. Kolmogorov*. Cambridge University Press
- Ge, Y., Cha, S.S., 2000: *Application of Neural Networks to Spectroscopic Imaging Velocimetry*, AIAA Journal, Vol. 38, pp 487-492
- Grün, A., 1985: *Adaptive Least Squares Correlation - A Powerful Image Matching Technique*, South African Journal of Photogrammetry, Remote sensing and Cartography Vol. 14, No. 3, pp 175-187
- Grün, A., Baltsavias, M., 1988: *Geometrically Constrained Multiphoto Matching*, Photogrammetric Engineering, Vol. 54, No. 5, pp 633-641
- Grün, A., 1994: *Digital close-range photogrammetry - progress through automation*. Keynote Paper, ISPRS Com. V Symposium, Melbourne, Australia, March 1-4. IAPRS Vol. 30, Part V
- Grün, A., Kinzelbach, W., Gyr, A., Maas, H.-G., 1996: *Entwicklung eines spatio-temporalen Zuordnungsalgorithmus für 3-D PTV*, Research Proposal, not published
- Guezennec, Y. G., Brodkey, R. S., Trigui, N., Kent, J. C., 1994: *Algorithm for fully automated three-dimensional Particle Tracking Velocimetry*, Exp. in Fluids 17, pp. 209-219
- Heist, D., Castro, I., 1996: *Point measurement of turbulence quantities in separated flows - a comparison of techniques*, Meas. Sci. Technol. 7 (1996), pp. 1444 - 1450, printed in the UK
- Hering, F., 1996: *Lagrangesche Untersuchungen des Strömungsfeldes unterhalb der wellenbewegten Wasseroberfläche mittels Bildfolgeanalyse*. PhD thesis, University Heidelberg, Heidelberg, Germany
- Hinsch, K. D., Hinrichs, H., 1996: *Three-Dimensional Particle Velocimetry*, in *Three-Dimensional Velocity and Vorticity Measuring and Image Analysis Techniques*, pp. 129-152, Kluwer Academic Publishers, printed in the Netherlands

- Jähne, B., 1997: *Digitale Bildverarbeitung*. 4. Auflage, Springer Verlag.
- Jørgensen, F., 2002: *How to measure turbulence with hot-wire anemometers - a practical guide*, Publication no. 9040U6151, Dantec Dynamics A/S, Denmark
- Kasagi, N., Nishino, K., 1990. Probing Turbulence with Three-Dimensional Particle Tracking Velocimetry. *Proceedings International Symposium on Engineering Turbulence - Methods and Measurements*, Dubrovnik, September 24-28
- Kasagi, N., Sata, Y., 1992: *Recent developments in three-dimensional particle tracking velocimetry*, Proc. 6th Int. Symp. Flow Vis., Yokohama, pp. 832-837
- Krake, A., Fiedler, K., 2002: *Laser 2 Focus Measurements and Flow Visualisation within the Rotating Rotor and the Side Channel of a Side Channel Compressor*, Proceedings of The 9th International Symposium on Transport Phenomena and Dynamics of Rotating Machinery, on CD-ROM, February 10-14, Honolulu, Hawaii, USA
- Kolmogorov, A. N., 1941a: *The local structure of turbulence in incompressible viscous fluid for very large Reynolds numbers*, Dokl. Akad. Nauk SSSR, 30, 299-303; for English translation see *Selected works of A. N. Kolmogorov*, I, ed. V. M. Tikhomirov, pp. 321-318, Kluwer
- Kolmogorov, A. N., 1941b: *Dissipation of energy in locally isotropic turbulence*, Dokl. Akad. Nauk SSSR, 32, 19-21; for English translation see *Selected works of A. N. Kolmogorov*, I, ed. V. M. Tikhomirov, pp. 324-327, Kluwer
- Kompenhans, J., Raffel, M., Willert, C., Wiegels, M., Kähler, C., Schröder, A., Bretthauer, B., Vollmers, H., Stasicki, B., 1996: *Investigation of unsteady flow fields in wind tunnels by means of Particle Image Velocimetry*, in *Three-Dimensional Velocity and Vorticity Measuring and Image Analysis Techniques*, pp. 113-127, Kluwer Academic Publishers, printed in the Netherlands
- Lai, J., He, Y., 1989: *Error considerations for turbulence measurements using laser-two-focus velocimetry*, J. Phys. E: Sci. Instrum. 22 (1989), pp. 108-114, printed in the UK
- Lai, W. T., 1996: *A new approach in experimental fluid research*, in *Three-Dimensional Velocity and Vorticity Measuring and Image Analysis Techniques*, pp. 61-92, Kluwer Academic Publishers, printed in the Netherlands
- Lockowandt, C., Löth, K., Ranebo, H., Jofs, B., Nilsson, J., Schneider, H., 1999a: *JET Growth Motion in Aerosols Module for MASER 8, Final Report*, SUM85111-D61, 8 November 1999, internal report, not published
- Lockowandt, C., Löth, K., Nilsson, J., Ranebo, H., Jofs, B., Schneider, H., Willneff, J., Dupont, O., Vedernikov, A., Legros, J.C., 1999b: *The JET Module, A Tool for Aerosol Particle Experiments in Microgravity*. 50th International Astronautical Federation Congress, Microgravity Sciences and Processes Symposium, IAF-99-J.5.07, Amsterdam, October 1999.
- Lüthi, B., Burr, U., Kinzelbach, W., Tsinober, A., 2001: Velocity derivatives in turbulent flow from 3d-PTV measurements. *Proceedings of the Second International Symposium on Turbulence and Shear Flow Phenomena*, Stockholm, 27-29 June 2001, eds. E. Lindborg et al. 2: 123-128.
- Lüthi, B., 2002: *Some Aspects of Strain, Vorticity and Material Element Dynamics as Measured with 3D Particle Tracking Velocimetry in a Turbulent Flow*, ETH Zürich, Ph.D. Thesis, 2002.
- Maas, H.-G., 1990: Digital Photogrammetry for the Determination of Tracer Particle Coordinates in Turbulent Flow Research. SPIE Proceedings Series Vol 1395, Part 1

References

- Maas, H.-G., 1991a: Digital Photogrammetry for the Determination of Tracer Particle Coordinates in Turbulent Flow Research. *Photogrammetric Engineering & Remote Sensing*, Vol. 57, No. 12, pp. 1593-1597
- Maas, H.-G., 1991b: Automated Photogrammetric Surface Reconstruction with Structured Light. International Conference on Industrial Vision Metrology, Winnipeg, Canada, 11.-12.07.1991
- Maas, H.-G., 1992a: *Complexity analysis for the determination of dense spatial target fields*. Robust Computer Vision (Eds.:Förstner/Ruwiede), Wichmann Verlag, Karlsruhe
- Maas, H.-G., 1992b: *Digitale Photogrammetrie in der dreidimensionalen Strömungsmesstechnik*. ETH Zürich - Dissertation Nr. 9665
- Maas, H.-G., 1993: *Determination of velocity fields in flow tomography sequences by 3-D least squares matching*, Proceedings of the 2nd Conference on Optical 3-D Measurement Techniques, Zurich, Oct. 4-7, Wichmann Verlag, Karlsruhe
- Maas, H.-G., Grün, A., Papantoniou, D., 1993: *Particle Tracking in three-dimensional turbulent flows - Part I: Photogrammetric determination of particle coordinates*. Experiments in Fluids Vol. 15, pp. 133-146
- Maas, H.-G., 1995: *New developments in multimedia photogrammetry, in Optical 3-D Measurement Techniques III*, (Eds.: A. Grün, H. Kahmen), Wichmann Verlag, Karlsruhe
- Maas, H.-G., 1996: *Contributions of Digital Photogrammetry to 3-D PTV, in Three-Dimensional Velocity and Vorticity Measuring and Image Analysis Techniques*, pp. 191-207, Kluwer Academic Publishers, printed in the Netherlands
- Maas, H.-G., Virant, M., Becker, J., Bosemann, W., Gatti, L., Henrichs, A., 1997: *Photogrammetric methods for measurements in fluid physics experiments in space*. 48th International Astronautical Congress, Torino/Italy
- Malik, N., Dracos, T., Papantoniou, D., 1993: *Particle Tracking in three-dimensional turbulent flows - Part II: Particle tracking*. Experiments in Fluids Vol. 15, pp. 279-294
- Melikhov, I. V., Vedernikov, A. A., 1995, *Jet growth (non-Brownian) random walk of crystals in aerosols*, Dokl. Phys. Chem. 340 505-8
- Merkel, G. J., Dracos, T., Rys, P., Rys, F. S., 1993: Flow Tomography by Laser Induced Fluorescence, XXV IAHR Congress, Tokyo, Japan
- Navab, N., Zhang, Z., 1992: Fusion of visual data through dynamic stereo-motion cooperation, IAPRS Vol. 29, Part B5, pp 932-939
- Netzs, Th., Jähne, B., 1993. *Ein schnelles Verfahren zur Lösung des Stereokorrespondenzproblems bei der 3D-Particle Tracking Velocimetry*, Mustererkennung 1993 (Eds. J. Pöppel and H. Handels), Springer-Verlag
- Ninomiya, N., Kasagi, N., 1993: *Measurement of Reynolds stress budgets in an axisymmetric free jet with the aid of three-dimensional Particle Tracking Velocimetry*, Proc. 9th Symp. on Turbulent Shear Flows 6.1.1-6.1.6, Kyoto
- Nishino, K., Kasagi, N., Hirata, M., 1989: *Three-dimensional Particle Tracking Velocimetry based on automated digital image processing*. Journal of Fluid Engineering, Vol. 111, pp. 384-391

- Nishino, K., Kasagi, N., 1989: *Turbulence statistics in a two-dimensional channel flow using a three-dimensional Particle Tracking Velocimeter*, Proceedings on the Seventh Symposium on Turbulent Shear Flows, Stanford University, August 21-23
- Nitsche, W., 1994: *Strömungsmesstechnik*, Springer-Lehrbuch, Springer-Verlag Berlin Heidelberg, ISBN 3-540-54467-4
- Papantoniou, D., Dracos, T., 1989: *Analyzing 3-Dimensional Turbulent Motions in Open Channel Flow by Use of Stereoscopy and Particle Tracking*. Advances in Turbulence 2 (Eds. Hernholz and Fiedler), Springer Verlag, Heidelberg
- Papantoniou, D., Dracos, T., 1990: *Lagrangian Statistics in Open Channel Flow by 3-D Particle Tracking Velocimetry*, Proceedings International Symposium on Engineering Turbulence - Methods and Measurements (Hrsg. Rodi, Ganic), Dubrovnik, September 24.-28. Elsevier Pub.
- Papantoniou, D., Maas, H.-G., 1990: *Recent advances in 3-D particle tracking velocimetry*. Proceedings 5th International Symposium on the Application of Laser Techniques in Fluid Mechanics, Lisbon, July 9-12
- Racca, R., Dewey, J., 1988: *A Method for Automatic Particle Tracking in a Three-Dimensional Flow Field*, Experiments in Fluids 6, pp. 25-32
- Raffel, M., Willert, C., Kompenhans, J., 1998: *Particle Image Velocimetry, A Practical Guide*, Springer Verlag, Berlin
- Rood, E. P. (ed), 1993: *Holographic Particle Velocimetry*, ASME FED 148
- Sata, Y., Kasagi, N., 1992: *Improvement toward high measurement resolution in three-dimensional particle tracking velocimetry*, Flow Visualization VI, Y. Tanida et al., eds., Springer-Verlag, pp. 792-796
- Sata, Y., Sato, K., Kasagi, N., Takamura, N., 1994: *Application of the three-dimensional particle tracking velocimeter to a turbulent air flow*, Proc. 3rd Asian Symp. on Visualization, Y. Nakayama et al., eds., Springer-Verlag, pp. 705-709
- Schimpf, A., Siekmann, H.E., Steinmann, A., 2002: *Stereo-PIV in aerated wastewater pond and side channel blower*, Proceedings of The 9th International Symposium on Transport Phenomena and Dynamics of Rotating Machinery, on CD-ROM, February 10-14, Honolulu, Hawaii, USA
- Schmundt, D., Münsterer, T., Lauer, H., Jähne, B., 1995: *The circular wind/wave facility at the University of Heidelberg, Air-Water Gas Transfer - Selected Papers from the Third International Symposium of Air-Water Gas Transfer*, Heidelberg, B. Jähne und E. Monahan (Hrsg.), Aeon Verlag Hanau
- Swedish Space Corporation, 1998: *Annual Report 1998*, www.ssc.se
- Swedish Space Corporation, 1999: *Annual Report 1999*, www.ssc.se
- Stüer, H., 1999: *Investigation of separation on a forward facing step*, ETH Zürich - Dissertation Nr. 13132
- Stüer, H., Maas, H.-G., Virant, M., Becker, J., 1999a: *A volumetric 3D measurement tool for velocity field diagnostics in microgravity experiments*, Meas. Sci. Technol. 10, pp 904-913, printed in the UK
- Stüer, H., Willneff J., Maas H.-G., 1999b: *Evaluation of image compression in 3D PTV*. Videometrics VI, Proceeding of SPIE, San Jose, California, 1999, Vol. 3641, pp 228-238

- Stüer, H., Willneff, J., Maas, H.-G., 2000: *The impact of image compression on three-dimensional particle tracking velocimetry data*, Journal of Flow Visualization and Image Processing (Publisher: Begell House), Vol.7 (2), pp.89-104
- Suzuki, Y., Kasagi, N., 1999: *Turbulent air flow measurement with the aid of 3-D particle tracking velocimetry in a curved square bend*, J Flow, Turbulence & Combustion, Vol. 63, pp. 415-442, Kluwer Academic Publishers, Netherland
- Suzuki, Y., Ikenoya, M., Kasagi, N., 2000: *Simultaneous measurement of fluid and dispersed phases in a particle-laden turbulent channel flow with the aid of 3-D PTV*, Exp. Fluids, Vol. 29, pp. 185-193
- Suzuki, Y., Ikenoya, M., Kasagi, N., 1999: *Three-dimensional PTV measurement of the phase relationship between coherent structures and dispersed particles in a turbulent channel flow*, 3rd Int. Workshop on Particle Image Velocimetry, pp. 107-112
- Tcl, 2003, Developer Xchange, Web-site: <http://www.scriptics.com/>
- Vedernikov, A. A., Melikhov, I. V., 1994, *Motion of growing crystals in gas in short-term microgravity experiments*, Proc. Int. Workshop on Short-Term Experiments under Strongly Reduced Gravity Conditions, Bremen, Germany, July 4-7, pp263-7
- Venas, B., Abrahamsson, H., Krogstad, P.-A., Löfdahl, L., 1999: *Pulsed hot-wire measurements in two- and three-dimensional wall jets*, Experiments in Fluids 27, pp 210-218, Springer-Verlag
- Virant, M., 1996: *Anwendung der dreidimensionalen "Particle Tracking Velocimetry" auf die Untersuchung von Dispersionsvorgängen in Kanalströmungen*, ETH Zürich - Dissertation Nr. 11678
- Wierzimok, D., Hering, F., 1993: *Quantitative Imaging of Transport in Fluids with Digital Image Processing*, Imaging in Transport Processes, Begell House, pp 297-308
- Willneff, J., 1999a: *Jet growth motion in aerosols module, Module Acceptance Review, Report Phase C/D, Contribution ETH*, internal project report, in cooperation with the Swedish Space Corporation, not published
- Willneff, J., 1999b: *Jet growth motion in aerosols module, Final Report Phase C/D, Contribution ETH*, internal project report, in cooperation with the Swedish Space Corporation, not published
- Willneff, J., Maas, H.-G., 2000: *Design and calibration of a four-headed camera system for use in microgravity research*, International Archives of Photogrammetry and Remote Sensing, XIXth ISPRS Congress Amsterdam 2000, Volume XXXIII, Part B5/2, Commission V, pp 894-899, 16-23 July 2000, Amsterdam, The Netherlands
- Willneff, J., Gruen, A., 2002: *A new spatio-temporal matching algorithm for 3D-Particle Tracking Velocimetry*, Proceeding of The 9th International Symposium on Transport Phenomena and Dynamics of Rotating Machinery, on CD-ROM, February 10-14, Honolulu, Hawaii, USA
- Willneff, J., 2002: *3D Particle Tracking Velocimetry based on image and object space information*, ISPRS Commission V Symposium, International Archives of Photogrammetry, Remote Sensing and Information Sciences, Volume XXXIV, Part 5, Commission V, September 2-6, Corfu, Greece

Curriculum Vitae

Dipl.-Ing. Jochen Willneff
Institute of Geodesy and Photogrammetry
ETH Zürich
8093 Zürich

Personal

Date of birth: March 14th, 1971
Nationality: German

Formation

1997- 2003:

Ph.D. student and assistant at Institute of Geodesy and Photogrammetry
Swiss Federal Institute of Technology Zurich, Switzerland
Ph.D. thesis: A Spatio-Temporal Matching Algorithm for 3D Particle Tracking Velocimetry

1991-1997:

Master of Geodetic Sciences at TH Karlsruhe, Germany
Master Thesis: 3D Modeling of Buildings at Institute of Photogrammetry and Remote Sensing

1990 - 1991: Military service

1982-1990: High school graduation, Oken Gymnasium, Offenburg, Germany

Employment:

1992-1994: ÖBVI Seitz & Stark, Offenburg, Germany, 20 weeks, practical training

Publications:

12 publications at conferences and in journals since 1999. A complete list of publications is available at: http://www.photogrammetry.ethz.ch/research/ptv/all_papers.html

Languages:

Native language: German
Foreign languages: English, French